INVESTIGATION ON DIELECTRIC RESONATOR AND DIELECTRIC LOADED ANTENNAS FOR DUAL-BAND AND WIDEBAND APPLICATIONS

P Anoop

INVESTIGATION ON DIELECTRIC RESONATOR AND DIELECTRIC LOADED ANTENNAS FOR DUAL-BAND AND WIDEBAND APPLICATIONS

A

Thesis Submitted

in Partial Fulfilment of the Requirements

for the Degree of

DOCTOR OF PHILOSOPHY

By

P ANOOP

DEPARTMENT OF ELECTRONICS AND ELECTRICAL ENGINEERING

INDIAN INSTITUTE OF TECHNOLOGY GUWAHATI

GUWAHATI - 781 039, ASSAM, INDIA

DECEMBER, 2020

Declaration

I hereby declare that the thesis entitled "**Investigation on Dielectric Resonator and Dielectric Loaded Antennas for Dual-Band and Wideband Applications**", submitted in the *Department of Electronics and Electrical Engineering, Indian Institute of Technology Guwahati, Assam, India*, for the award of the degree of **Doctor of Philosophy**, has been carried out by me under the supervision and guidance of Prof. Ratnajit Bhattacharjee. The results embodied in this thesis are original and have not been submitted to any other University or Institute for the award of any degree or diploma.

Dated: 31/12/2020

Place: Guwahati

P Anoop
Research Scholar
Dept. of Electronics and Electrical Engineering
Indian Institute of Technology Guwahati
Guwahati - 781039, Assam, India.

Certificate

This is to certify that the thesis entitled "**INVESTIGATION ON DIELECTRIC RESONATOR AND DIELECTRIC LOADED ANTENNAS FOR DUAL-BAND AND WIDEBAND APPLICATIONS**", submitted by **P Anoop** (136102003), a research scholar in the *Department of Electronics and Electrical Engineering, Indian Institute of Technology Guwahati*, for the award of the degree of **Doctor of Philosophy**, is a record of an original research work carried out by him under our supervision and guidance. The thesis has fulfilled all requirements as per the regulations of the institute and in my opinion has reached the standard needed for submission. The results embodied in this thesis have not been submitted to any other University or Institute for the award of any degree or diploma.

Dated: 31/12/2020
Guwahati.

Prof. Ratnajit Bhattacharjee
Professor
Dept. of Electronics and Electrical Engg.
Indian Institute of Technology Guwahati
Guwahati - 781 039, Assam, India.

To my Family

Acknowledgements

First and foremost, I feel it as a great privilege in expressing my deepest and most sincere gratitude to my supervisor Prof. Ratnajit Bhattacharjee, for his excellent guidance and encouragement throughout my Ph.D. tenure. His patience, kindness, attention and the mental support in many situations of my life, during this research has been a source of great inspiration and motivation to me. His advice has taught me innumerable lessons and insights on the workings of an academic research, that enriched my life as a researcher as well as an individual. I thank him from the bottom of my heart for always being there with me during all kinds of distress and grieve.

I would like to thank my Doctoral Committee members, Prof. Rakhesh Singh Kshetrimayum, Dr. Sisir Kumar Nayak and Dr. Mahima Arrawatia for sparing their valuable time out of a busy schedule to evaluate my progress and enrich this thesis work with their valuable suggestions and feedbacks. I would also like to thank Prof. A. K. Gogoi who have been in my Doctoral Committee until retirement. His suggestion towards my research and on the future prospect of me as a researcher and an individual have been a great support and inspiration. I also thank Prof. Rohit Sinha, Head of the Department, EEE, for his kind help and timely intervene in all the academic matters during my Ph.D. I would also like to extend my thanks to the other faculty members of IIT Guwahati, who have been with me and supported towards my research work in innumerable ways.

I sincerely thank Prof. P. Mohanan, Department of Electronics, CUSAT for his kind support in availing research facilities at Centre for Research in Electromagnetics & Antennas (CREMA). I also extend my thanks to Ants Ceramics, Pune and Kumar Ceramics, Bhubaneswar for providing me with the materials required for carrying out this research.

I am also grateful to my senior Dr. Haris B. C, for his advice and moral support during my Ph.D. I also sincerely thank my seniors Dr. Rajib Jana and Dr. Somen Bhattacharjee, and my dear colleagues Mrinmoy Bharadwaj and Dr. Jitendra Prajapati for their support and feedbacks during this research. I sincerely thank my dear friends Dr. Pawan Kumar, Rahul Chhatwani, Prateek Rathore, Arijit Roy, Kaushik Debbarma for making my stay at IIT Guwahati, beautiful. I specially thank Dibya Jyoti Das, Mrinmoy Bharadwaj and Himangshu Jyoti Das for the discussions we had, apart from research in the leisure time, which were one of the unforgettable memories during this research life. I also thank rest of my fellow scholars and inmates, for their support during my stay at IIT Guwahati.

I wholeheartedly thank all the Malayaleese who made my life during this Ph.D., a most beautiful and memorable experience, which I never had before. I thank my dear friends Sajith and Arun Mathew, who were always with me at every moment of life at IIT Guwhati. I also thank Dr. Haris B.C, Dr. Jiss J. Nallikuzhy, Dr. Sandeep P, Dr. Sonu J.K, Vishnu V. Thuruthiyil, Dr. Piyoosh P, Dr. Vivek Lukose, Dr. Vasudevan M.S, Anoop Raveendran, Arjun Puthussery, Bino Albert, Nidhin A.K, Jeevan Kuriakose, Abdul Kareem, Jith J.R, Dileep P, Dr. Suresh B.M, Dr. Renjith Bhaskar, Dr. Hari Narayanan, Sajeer K.P, Fahad M, Vijith K.P, Hrishikeshan V. M, Thomas T. Daniel, Mathew Francis, Dr. Vivek Venugopal, Suvin V, Amrutha Suresh, Dhanya, Lakshmi, Anu, Reshma, Anjali, Alaka, Rahul R. Nair, for being with me and making my stay at IIT Guwahati, one of the unforgettable memories of my life. I also sincerely thank Dr. A. Rajesh and Dr. Tony Jacob for their support and care which, I received during my stay at IIT Guwahati.

I express my deepest appreciation towards my wife, Hima for her unconditional support and sacrifices, in all my hardship and struggle for this thesis. This Ph.D. would not have been possible without all her mental and moral support. I also extend my love and appreciation to my dear little daughter, Ridhibala for abiding my ignorance and the patience she showed during this research. This journey would not have been possible without the prayers and unconditional love from my Parents, Balachandran and Sushama. I am especially grateful to them, who supported me emotionally and financially throughout this life for pursuing my dream and ambitions. I also appreciate all the love and support from my sister Arunima, and her special care and attention which she gave during my absence in the family, during this research. I sincerely thank my Father-in-law, Balan and Mother-in-law, Mallika, for all their prayers and emotional support in every difficulty, and the kind attention of in-laws to my family in my absence, during this research. I also thank my intimate friend since childhood, Remith Manohar for his timely intervene and emotional support for completing this research.

Lastly, I extend my sincere thanks to all the staffs in the Department of Electronics and Electrical Engineering and IIT Guwahati administration for helping me in all sorts of ways during this research and my stay, at the prestigious campus of Indian Institute of Technology, Guwahati.

P. Anoop

Abstract

In this thesis, we investigate an Equilateral Triangular shaped and a Rhombic shaped Dielectric Resonator Antenna, and their potential for dual-band and wideband applications. The dielectric loading effects has been observed while designing practical Dielectric Resonator Antennas presented in this thesis and in the context of this, an investigation on some of the aspects of dielectric loading effect is also presented. The investigations reported in this thesis have resulted into several contributions. The quality factor of Equilateral Triangular shaped Dielectric Resonator Antenna operated in the dominant $TM_{10\delta}$ mode has been studied in detail. An expression for calculating the quality factor for this operating mode is also developed for the case of most commonly used aspect ratios of the dimensions and the dielectric constant values of the materials used in the design of practical Equilateral Triangular shaped Dielectric Resonator Antenna. Further, this investigation has been extended to study the bandwidth performance for this dominant mode and relevant closed form expression for estimating the practical impedance bandwidth for this antenna geometry in this dominant operating mode is also presented. The Equilateral Triangular shaped Dielectric Resonator Antenna is also investigated for its potential as a dual-band antenna for WLAN application in the frequency bands of 2.4-2.5 GHz and 5.75-5.85 GHz. Two configurations of the dual-band Equilateral Triangular shaped Dielectric Resonator Antennas are proposed namely, Configuration-I and Configuration-II, and their performance with other dual-band Dielectric Resonator Antennas, reported in the literature, are compared. Based on various observations in the design of proposed dual-band antenna configurations, some of the challenges in the design of dual-band/ multi-band Dielectric Resonator Antennas have also been highlighted. A Rhombic shaped Dielectric Resonator Antenna, having unequal diagonals, has been investigated for the first time and is presented in this thesis. The dominant and a few of the higher order TE modes excited inside this basic antenna geometry have been identified through Eigen mode analysis with

the aid of Electromagnetic simulations performed using CST Microwave Studio. Empirical formulae for calculating the resonant frequencies of these modes have been developed separately for the x- and y- polarized cases, through curve-fitting approximations. Suitable feeding techniques that can be used for exciting these modes have also been presented. The nature of radiation characteristics of these modes have been identified, and presented to give an insight into the behavior of these modes excited inside this proposed Dielectric Resonator Antenna. A prototype of this antenna has been fabricated and its performance is verified experimentally. A preliminary investigation on the special case of this antenna geometry with low profile configuration has also been presented. Further, by fine-tuning the feed position, the proposed Rhombic Dielectric Resonator Antenna is also found to exhibit wideband characteristics. Some aspects of dielectric loaded monopole antenna has also been investigated and presented in this thesis. This investigation includes the effect of size, shape, volume and dielectric constant of the dielectric load on the impedance bandwidth and radiation characteristics of a monopole antenna. Dual-band dielectric loaded monopole antennas for WLAN applications in the bands 2.4-2.5 GHz and 5.75-5.85 GHz have been proposed. Appropriate mathematical model and a closed form expression, useful in the design of such dual-band antennas have also been discussed.

Contents

List of Figures

List of Tables

Glossary

AR	Axial Ratio
CDRA	Cylindrical Dielectric Resonator Antenna
CP	Circular Polarization
CST	Computer Simulation Technology
DRA	Dielectric Resonator Antenna
EBG	Electronic Band Gap
EM	Electromagnetic
ETDRA	Equilateral Triangular Dielectric Resonator Antenna
HDRA	Hemispherical Dielectric Resonator Antenna
HEM	Hybrid Electromagnetic
HFSS	High Frequency Structure Simulator
RDRA	Rectangular Dielectric Resonator Antenna
TE	Transverse Electric
TM	Transverse Magnetic
UWB	Ultra Wide Band
VSWR	Voltage Standing Wave Ratio
WiMAX	Worldwide Inter-operability for Microwave Access
WLAN	Wireless Local Area Network

List of Symbols

λ_o	Free space wavelength
ϵ_r	Relative permittivity of the material
ω	Angular frequency
Q	Quality factor
$Q_{radiated}$	Radiation quality factor
Q_{loss}	Loss quality factor
$\overrightarrow{E}$	Electric field intensity vector
$\overrightarrow{H}$	Magnetic field intensity vector
$\overrightarrow{n}$	Unit normal vector
a	Length of side of a DRA
a_e	Effective value of length of side of an ETDRA
h	Height of the DRA above goundplane
h_e	Effective value of height of an ETDRA above goundplane
χ	Composite wave number in x and y direction together
$T(x, y)$	Amplitude distribution function
k_z	Wave number along z- direction
$f_{m,n,p}$	Resonant frequency of TM modes of an ETDRA
$f_{modified}$	Modified resonant frequency of TM modes of an ETDRA
f_r	Resonant frequency of an antenna
s	Voltage standing wave ratio
T	Degree of impedance matching
Z_0	Characteristic impedance of a transmission line
R_0	Resistive part of the input impedance of an antenna
Q_{10}	Q-factor of an ETDRA having ϵ_r=10, operated in $TM_{10\delta}$ mode

$\triangle Q$	Correction factor for Q-factor of an ETDRA having ϵ_r=10, operated in $TM_{10\delta}$ mode
BW	Fractional impedance bandwidth
$\triangle f$	Relative bandwidth of an antenna
$\triangle f_{max}$	Maximum impedance bandwidth of an ETDRA operated in $TM_{10\delta}$ mode
$\triangle f^{'}$	Correction factor for impedance bandwidth of an ETDRA operated in $TM_{10\delta}$ mode
$\|S_{11}\|$	Magnitude of the return loss of an antenna
d_1	Length of longer diagonal of a Rhombic DRA
d_2	Length of smaller diagonal of a Rhombic DRA
d_{1eff}	Effective value of longer diagonal of a Rhombic DRA
d_{2eff}	Effective value of smaller diagonal of a Rhombic DRA
h_{eff}	Effective value of height of a Rhombic DRA
$(TE_n)^y$	X-polarized TE mode of a Rhombic DRA of order n
$(TE_n)^x$	Y-polarized TE mode of a Rhombic DRA of order n
$f_{(TE_n)^y}$	Resonant frequency of $(TE_n)^y$ mode of Rhombic DRA
$f_{(TE_n)^x}$	Resonant frequency of $(TE_n)^x$ mode of Rhombic DRA
$f_{(TE_1)}$	Resonant frequency of $(TE_1)^y$ and $(TE_1)^x$ mode of a low profile Rhombic DRA
$tan\ \delta$	Loss tangent value of a dielectric material
ϕ_{1d}	Half power beamwidth in one plane (degrees)
ϕ_{2d}	Half power beamwidth in the plane right angle to the other (degrees)
G_0	Empirical value of gain of an antenna

1

Introduction to the Dielectric Resonator Antennas

Contents

This chapter presents the introduction to Dielectric Resonator Antennas, popularly known as DRA. The major characteristics of this antenna are discussed to highlight their significance compared to other small antennas. Survey of relevant literature is then presented to understand where they stay in the current state of the art. The motivation of this thesis is discussed following the state of the art on the analysis and design of Dielectric Resonator Antennas. The contributions of this thesis are then presented and the chapter wise organization of the works discussed in this thesis are also summarized.

1.1 Dielectric Resonator Antennas

The dielectric resonators were first presented by R. D. Richtmyer in the form of dielectric spheres in 1939 in [1]. This structure was introduced as a very high quality factor (Q-factor) microwave resonator and not as a radiator. The modes excited inside such resonator was first analyzed by Okaya and Barash and presented in [2] in the early 1960's. As the geometry of dielectric resonators were very compact due to the use of very high dielectric constant material ($\epsilon_r > 200$), they easily replaced the conventional waveguide cavity resonators. They were mainly used as filters and oscillators, with low loss and Q-factor as high as 10,000 and even more. As the Q-factor of the dielectric resonators were very high, the losses happening within such resonators in the form of radiation were feeble. It was until 1983, the dielectric resonators were not investigated as a radiator, when S. A. Long, McAllister and Shen introduced cylindrical [3], rectangular [4] and hemispherical [5] dielectric resonators as antennas which radiates electromagnetic fields outside such cavities. The radiated fields are enhanced by proper choices of the dimensions and materials which have lower dielectric constant values varying in the ranges of $5 \leq \epsilon_r \leq 20$. By choosing lower values of dielectric constant, these resonator antennas will have lower Q-factor, making them better radiators at their resonant frequencies. A radiating mode, which is excited at its resonant frequency, has a unique standing wave field distribution based on the geometry of the DRA. The radiated fields of such excited modes from the DRA resembled the radiation patterns of the conventional short electric or magnetic dipoles. However, some of the inherent properties of DRA gave them a special attention of the research community.

The research studies on the DRA started three decades ago. In the early 1980's the research mainly focussed on the analysis on the resonant modes of such antennas [3–5]. However, in the early 1990's the investigation were still focused with individual DRAs on their feeding mechanism, input impedances, Q-factor and radiation characteristics [6–12]. In the later stages of 1990's the DRAs

were more investigated to improve the impedance bandwidth, although a few related works were also reported previously in the literature [13–21]. The analysis and theoretical investigation on rectangular DRA (or RDRA) and cylindrical DRA (or CDRA) were also well developed before the start of this century. Improving antenna characteristics like gain and developing circularly polarized design also became quite popular using RDRA and CDRA, since early 1990's. Some of the early literature include [22–27] on circular polarization and [28–30] are for high gain designs.

The DRAs which is classified among the small antennas, continued as a popular topic of research invoking many researchers all over the world to develop simple as well as novel geometries of such antennas to achieve broadband, high gain, linear as well as circularly polarized characteristics. Some of the properties of the DRA make them an outstanding candidate among the small antennas. The early investigations on the DRA summarizes the characteristics of this small antenna as:

- The overall size of a radiating dielectric resonator is proportional to $\lambda_o/\sqrt{\epsilon_r}$, where λ_o is the free space wavelength and ϵ_r is the dielectric constant of the material used to form the DRA. By proper choice of material and ϵ_r value, the size of the antenna can be considerably reduced.

- By proper choice of antenna dimension and ϵ_r value, the DRAs can be made of several shapes or geometries. Further, the dimension and dielectric constant of the material can be varied to affect the resonant frequency of the excited modes of such antennas, thereby allowing a high degree of flexibility in the realization of DRA to operate between a wide range of frequencies.

- Unlike the other conventional small radiators like patch antenna, the DRAs do not suffer from conductor losses or rather such effects are often insignificant. By choosing low loss dielectric materials the DRA can be designed to provide a very high radiation efficiency.

- The modes of the DRA can be excited using simple feeding techniques. The conventional feeding techniques like coaxial probe, microstrip lines, coplanar waveguide lines, slots etc can be used to efficiently excite such antennas, allowing them to easily integrate with various existing technologies.

- The radiation patterns of the excited modes of the DRA are similar to patterns of short electric or magnetic dipoles which produces either broadside or omnidirectional patterns. Due to their high radiation efficiency, the DRAs therefore can easily replace other conventional small antennas producing similar radiation characteristics.

We have mentioned that, the DRAs provide high degree of flexibility to the antenna designers to realize their design in any complex geometry. Generally, the dielectric materials used in the realization of such antennas are cheap and easily available. By proper machining of the commercially available dielectric block, the DRAs of any desired geometry can be developed. However, in certain cases the drilling of the material may be required if the antenna is excited using a coaxial feed. The popular feeding techniques used to excite the DRA will be discussed later in this chapter.

1.2 Fundamentals of Dielectric Resonator Antennas

As discussed before, the dielectric resonators, were not intially used as radiators instead as microwave resonators, of very high Q-factor. The Q-factor of a dielectric resonator is described as in [1, 31];

$$Q = \omega \frac{average\ energy\ stored}{energy\ loss/second} \tag{1.1}$$

The energy lost per second or the power lost in the dielectric resonators are mainly in the form of radiations as they are not significantly effected by conductor losses. A magnetic wall exist at the boundaries of the dielectric resonator and mathematically which is expressed as given in [12, 32];

$$\overrightarrow{n} \times \overrightarrow{H} = 0 \tag{1.2}$$

$$\overrightarrow{E} \cdot \overrightarrow{n} = 0 \tag{1.3}$$

where, $\overrightarrow{n}$ is the unit normal vector to the dielectric resonator boundaries. The quantities $\overrightarrow{E}$ and $\overrightarrow{H}$, represents the Electric and Magnetic field vectors, respectively. We can also physically interpret the above equations as the condition, where the dielectric-air boundaries existing at the edges of dielectric resonators do not allow the fields inside this dielectric cavity to escape into the free space. Such a situation is maintained by making use of a very high dielectric constant material in the design of dielectric resonators. As the losses happening inside such cavity in the form of electromagnetic radiation are very insignificant, the Q-factor of dielectric resonators are very high. However, the radiated fields outside dielectric resonators cannot be zero, as they would exhibit infinite Q-factor which is impractical. A small amount of fields has to exist at the outer walls of dielectric resonators which escape into the free space as radiation. The Cohn model presented in [33] explains that the fields inside the dielectric resonator does not vanishes abruptly at the dielectric-air boundary, instead they gradually decreases while moving away from such boundaries. A similar model was also presented by Itoh and

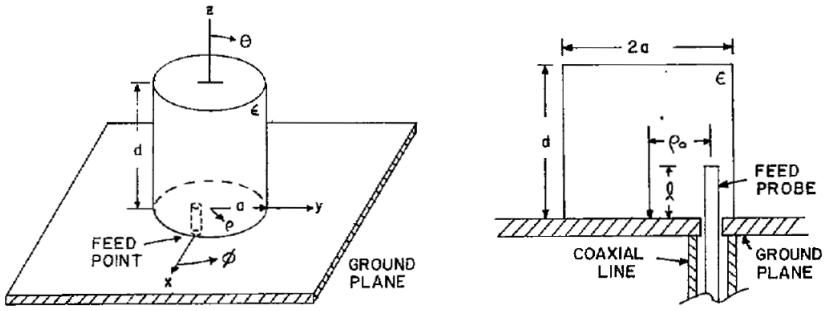

Figure 1.1: The antenna configuration of CDRA introduced by S. A. Long in [3]

Rudokas [34] in which the fields outside the dielectric cavity decays monotonically while moving radially outward. Usually, to prevent any radiation the dielectric resonators used in the microwave filters and oscillators are also shielded by metal cavities, so that a high Q-factor is maintained. However, if the shielding is removed and the high Q-factor of a dielectric resonator is reduced, the radiated fields from such a dielectric cavity can be enhanced. This is achieved by choosing relatively lower dielectric constant materials in the design of dielectric resonators. S. A. Long, who introduced dielectric cavity resonators as an antenna, mentioned the values of dielectric constant can typically vary from $5 \leq \epsilon_r \leq 20$. The CDRA, which was first reported by S. A. Long in [3], is shown in Figure 1.1. The antenna arrangement has a cylindrical dielectric block of appropriate dimensions and chosen dielectric constant value, which can support the excitation of fundamental TM_{110} mode and some of the higher order modes. The antenna is excited by a conventional coaxial feed. The DRA is placed on a conducting groundplane and the coaxial feeding probe protrude into the cylindrical dielectric block through the base of the groundplane. The coaxial probe is placed at an appropriate position to have proper excitation of fundamental as well as some of the higher order modes of the CDRA. The drilling of the DRA is required to have maximum coupling between the coaxial probe and the fields of the excited modes inside the cylindrical dielectric block. For any DRA, the standing wave field distribution of an excited mode is unique, which produces a corresponding radiation pattern in the far field. In general, the modes excited inside a DRA can be classified into TE, TM or HEM. The nomenclature followed in assigning the modes of DRA are presented in [10]. The TM_{110} mode excited inside the CDRA in [3] produces a broadside radiation pattern. Such enhanced radiation pattern from the DRA is a result of low Q-factor of this excited mode inside the proposed DRA.

1.3 Survey of relevant literature

The DRAs have been an active area of research since the last three decades, and still continuing as a promising research topic among the researchers. The contribution to the literature on the DRA so far has been very significant and relevant to meet the design requirements of most of the existing technologies. They are more convenient to operate at the microwave frequencies from L- band to X-band. However, such antennas are even reported for applications at millimeter wave frequencies [35–38]. We will therefore classify the investigation on the DRAs reported in the literature based on (i) geometry or shape and (ii) utility. This classification will help the readers to have an understanding of the trends and the state of the art on the design of dielectric resonator antennas based on which, the research carried out in this thesis is presented.

1.3.1 Survey of DRA shapes

In the early stages of DRA research, three basic shapes of such antennas were prominent; which are cylindrical, rectangular and hemispherical. The cylindrical and rectangular DRA have geometrically better degree of freedom and therefore have high design flexibility when compared to the hemispherical geometry. Although the exact analytical solutions to the fields of hemispherical DRA (or HDRA) exist, such antennas had practically limited usage due to the difficulty involved in their fabrication. However, as discussed before, the RDRA and CDRA were rigourously investigated by the research community on their excited modes, Q-factor and radiation characteristics, which are detailed in some of the popular textbooks [39, 40] in the area of antennas and wave propagation. The wideband, circularly polarized and high gain designs with DRA and some of the techniques to achieve such characteristics which are available in the literature, will be separately discussed later in this chapter.

The ring DRA, which is a variant of CDRA was presented in [41]. Some of the early investigations on such resonator was discussed in [42–44]. As the central portion of such antennas are hollow, their Q-factors are lower than CDRAs. However, for the same reason their resonant frequencies are higher than the CDRA. Some of the designs using ring DRA which are available in the literature are presented in [45–49]. Another basic DRA which did not receive much attention by the antenna community is the equilateral triangular DRA (or ETDRA). This DRA was introduced in the literature as low profile design, where the height of the DRA is very small compared to the rest of its dimensions [50,51]. Some of the early analysis of ETDRAs are reported in [52–57]. The investigations on this DRA geometry

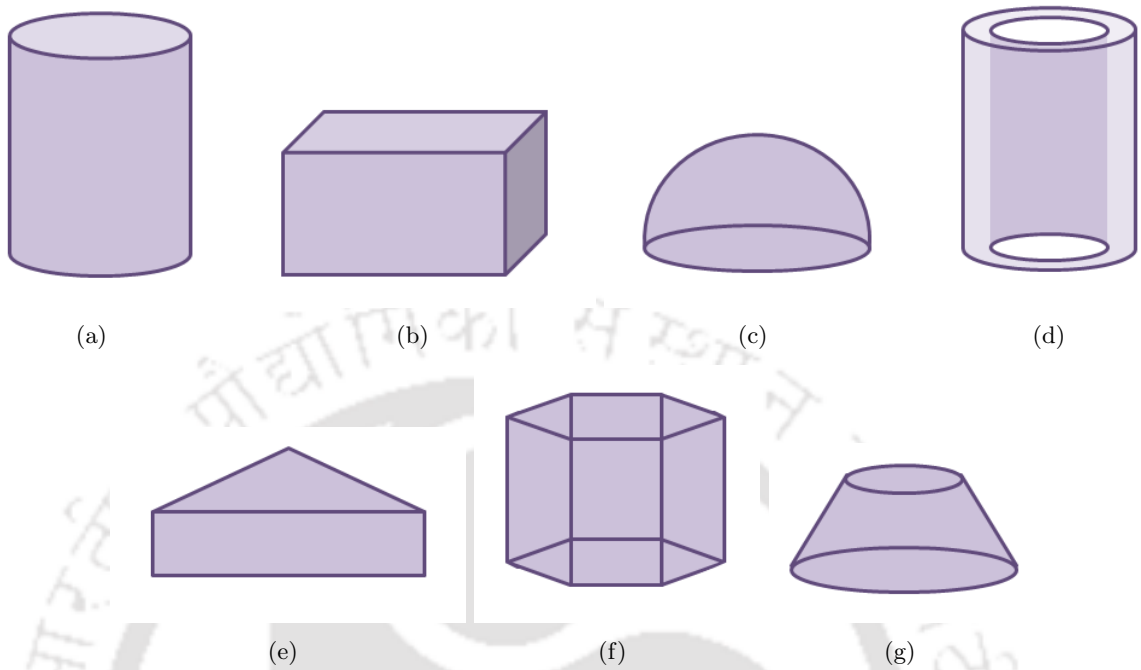

Figure 1.2: Geometry of some of the DRA shapes: (a) CDRA, (b) RDRA, (c) HDRA, (d) Ring DRA, (e) ETDRA, (f) Hexagonal DRA and (g) Conical DRA.

are found very limited in the literature; some of the available works are reported in [58–62] and recently in [63–67]. Other forms of triangular shaped DRAs are also reported recently in the literature in [68–70].The DRAs of other miscellaneous cross-section available in the literature includes, conical DRA [71, 72], pyramidal DRA [73, 74], elliptical DRA [75–79], tetrahedral DRA [19, 80], hexagonal DRA [81–83]; most of which are not yet investigated rigourously. The geometry of some of the available and popular DRAs in literature are shown in Figure 1.2. With the requirement of ultra-wideband (UWB) design and circular polarization with wide axial ratio bandwidth, the antenna designers modified the basic geometries as well as incorporated new improved feeding techniques to realize novel and compact DRA designs, since the last two decades.

1.3.2 Survey based on utility and performance

In the previous sub-section we have discussed various DRA geometries introduced in the literature. The theoretical analysis of some of such DRAs were developed and some of the characteristics of such DRAs which have been reported in the literature include wide bandwidth, high gain and type of polarization. In this section, we discuss the techniques used in the literature to improve such characteristics and some of the novel designs and trends in achieving such antenna characteristics

using DRA.

1.3.2.1 Survey on broadband DRAs

The broadband or wide impedance bandwidth for DRAs, as reported in the literature, are achieved mainly by: (i) introducing air gap, (ii) improving feeding technique, (iii) exciting multiple modes and (iv) layering or stacking of the DRAs. Introducing air gap is one of the early techniques used by the antenna designers to improve the impedance bandwidth, which are reported in the literature [15] [16, 84–90]. The investigation shows that upon introducing air gap between the DRA and the ground plane, the impedance matching can be achieved over wider frequencies with reduced Q-factor; however, the resonant frequency of the antenna increases. Another method followed in the literature during the early period of DRA research is making both the feed and the antenna to resonate at nearby frequencies. Through proper fine tuning, impedance matching can be brought over a broad frequency range. Such a technique is proposed in [48], where in a coaxially excited DRA, both the probe and the DRA resonate at nearby frequencies and wide impedance matching is achieved. Similar wideband DRAs are also reported in [49, 91, 92]. Improving the feeding technique is yet another method used in the literature to improve the impedance bandwidth. Use of ring aperture feed [93,94], U-shaped aperture feed [95], cavity backing [20], improved microstrip feeding [96,97] and many other novel approaches modifying the conventional feeding techniques [98–106] are also reported in the literature for enhancing the bandwidth. However, the broadening of the impedance bandwidth does not always happens due to such feeding techniques alone. The improved feeding techniques also excite multiple modes of the DRA and the broad impedance bandwidth is the result of having close resonant frequencies of these excited modes. Wideband DRAs design using such technique of exciting multi-modes of the DRA are also reported in [107–113].

The broadening of the impedance bandwidth using multiple modes are also achieved by exciting multiple DRAs. The broad impedance bandwidth is achieved by exciting modes of each DRA which resonates at nearby frequencies. Stacking of DRAs [13,21,114–116], use of coplanar DRAs [14,117,118], embedding [18, 119, 120], layering [121–124] of the DRAs are some of the techniques used in this method for broadening the bandwidth. Such multiple resonances are also brought using fractal design technique. In this technique DRA of complex patterns are made out of similar DRAs of different scales and which are created by repeating the same or a similar set of process over and over. Some of the wideband fractal DRAs reported in the literature includes [125–129]. Such DRA designs are very

complex from the fabrication point of view; however, they provide very high percentage bandwidths. The percentage impedance bandwidth using such technique are found as high as 64% and 66%, which are reported in [126] and [129].

The similar techniques used for broadening the impedance bandwidth are also practiced by the antenna designers for achieving UWB DRAs. M. Lapierre and Y. M. M. Antar developed ultra wideband antenna using monopole and ring DRA in [92]. A similar hybrid antenna for UWB operation is also reported later by D. Guha and B. Gupta along with Y. M. M. Antar in [130, 131], with an improved bandwidth of 22% compared to the previously reported design in [92]. Such hybrid antenna is also reported by M. N. Jazi and A. R. Sebak in [132], with an ultra wide bandwidth in the range of 1.8-12 GHz. Hybrid antenna with stacking of the cone shaped DRA is also reported by C. Ozzaim and N. Tarim in [133] with a fractional impedance bandwidth of 136% covering a frequency range of 1.8-9.4 GHz and Ring DRA loaded on a monopole is presented by K. H. R. Zheng and Le Wei Li in [134], having a bandwidth of 110%. An UWB DRA for digital video broadcasting (DVB) and GSM application is reported by L. Huitema and T. Monediere in [135] having a bandwidth of 70%. The UWB antenna using DRA with band rejection in the frequency range of 3.1-10.6 GHz is reported in [136], by T. A. Denidni and Z. Weng. Such UWB DRA with band rejection is also reported in [137], using hybrid design technique by M. N. Jazi and T. A. Denidni. A UWB design with a band rejection around 5.8 GHz is also reported by M. Abedian and S. K. A. Rahim in [138]. Later, they have developed a compact UWB DRA with band rejection in WiMAx/WLAN bands, reported in [139]. However, the compact UWB DRA is presented much earlier by Y. Ge and K. P. Esselle in [140], having an operating bandwidth in the range of 3.1-10.6 GHz. Compact UWB antenna is also presented by M. Abedian and M. Khalily in [141], using two segment Z-shaped DRA having an operating bandwidth in the range of 2.5-10.3 GHz. Another version of this two segment Z-shaped DRA having the same operational bandwidth is presented in [142].

The UWB design using DRAs are not limited in the literature discussed so far, some of the other noted designs include UWB DRA mounted on a vertical ground plane presented in [143, 144], UWB DRA with low cross-polarization discussed in [145], UWB DRA with low cross-polarization as well as consistent omni-directional pattern over the operating bandwidth, reported in [146] and PMA loaded DRA for UWB applications presented in [147].

1.3.2.2 Survey on multi-band operating DRAs

Multi-band DRAs reported in the literature are developed by achieving multiple resonant frequency and the impedance matching is improved around each of the resonant frequency. The impedance matching is improved around those frequencies over which the antenna is operated. A mode is excited at those resonant frequencies to provide desired radiation characteristics. The techniques used in the design of multi-band DRAs are similar to the broadband DRAs, and approaches like stacking, layering, use of mutliple DRAs are reported in the literature. However, based on operation, we divide the mutli-band DRAs into (i) dual-band DRAs, (ii) triple-band DRAs and (iii) DRAs with more than three bands.

In the dual-band DRAs reported in the literature, impedance matching around the two operating resonant frequencies are achieved by utilizing single DRA as well as two DRAs. In single DRA dual-band antennas, multiple modes of single DRA are excited directly using conventional excitation techniques to achieve dual-band operation [148–155]. However, improved feeding techniques are also applied while exciting the DRA to achieve such antenna characteristics [156–159]. Multiple feeding of a single DRA is also used as a technique to achieve dual-band characteristics which is reported in [76]. Other techniques like cavity backing [160], integrating DRA with slots [161], defective ground plane [162] and introducing fractal geometry [163] of the DRA are also reported in the literature to achieve dual-band operation. However, in multiple DRA dual-band design, each DRA resonates within corresponding operating bands of the dual-band DRA. A stacked dual-band CDRA is reported in [164]. Similar approaches in the design of dual-band DRAs are also followed in triple-band and other multiple-band DRAs reported in the literature. Single DRA with triple-bands utilizing multi-modes are reported in [81]. Single DRA with modified feed for tri-band operation is reported in [165]. DRA with metallic coating for tri-band operation is also reported in the literature as detailed in [166]. The tri-band antenna utilizing multiple DRAs with the technique of stacking is reported in [167]. Another technique which introduce variation of permittivity values along the azimuth variation, to achieve tri-band design using DRA is detailed in [168]. The DRAs with more than three operating bands reported in the literature are very limited; however one such antenna is described in [82], which achieved four operational bandwidths, by exciting multiple modes of an hexagonal DRA.

1.3.2.3 Survey on high gain DRAs

The high gain DRAs reported in the literature can be classified into two categories (a) DRAs with only high gain [28, 29, 35–38, 127, 169–185] and (b) DRAs with high gain as well as broad impedance bandwidth [30, 115, 124, 186–193]. In the investigation on high gain DRAs, the antenna designers often focussed on attaining higher gain with simple DRA shapes, some of which are reported in [28,29,35,172–175,177–179,183,185]. An old technique of improving the gain is by layering of RDRA of different permittivity values, reported by Y. Hwang, Y.P. Zhang and K.M. Luk in [28] where, a gain of 6.2 dBi is achieved. Improving the coupling mechanism is also used to enhance the DRA gain. The DRA reported by K. W. Leung and K. M. Luk in [29] is one such early reported work in the literature that achieved a gain of 4 dBi using very high permittivity material. A similar technique is used by S. Fakhte and M.H.V. Samiei using a loaded patch antenna on the RDRA to achieve a gain of 11.5 dBi in 3.75-6.75 GHz bandwidth and, A. Rashidian and L. Shafai in [178] to achieve a gain of varying from 4.2-5.5 dBi in 4.3-4.6 GHz bandwidth using RDRA loaded with tall metal microstrip line. Another technique reported in the literature makes use of higher order mode excited in the DRA to enhance gain performance [172–174, 177, 179]. They include broadside high gain CDRA reported by Guha in [172, 174], having a gain more than 8 dBi in the operating frequencies at which $HEM_{12\delta}$ like modes are excited. Another RDRA presented by A. Petosa and S. Thirakoune in [173], excited higher order modes in such DRAs to enhance the gain upto 5 dBi than the gain of the fundamental mode. In [177], L. Y. Feng and K. W. Leung presented a CDRA whose gain is enhanced by exciting TM_{015} mode. The antenna provided a gain of 2.3 dB higher than that of the fundamental TM_{011} mode. However, not the last, M. Michal and Z. Raida presented enhanced gain CDRA based on the combination of higher order modes to achieve a gain of 11.6 dBi at 5.8 GHz by exciting HEM_{133} and HEM_{123} modes.

Other techniques reported in the literature for increasing the gain includes, incorporating electromagnetic bandgap (EBG) structures [37,170,171], use of fractal geometries presented in [127,169]. It is also noted that, in the recent reported DRA design [182], a technique where a flat reflecting surface in the antenna arrangement is used to enhance the gain. However, a similar approach is also presented in the literature little early by Nasimuddin and K.P. Esselle in [30]; where, a short horn covers a RDRA arrangement to enhance gain in the broadside direction. A gain of 8.5 dBi was achieved through this arrangement. Also, this antenna provided a percentage impedance bandwidth of 25%, making it a

high gain broadband DRA. A similar design is also reported in [186], where a gain better than 9 dBi is achieved, with a percentage bandwidth of 21.3%, over the range of 6.07-7.52 GHz.

In the design of high gain broadband DRAs one of the early work was reported by K. M. Luk in [115]. The configuration uses multiple CDRAs which are stacked one above the other. A small air gap is introduced and the DRA on the top is placed little away from the axis of bottom antenna to enhance bandwidth as well as gain. A maximum gain of 6.4 dBi and a percentage impedance bandwidth of 37% is achieved. Such stacked arrangement of the DRAs with high gain and wideband characteristics is also reported in [124] by Y. M.Pan. This antenna is made very compact by using low profile rectangular shaped DRAs. The antenna provides a gain of 9 dBi with a percentage impedance bandwidth of 40%. However, a compact DRA reported little early by Wang in [187], achieved a gain of 11 dBi. This proposed high gain broadband DRA has a percentage bandwidth of 23% covering a frequency range of 5.4-6.8 GHz. The antenna arrangement has a intermediate layer and a metallic cylinder along with the CDRA to enhance gain as well as impedance bandwidth. Other noted work in the literature includes DRAs with fractal geometries to enhance bandwidth and gain. A fractal design using RDRA is reported by P. Patel in [188]. The antenna provides a gain of 7.2 dBi and an impedance bandwidth of 2.4 GHz, which find application for WiMAX and WLAN operations. The fractal geometries were very well utilized to design wideband DRAs as we have already seen in section 1.3.2.1. Another technique for enhancing gain as well as bandwidth of DRAs is introducing EBG structures. Some of the reported literature includes a novel hemispherical DRA with EBG structure as in [189] having a gain of 9 dBi and percentage bandwidth of 30%, a wideband EBG resonator antenna reported by Hashmi and Esselle in [191] having a peak measured gain of 15.6 dBi and 3 dB gain-bandwidth of 27%. A reported technique in the literature that enhance bandwidth and gain uses metameterials as in [190], where a maximum gain of 9.8 dBi is achieved with a percentage bandwidth of 32.8%. Other noted geometries reported in the recent period in the literature for enhancing the bandwidth as well as gain includes; a compact filtering DRA proposed by P.F. Hu in [192], with an impedance band of 20.3% and gain of 9.05 dBi, and a mushroom shaped DRA proposed recently by R.Cicchetti in [193], having a fractional bandwidth of 65% and a maximum gain of more than 14 dBi.

1.3.2.4 Survey on circularly polarized DRAs

The circular polarization (CP) in a DRA is generated by exciting degenerate modes which are in phase quadrature and spatially orthogonal to each other. Such polarization can be achieved by

suitable excitation mechanism in which the feed is positioned appropriately to excite spatially orthogonal degenerate modes. The modes can be excited by single or dual point feeding technique [40]. One of the early reported single point feed circularly polarized DRA is a chamfered DRA presented in [194]. The DRA has square cross-section which is cut at its opposing corners. The DRA has a 3-dB axial ratio (AR) bandwidth of 4%. In another approach RDRA is fed diagonally to obtain CP, as reported in [22, 24, 195, 196]. Arranging cross-shaped DRA presented by Ittipiboon in [197] is another technique to excite two spatially orthogonal modes to generate CP. The two arms of the cross are assumed as two linearly polarized RDRA. The antenna provides a 3-dB AR of 4%. These techniques described in the above reported articles presents single fed DRA in which the arrangement of DRA is modified to achieve CP. However, it is also possible that the feed itself can be modified to excite spatially orthogonal modes of the DRA as reported in [25, 26] by C. Y. Huang. The arrangement uses cross slot aperture coupled microstripline feeding technique to excite degenerate modes of CDRA to generate CP. The approach does not require modification of the DRA, so that the geometry remains simple. The CDRA reported in [25] has a 3-dB AR of 4% around 2.04 GHz. Annular slot aperture for exciting the degenerate modes of required amplitude and phase for CP is another technique which are reported in [198–201]. Back cavities are also introduced below the slots to suppress backlobe radiations in [198, 201]. A 3-dB AR bandwidth of 4% is reported for these DRAs using such feeds. Other aperture slot coupled DRAs generating CP available in the literature are reported in [201–207].

Apart from the aperture slot coupled feeding, a technique reported in the literature introduced parasitic slots as in [208] by C. Y. Huang, where a CDRA is excited to generate CP. The input impedance of such antenna is matched by the exciting aperture feed and the low AR is maintained by adjusting the parasitic slots. A maximum 3-dB AR bandwidth of 2.7% has been achieved by this feeding technique. However, it was later reported that the parasitic slots can be replaced by parasitic strips in the form of metal strips or patches on the DRA as discussed in [27, 209–213]. The CP can be generated by appropriately fine tuning the dimensions as well as choosing the position of the metallic strips. The 3-dB AR bandwidth achieved with this technique reported in [27, 209–213] varied from 1% to 3%. Developing fractal geometries are yet another technique which are reported in the literature which has the potential to generate CP. Although, such reported geometries are limited, some of the noted designs are presented in [214, 215]. In [214], S. Dhar proposed a Minkowski fractal design developed from RDRA, which gave a 3-dB AR bandwidth of 5.83%. In [215], a spidron fractal DRA

is proposed by Altaf using a C-shaped slot excitation. The DRA provides a 3-dB AR bandwidth of 11.57%.

The reported circularly polarized DRAs discussed so far, except a few has very limited AR bandwidth. However, to improve the 3-dB AR bandwidth, a technique has been reported in [216, 217], known as sequential rotation of a set of linearly polarized antennas. Some of the early circularly polarized DRAs developed using such technique are proposed in [194, 218–221] and their 3-dB AR bandwidths are reported as enhanced upto 20%. This technique of generating circularly polarized DRAs is also followed in some of the articles reported thereafter, as in [222, 223]. In [222], reported by Fakhte, has a novel low cost DRA by stacking four RDRA, which are rotated 30^0 relative to each other to achieved CP of 6% 3-dB AR bandwidth. Similarly in [223], reported by Wang and Wong, in which a rotated stair shaped DRAs are placed appropriately to achieve CP. The arrangement provides a wide 3-dB AR bandwidth of 18.2% and an average gain around 4.5 dBi.

Some of the wideband circularly polarized DRA reported in the literature using other approaches are discussed in [224–229]. A CDRA excited with 90^0 hybrid coupler is presented by Khoo in [224], which provides an AR bandwidth of 25.9%. A similar approach is also available in [225], proposed by Lim and Leung, where a 3-dB AR bandwidth of 20% is reported. In [226], Pan and Leung proposed a trapezoidal shaped DRA having an AR bandwidth of more than 20%. The impedance matching is improved by providing a notch on the top of the DRA. Using the technique of adding parasitic strips to the lateral slots of the DRA, Pan and Leung have also enhanced the AR bandwidth of the DRA by 25.4%, as reported in [227]. The antenna also exhibit omni-directional radiation pattern throughout the operating bandwidth. Another technique is presented by Han in [228]; where, the DRA is excited by dual-feed to achieve wide AR bandwidth of 47.69%. Apart from wideband circularly polarized DRA, a few noted dual-band circularly polarized DRAs [200, 230–232] are also reported in the literature.

1.4 Motivation of the Present Work

(i) The cylindrical and rectangular DRAs reported in the literature underwent a thorough investigation by the research community. This basic DRA geometries were also efficiently utilized by the research community to achieve antenna characteristics and their performance are enhanced by techniques which we have discussed in the previous section. Among the DRA with basic geome-

tries, the hemispherical DRA did not became much popular due to their low degree of freedom and therefore, very limited designs using such DRA were reported in the literature. However, the research community also gave very less attention to the Equilateral Triangular DRA (ETDRA), although this DRA geometry is flexible to fit into any space and adaptable with the existing technologies to realize all the antenna characteristics. A very limited works based on such DRAs were reported in the literature until a few years ago [19, 29, 50, 51, 54, 58–61, 80].

(ii) Although, the analysis of excited modes within the ETDRA were developed [52–54, 56, 57] and later in [62]; like rectangular and cylindrical DRAs, the expression for quality factor for the excited modes inside the ETDRA were not developed. Further, upon estimating the quality factor, it would be directly possible to estimate the impedance bandwidth of such DRAs, while they are excited with a particular radiating mode.

(iii) In the detailed survey of available DRA literature, it is also found that, the potential of the ETDRAs for dual-band operation is not adequately investigated and reported in the literature [60]. A recent investigation on dual-band ETDRA is reported in [64]. It is to be noted that, the DRAs are small antennas which are usually designed to resonate at a particular operating frequency. Based on the desired radiation characteristics and design requirement, a suitable geometry is chosen and an appropriate radiating mode is excited. However, at frequencies of operation where any of the radiating modes of the DRA is not excited; at those frequencies the DRA can act as a dielectric load. The dielectric loading basically effects the impedance matching of the antenna around the desired operating frequency. However, these effects can be severe, when DRAs are designed to operate as a dual-band antenna, and which make use of multiple DRAs which are closely spaced in the antenna configuration. It is possible that in such compact antenna design the radiated fields of a higher order mode of one DRA have better chances of interfering with radiated fields of an excited mode of another closely spaced DRA, if both the former and later radiating modes have close values of their resonant frequency. Dual-band DRA design using ETDRAs, with emphasis on various effect on the impedance matching and desired radiation characteristics are not properly addressed in the literature. Further, the potential of ETDRA, in single as well as multiple DRA configurations for dual-band operation has also not been investigated in detail and reported in the literature.

(iv) In the design of wideband DRA, a variant of square DRA is reported in the literature, which is a rotated version of a square DRA to form a Rhombic DRA [233]. The diagonals of this DRA has equal length. However, if we assume two ETDRAs joined at one of their sides to form a Rhombic DRA having unequal diagonals, the field distributions of the excited modes are different from that of the excited modes of Rhombic DRA formed by rotated version of the square DRA. Such rhombic DRA have not been investigated and reported in the earlier literature. Due to unequal lengths of the diagonal, this DRA geometry can be excited to achieve wide impedance bandwidth.

(v) We already discussed that, the dielectric loading effects are used in the antenna design, where the resonant frequency of an antenna is to be reduced while keeping its size smaller. This phenomena is observed usually in the DRA design having multiple DRAs. This effect becomes significant when the arrangement of DRAs in the design are very closely spaced such that, the presence of one DRA effects the resonant frequency as well as impedance matching of the neighbouring DRA in the design. The impedance bandwidth and the antenna performance can degrade. Moreover, it is observed that developing dual-band/ multi-band designs using DRA becomes quite challenging. However, understanding this phenomena of dielectric loading in a broader perspective can resolve some of the challenges in the design of multi-band antennas. It is noted that dielectric loading effect is favourably used in the literature, even in the design of monopole and dipole antennas. The effect of dielectric loading of a thick monopole on radiation characteristics was reported in [234]. The effect on efficiency-bandwidth product on the volume of the dielectric load is also investigated in detail and presented in [235]. However, the effect of such loading over the impedance matching, while varying the size and dielectric constant for different geometry of the dielectric load have not been investigated so far.

1.5 Thesis Contribution

The research work carried out on the investigation on dielectric resonator and dielectric loaded antennas include theoretical as well as simulation study which focus mainly on the Equilateral Triangular DRA and the proposed new Rhombic DRA having unequal diagonals. Characteristics like dual-band, wideband and high gain performances are achieved by proposing novel design guidelines. The performances are also verified with fabricated prototypes through measurements. As a case study,

some aspects of dielectric loaded antennas are also investigated, the prime objective of which is to demonstrate on the phenomena of dielectric loading and how, volume and shape of the load effect the impedance matching.

The main contributions of this thesis are summarized and listed below:

(i) Quality factor of an ETDRA excited with dominant $TM_{10\delta}$ mode is presented. A closed form expression for the calculation of same is also developed.

(ii) The impedance bandwidth performance of $TM_{10\delta}$ mode is presented. By utilizing the expression for the quality factor, a closed form expression is also developed to calculate the practical bandwidth of an ETDRA excited with such mode.

(iii) Dual-band antenna for WLAN applications are proposed using single as well as two ETDRAs, configuration-I and configuration-II. The radiation characteristics of higher order $TM_{3-3\delta}$ mode in ETDRA is discussed, which is operated in the upper band of the proposed ETDRA configuration-I. The configuration-II presents dual-band ETDRA with similar radiation characteristics in both the operating bands. The effect of unwanted higher order mode in the design of such dual-band DRAs and techniques to suppress the same is also discussed. Further, in the context of the proposed dual-band ETDRA configurations, the importance of dielectric loss tangent is briefly highlighted. Some of the challenges and considerations in the design of dual-band/ multi-band DRAs are also discussed.

(iv) A new Rhombic DRA having unequal diagonals is proposed. Dominant and some of the TE modes excited inside such DRAs are identified and their field distributions are presented. The expression for calculating the resonant frequency of these modes are developed and their radiation characteristics are also presented.

(v) Appropriate feeding techniques for exciting the TE modes of the new Rhombic DRA is presented and suitable feed positions are identified to achieve a wide impedance bandwidth. Using a simple coaxial probe excitation this proposed DRA with basic geometry achieved a bandwidth of 31.64%.

(vi) The effect of shape, volume and permittivity of the dielectric loading on a monopole strip are investigated. Appropriate closed form expression is developed, which is useful in the design of dielectric loaded monopole antenna for dual-band operation.

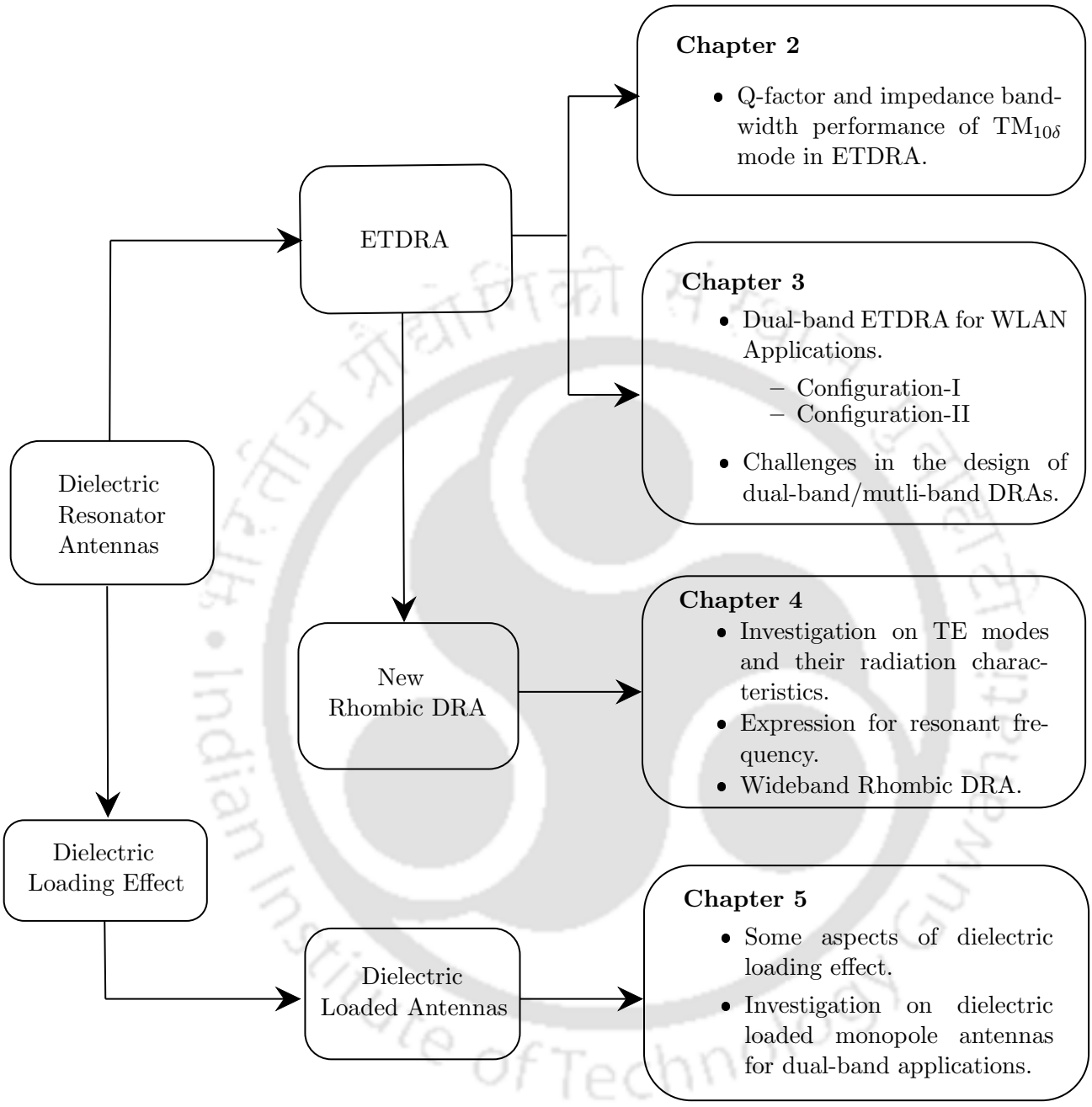

Figure 1.3: Thesis contribution tree

A pictorial representation of the contributions of this thesis is shown in Figure 1.3.

1.6 Thesis Organization

This thesis is organized into six chapters. The summary of each chapter is briefed as follows.

Chapter 1: In this chapter, an overview of Dielectric Resonator Antennas, survey of relevant literature and the motivation of this thesis is presented.

Chapter 2: This chapter discusses initially about the TM mode solutions of Equilateral Triangular DRA and some of the factors effecting the resonant frequency of the excited modes in such DRAs. This is followed by discussion on the Q-factor of $TM_{10\delta}$ mode excited inside such DRAs. The Q-factor curves are presented for the $TM_{10\delta}$ mode. A closed form expression for calculating the Q-factor for such mode is discussed and the validation of the same by comparing with practical results are also presented. The chapter concludes with the discussion on bandwidth performance of TM mode excited in ETDRA.

Chapter 3: The Chapter 3 presents the investigation on the design of dual-band ETDRAs for WLAN applications. The chapter intially discusses a preliminary investigation on the design and performance characteristics of the proposed dual-band antenna. The subsequent section discusses about the design modifications to improve the radiation characteristics in the initial design. A detailed investigation on the potential of an ETDRA as a dual-band antenna is presented and two configurations of the same is proposed; namely, Configuration-I and Configuration-II, which are discussed in separate sub-sections. Further, the performance of the proposed configurations of the dual-band ETDRAs are also compared with other dual-band DRAs reported in the literature. The chapter concludes by discussion on some the challenges and issues in the design of dual-band/ multi-band DRAs, which are summarized based on various observations in the investigation of the proposed dual-band ETDRAs.

Chapter 4: In this chapter investigation on a new Rhombic DRA is presented. The chapter initially introduces the geometry of the proposed Rhombic DRA and discusses the motivation of developing such a DRA geometry. This is followed by discussion on some of the excited TE modes in such DRAs. The field distributions of the excited modes are presented for better understanding of these excited TE modes. A discussion on the calculation of resonant frequency of the excited TE modes are then presented, followed by a brief discussion on the feeding techniques which will be useful in the excitation of such modes. The radiation characteristics of dominant and some of the higher order TE modes excited inside such Rhombic DRA are then presented in this chapter. A special case of this proposed DRA having a low profile geometry, where the height of the DRA is very small

compared to the other dimensions of this antenna geometry is also presented in the subsequent section. The chapter concludes with the design of a compact wideband Rhombic DRA.

Chapter 5: In this chapter some aspects of dielectric loaded antennas are presented. The chapter initially discusses the design of dielectric loaded monopole antenna for dual-band operation which can be operated in the WLAN frequency bands of 2.4-2.5 GHz and 5.75-5.85 GHz. Modeling of this proposed dual-band antenna is presented in the following section. A discussion on dielectric loading with different dielectric shapes are then presented and case studies, where deviations in the modeling of the proposed antenna are observed, are also presented in the subsequent section. The chapter concludes with discussion on the practical observations of proposed dielectric loaded dual-band antenna.

Chapter 6: In this chapter, the summary of the works presented in this thesis on dielectric resonator and dielectric loaded antennas are presented. Scopes of future research based on the works reported in this thesis are also discussed.

1.7 Summary

In this chapter we have discussed the features and properties of a dielectric resonator antenna. A detailed survey of the DRAs reported in the literature are presented classifying them based on the geometry as well as utility and their applications. Based on the state of the art of this popular antenna, motivation of the research work presented in this thesis are discussed. This chapter also summarizes the contributions of this thesis and the chapter wise organization of the research works carried out by the author.

2

Investigation on Equilateral Triangular Dielectric Resonator Antenna

Contents

In this chapter[1], we discuss about the Q-factor and impedance bandwidth performance of ETDRA excited with the dominant $TM_{10\delta}$ mode. A method for calculating the Q-factor of such antennas excited with this mode is developed, which is obtained through curve fitting approximation technique. The Q-factor is expressed as a function of aspect ratio (a/h) and the material dielectric constant (ϵ_r) of the DRA. This method is also utilized further in obtaining an approximate expression for calculating the impedance bandwidth around the resonant frequency of such DRA, when excited with the $TM_{10\delta}$ mode. Moreover, the bandwidth performance of such mode around the resonant frequency for different degrees of impedance matching is also discussed.

In this thesis, the research work carried out with ETDRA mainly concentrates with the dominant $TM_{10\delta}$ mode. We therefore start our discussion with $TM_{m,n,p}$ mode solutions of ETDRA in a more generalized perspective and then present the standing wave field distribution of the dominant $TM_{10\delta}$ mode excited inside an ETDRA. The early analysis reported in the literature [50, 52–55] assumed the ETDRA as a waveguide of equilateral triangular cross section. However, in ETDRA we do not have a travelling wave and instead have a standing wave field pattern for an excited mode at its resonant frequency. The comprehensive analysis of the TM modes of an ETDRA presented in this chapter also discusses the field distribution of some of the higher order $TM_{m,n,p}$ modes, a few of which has not been discussed in the literature.

2.1 $TM_{m,n,p}$ mode solutions of ETDRA

The TM field distribution of an ETDRA having side 'a' and height 'h'(above the groundplane) whose geometry is shown in Figure 2.1, can be expressed using the field quantities which are described in Appendix A as:

$$E_z = A_c \left(\frac{\chi^2}{j\omega\varepsilon}\right) T(x,y)P(z) \tag{2.1}$$

$$\begin{aligned} E_x \;=\; & \left[\frac{A_c(k_z sin(k_z z))}{j\omega\epsilon}\right]\left(\frac{2\pi}{\sqrt{3}a}\right) \times \{lsin(\theta_x l)cos[\theta_y(m-n)] + msin(\theta_x m)cos[\theta_y(n-l)] \\ & +nsin(\theta_x n)cos[\theta_y(l-m)]\} \end{aligned} \tag{2.2}$$

[1]The work reported in this chapter has been presented in the following conference publications:
Anoop P, Bhattacharjee R, "Expression for Quality factor of $TM_{10\delta}$ mode in Equilateral Triangular DRA", *IEEE-INAE Workshop on Electromagnetics (IIWE 2018)*; Dec.2018,Trivandrum, India.
Anoop P, Bhattacharjee R, " Impedance bandwidth performance of $TM_{10\delta}$ mode in Equilateral Triangular DRA," *14th European Conference on Antennas and Propagation, EuCAP 2020*, Copenhagen, Denmark, March 15-20, 2020.

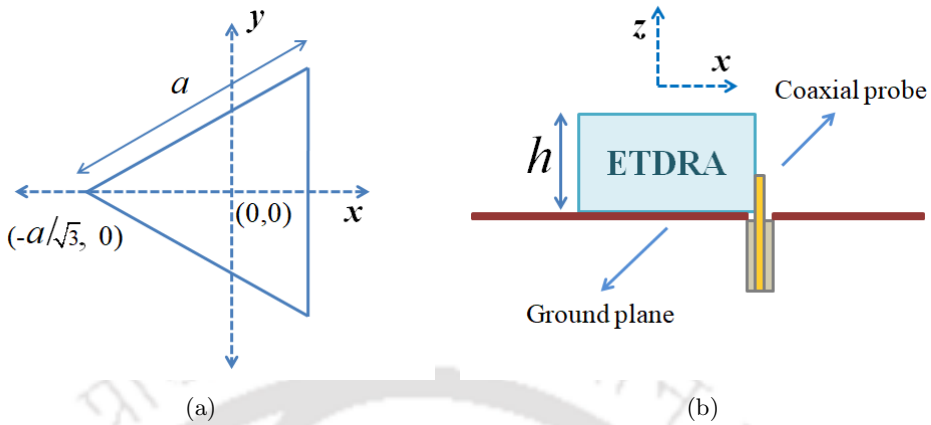

(a) (b)

Figure 2.1: Geometry of Equilateral Triangular DRA: (a) 2-D top view and (b) side view with the coaxial cable to excite dominant mode.

$$E_y = \left[\frac{A_c(k_z sin(k_z z))}{j\omega\epsilon}\right]\left(\frac{2\pi}{3a}\right) \times \{(m-n)cos(\theta_x l)sin[\theta_y(m-n)] + (n-l)cos(\theta_x m) sin[\theta_y(n-l)] + (l-m)cos(\theta_x n)sin[\theta_y(l-m)]\} \quad (2.3)$$

$$H_x = -A_c(cos(k_z z))\left(\frac{2\pi}{3a}\right) \times \{(m-n)cos(\theta_x l)sin[\theta_y(m-n)] + (n-l)cos(\theta_x m) sin[\theta_y(n-l)] + (l-m)cos(\theta_x n)sin[\theta_y(l-m)]\} \quad (2.4)$$

$$H_y = A_c(cos(k_z z))\left(\frac{2\pi}{\sqrt{3}a}\right) \times \{lsin(\theta_x l)cos[\theta_y(m-n)] + msin(\theta_x m)cos[\theta_y(n-l)] + nsin(\theta_x n)cos[\theta_y(l-m)]\} \quad (2.5)$$

where, A_c is a constant and k_z is the wave number along z direction (along height h from ground plane), given by

$$k_z = \frac{p\pi}{2h}, \qquad p=1,2.. \quad (2.6)$$

The resonant frequency of $TM_{m,n,p}$ modes excited inside an ETDRA can be expressed as in [52–54] given by

$$f_{m,n,p} = \frac{c}{2\pi\sqrt{\varepsilon_r}}\sqrt{\left(\frac{4\pi}{3a}\right)^2(m^2+n^2+mn) + {k_z}^2} \quad (2.7)$$

The resonant frequency is described by side a, height h and the dielectric constant (ϵ_r) of the material used to realize an ETDRA. The aspect ratio (a/h) describes the size of the ETDRA. However, for the cases where $a >> h$, the resonant frequency of the modes mainly depend on h, as the terms containing $1/a$ in equation 2.7 becomes insignificant. Therefore, the expression for resonant frequency further

reduces to;

$$f_{m,n,p} = \frac{c}{2\pi\sqrt{\varepsilon_r}}\left(\frac{p\pi}{2h}\right) \tag{2.8}$$

The equations 2.2 2.3 2.4 2.5 can be used to obtain standing wave field distribution of the various excited modes inside the ETDRA. The field distribution of dominant and a few of the higher order TM modes excited inside an ETDRA are shown in Figures 2.2, 2.3, 2.4, 2.5, 2.6. The dominant mode excited inside an ETDRA is $TM_{10\delta}$ mode. The E-field and H-field distributions of this excited mode inside this DRA are shown in Figure 2.2(a) and Figure 2.2(b), respectively. The isometric view of E-field and H-field obtained using eigen mode simulation performed using commercial EM simulator, CST Microwave Studio is also shown, as in Figure 2.2(c) and Figure 2.2(d), respectively. The same has also been shown for higher order TM modes in Figures 2.3, 2.4, 2.5, 2.6. The $TM_{10\delta}$ mode can be easily excited using a conventional coaxial probe. By convention, the feed should be placed at the point where, a maximum coupling between the source and the fields of the mode (which is to be excited) exist. For a fundamental $TM_{10\delta}$ mode, the maximum coupling exist when the probe is kept at the center of one of the sides of the ETDRA. Figure 2.1(b) shows the schematic diagram of exciting the dominant mode of an ETDRA. The higher order TM modes can also be similarly excited by properly placing the feed. For example, the field distribution of $TM_{11\delta}$ mode is shown in Figure 2.3. This mode can be excited by placing the coaxial feed at the centroid of the DRA. Drilling of the DRA is therefore, required in this type of feeding technique. However, this can be avoided by choosing aperture coupling. The field distributions of higher order modes like $TM_{2-2\delta}$, $TM_{12\delta}$ and $TM_{3-3\delta}$ modes, are shown in Figure 2.4, Figure 2.5 and Figure 2.6, respectively. Excitation of such modes need not require any drilling of the DRA for the case of a coaxial probe excitation and therefore, can be excited by similarly placing the feed, as in the case of $TM_{10\delta}$ mode. The Table 2.1 shows the resonant frequency of these excited modes, which has been obtained for an ETDRA having side a=20 mm for various aspect ratios (a/h) and dielectric constant (ϵ_r) values, using eigen mode simulations performed using CST Microwave Studio.

2.1.1 Issues effecting resonant frequency of the excited modes inside ETDRA

The equation 2.7 gives the theoretical resonant frequency of $TM_{m,n,p}$ modes excited inside an ETDRA. However, it is observed that the practical resonant frequency of the excited modes are occurring above their corresponding theoretical values. The deviations are observed to a greater

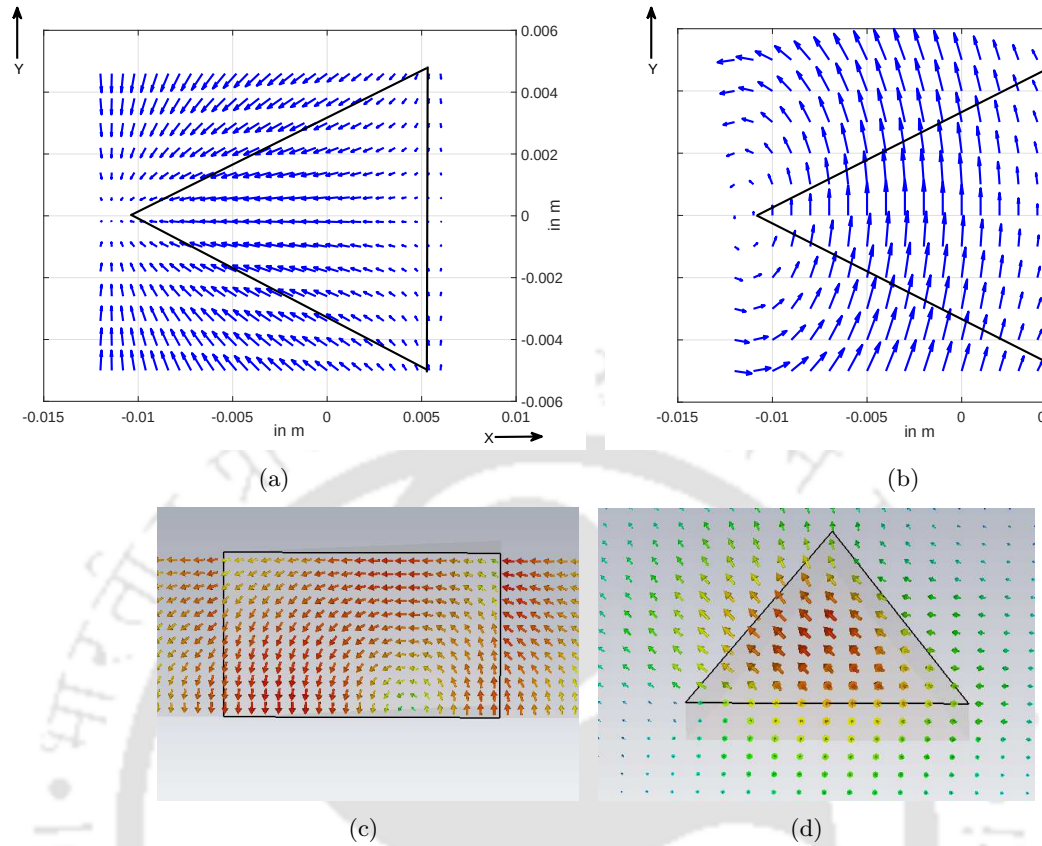

Figure 2.2: Field distribution of $TM_{10\delta}$ mode(a) E-field (analytical) in XY plane,(b) H-field (analytical) in XY plane, (c) E-field (CST) isometric view,(d) H-field (CST) isometric view.

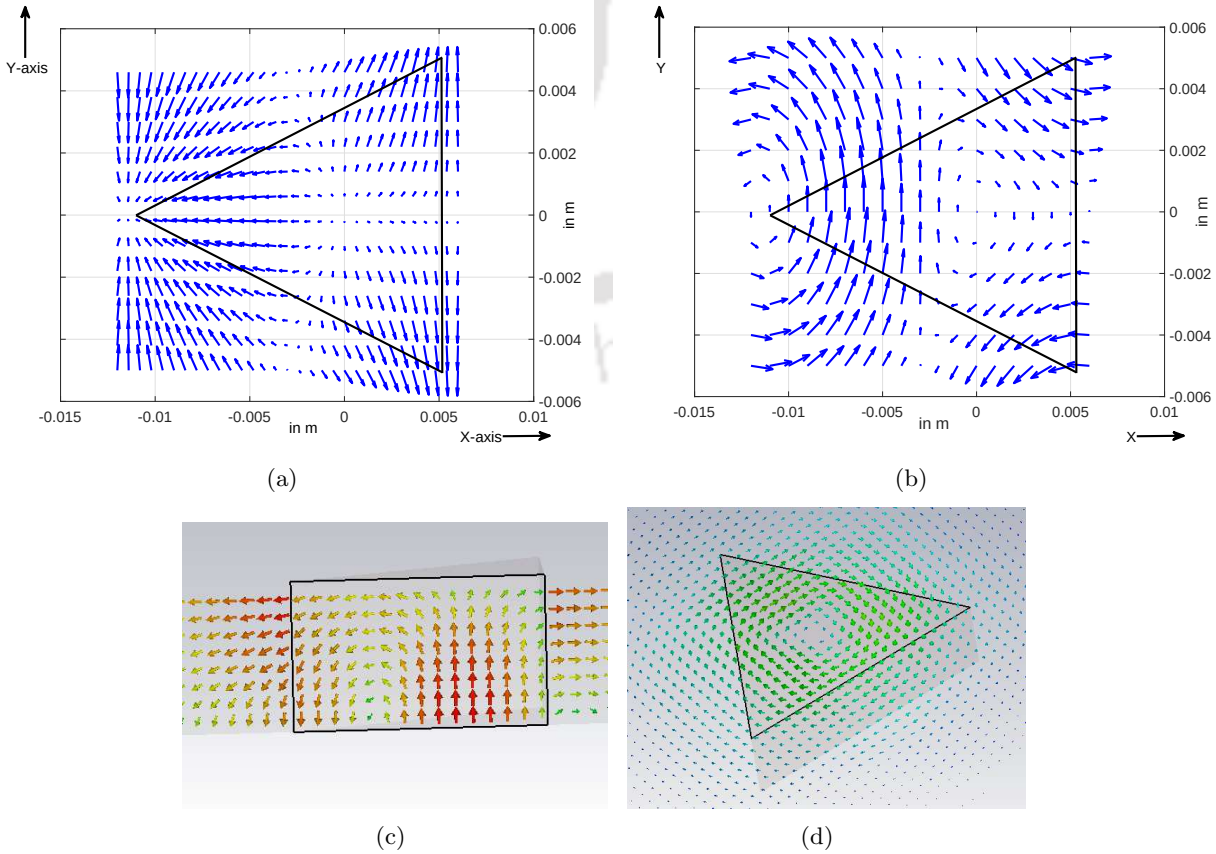

Figure 2.3: Field distribution of $TM_{11\delta}$ mode (a) E-field (analytical) in XY plane,(b) H-field (analytical) in XY plane, (c) E-field (CST) isometric view,(d) H-field (CST) isometric view.

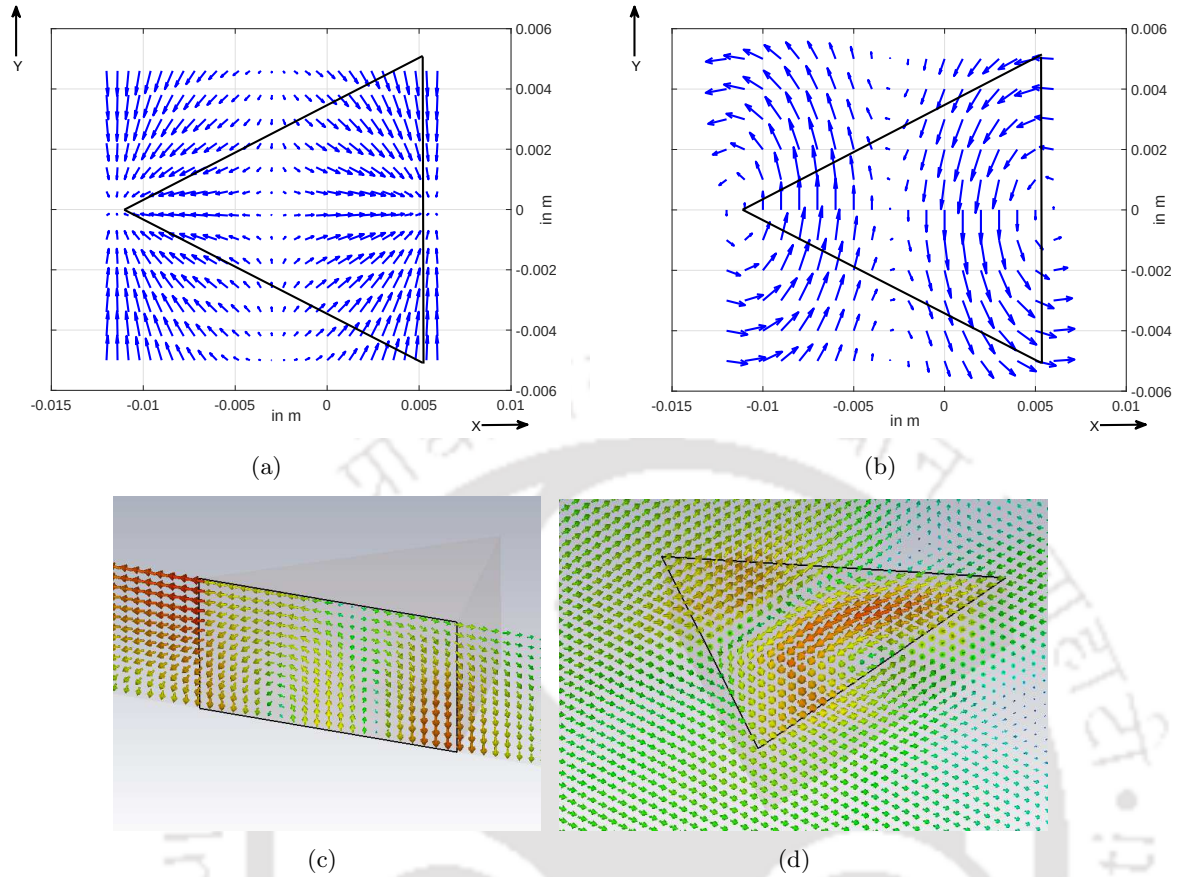

Figure 2.4: Field distribution of $TM_{2-2\delta}$ mode (a) E-field (analytical) in XY plane,(b) H-field (analytical) in XY plane, (c) E-field (CST) isometric view,(d) H-field (CST) isometric view.

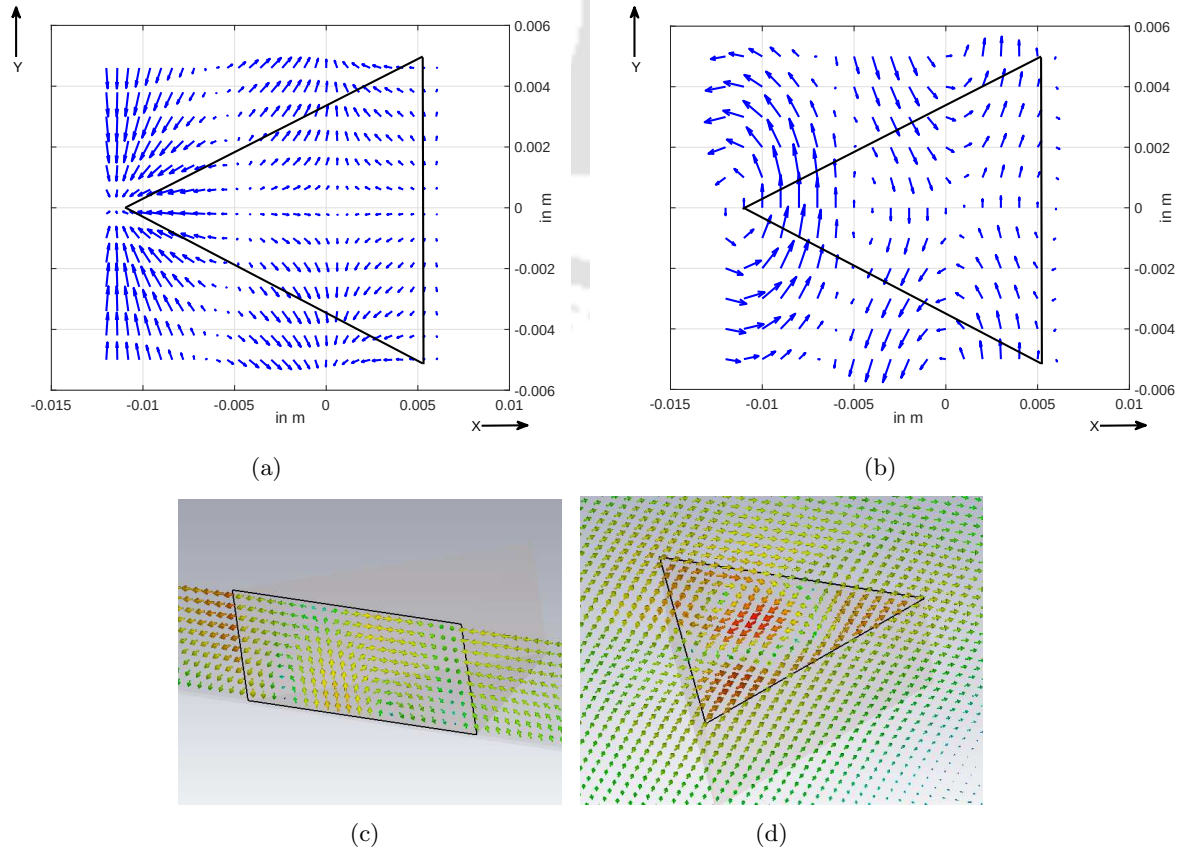

Figure 2.5: Field distribution of $TM_{12\delta}$ mode (a) E-field (analytical) in XY plane,(b) H-field (analytical) in XY plane, (c) E-field (CST) isometric view,(d) H-field (CST) isometric view.

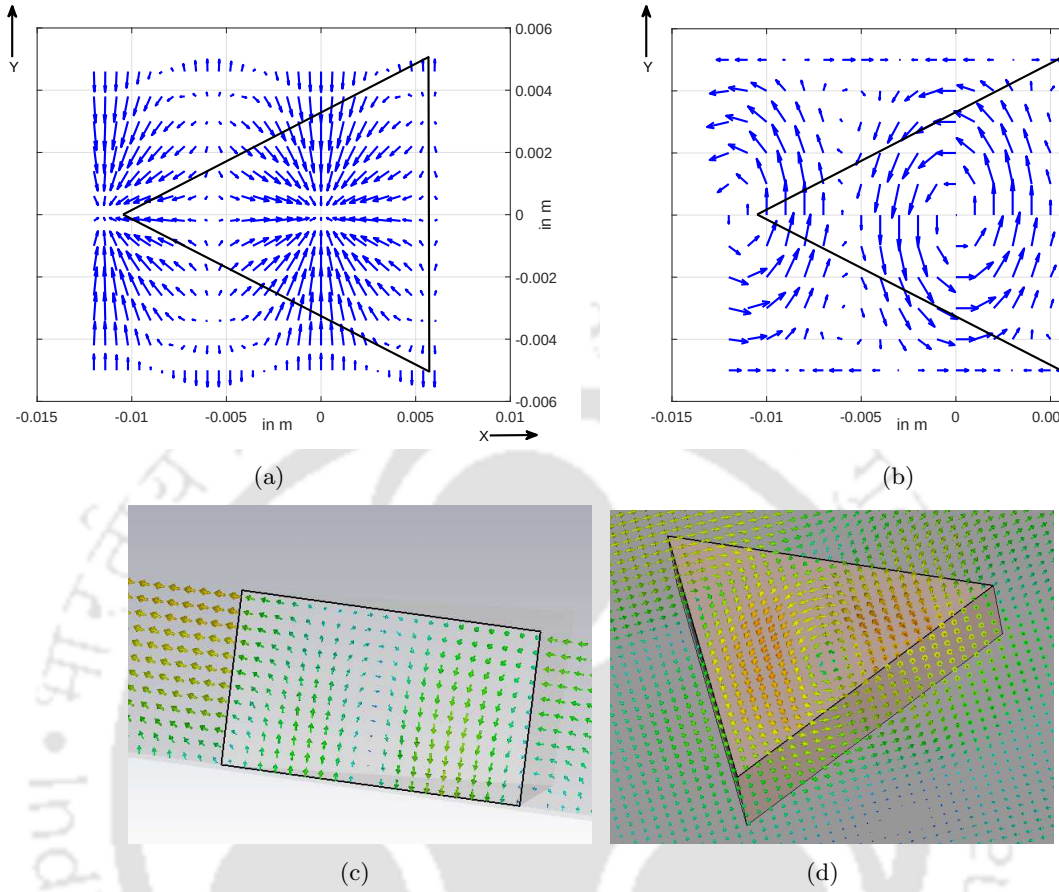

Figure 2.6: Field distribution of TM$_{3-3\delta}$ mode (a) E-field (analytical) in XY plane,(b) H-field (analytical) in XY plane, (c) E-field (CST) isometric view,(d) H-field (CST) isometric view.

extent while we excite higher order modes inside this DRA. Such deviations in the resonant frequency of TM$_{m,n,p}$ mode was first reported by Yoshihiko in [53]. However, a detailed investigation is reported later in [62]. The investigation focused on the resonant frequency of various modes excited inside the ETDRA, which are practically observed different from their corresponding theoretical values. The investigation pointed out that the field distributions of these excited modes inside such DRA remains confined to the regions except at the corners of the antenna geometry. Such phenomenon reduces the effective dimensions of ETDRAs and causes a significant difference in the measured resonant frequency from their corresponding theoretical value. Through proper curve fitting technique an approximate expression for calculating the effective dimensions of the ETDRA are also developed and provided in [62], given by equations 2.9 2.10, where 'a_e' is the effective value of side a and 'h_e' is the effective

Table 2.1: Eigen mode frequency obtained using CST simulations for various TM modes of ETDRA having (a) ϵ_r=10.2, side a= 20mm, for various aspect ratios (a/h) and (b) side a= 20mm, height h=8mm, for various ϵ_r values.

(a)

Modes	Resonant Frequency (GHz)		
	a/h=1.5	*a/h=2*	*a/h=2.5*
$TM_{10\delta}$	4.24	4.64	5.02
$TM_{11\delta}$	5.27	6.19	6.78
$TM_{2-2\delta}$	5.54	7.30	7.78
$TM_{12\delta}$	5.59	7.304	8.89
$TM_{3-3\delta}$	5.61	7.35	9.06

(b)

Modes	Resonant Frequency (GHz)		
	ϵ_r=10.2	ϵ_r=9.4	ϵ_r=6.15
$TM_{10\delta}$	5.02	5.20	6.23
$TM_{11\delta}$	6.78	6.99	8.04
$TM_{2-2\delta}$	7.78	8.04	9.01
$TM_{12\delta}$	8.89	8.91	9.04
$TM_{3-3\delta}$	9.06	9.08	9.10

value of height h of the ETDRA, given by;

$$a_e = a \times (1.003 \times e^{-0.0001747t} - 0.4172 \times e^{-0.4967t}) - 0.01 \times \left(\frac{h}{a}\right) \times \varepsilon_r^{-1.75}; t = |m| + |n| \tag{2.9}$$

$$h_e = h \times (1 - \varepsilon_r^{-1}) \tag{2.10}$$

The modified resonant frequency of ETDRA can be then expressed as detailed in [62], given by;

$$f_{\text{modified}} = \frac{c}{2\pi\sqrt{\varepsilon_r}} \sqrt{\left(\frac{4\pi}{3a_e}\right)^2 (m^2 + n^2 + mn) + \left(\frac{p\pi}{2h_e}\right)^2} \tag{2.11}$$

The closed form expressions given by equations 2.9 2.10 can be used to calculate the effective values, so that the resonant frequency of $TM_{m,n,p}$ mode using equation 2.11 will utmost have 4% error from their corresponding practically observed value.

In the investigation presented in this thesis on ETDRA, we use the modified expressions given by equations 2.9 2.10 2.11 for the calculation of resonant frequency of various modes excited inside this DRA. The development of this expression is one of the recent investigation found in the literature on ETDRAs after a long dormant period. Further, it is also found that, the ETDRA remain unexplored in many aspects, that include theoretical as well as in the practical utilization. We now present the investigation on two such important characteristics of ETDRA (i) Q-factor and (ii) impedance bandwidth performance, which have not been reported previously in the literature.

2.2 Quality factor of $TM_{10\delta}$ mode in ETDRA

As reported in [236], near the resonant frequency of a mode excited within an antenna, the behaviour of its input impedance can be modeled through a series or parallel resonant circuit. It is well

known that, the fractional bandwidth of an antenna is inversely proportional to its Q-factor and hence, proper calculation of Q-factor of the antenna operated with a particular mode provides a precise information about the achievable bandwidth. In this investigation we focus only on the dominant $TM_{10\delta}$ mode excited inside an ETDRA. We will start our discussion with some of the theoretical aspects required for the calculation of Q-factor and impedance bandwidth. Then, we will focus on the nature of the Q-factor curves for such modes as a function of material dielectric constant(ϵ_r) and aspect ratio of the dimensions (a/h). The curves are plotted by calculating the Q-factor of individual ETDRA (of specific dimension and ϵ_r value) using the results obtained from the simulations performed using Ansys High Frequency Structure Simulator (HFSS™) Version 15 [237]. The motive of using results from the commercial software is to get a more precise value of the Q-factor, as the analytically calculated values are observed very high compared to their corresponding practical values, as reported in [62].

2.2.1 Theoretical Background

The Q-factor or the total quality factor, Q of a resonating antenna depends on the loss of its energy. The loss of energy can be either in the form of desired radiation or else in the form of unwanted dissipation in the antenna structure. We express Q-factor mathematically as given in [39] as;

$$Q = \omega \frac{average\ energy\ stored}{energy\ loss/second} \tag{2.12}$$

The total Q-factor can be separated into radiation Q-factor, $Q_{radiated}$ and a dissipation/loss Q-factor, Q_{loss} that accounts from the losses happening within the antenna . They mainly include (i) conduction losses and (ii) dielectric losses. Conduction losses happen due to finite conductivity of the conducting material used in the antenna. The losses due to dielectric materials are described in terms of their loss tangent value. Higher loss tangent value indicates more lossy dielectric material. Therefore we express;

$$\frac{1}{Q} = \frac{1}{Q_{radiated}} + \frac{1}{Q_{loss}} \tag{2.13}$$

For a perfectly matched dielectric resonator antenna with a lossy dielectric material, excited with a source having characteristic impedance Z_0, the Q-factor can be expressed in terms of fractional impedance bandwidth *(BW)* as given in [236], [40],

$$BW = \frac{\triangle f}{f_r} = \frac{s-1}{Q\sqrt{s}} \tag{2.14}$$

where, f_r is the resonant frequency, s is the maximum acceptable voltage standing wave ratio (VSWR) and $\triangle f$ is the relative bandwidth $(f_2 - f_1)$ with f_1 and f_2 being the lower and upper edge frequencies respectively for which VSWR= s. Hence, the quality factor serves as a useful information about the bandwidth of the antenna operated with a particular mode at a specific resonant frequency. Around this resonant frequency, the nature of input impedance of the mode excited inside an antenna can be modeled as an equivalent series or parallel resonant circuit. Ideally at the resonant frequency, the input impedance of the antenna is purely resistive (R_0) which is matched to the characteristic impedance (Z_0) of the source. Under this perfectly matched condition the fractional impedance bandwidth can be expressed in terms of Q-factor using equation 2.14 for both series as well as parallel resonance. However, in practice, a perfect impedance matching may not occur at the resonant frequency and equation 2.14 generalizes to as given in [236], which is expressed as;

$$BW = \frac{\triangle f}{f_r} = \frac{1}{Q}\sqrt{\frac{(Ts-1)(s-T)}{s}} \tag{2.15}$$

where,

$$T = \begin{cases} R_0/Z_0, & \text{for parallel resonance} \\ \\ Z_0/R_0, & \text{for series resonance} \end{cases} \tag{2.16}$$

A properly excited $TM_{10\delta}$ mode of an ETDRA whose resonant frequency is quite away from the higher order modes excited inside such antennas, can be thus assumed as an equivalent electrical model whose input impedance behaves either as a series or as a parallel resonance circuit. The bandwidth *(BW)* of this antenna operated with such mode can be estimated from its quality factor Q.

2.2.2 Q-factor curves for $TM_{10\delta}$ mode in ETDRA

We now, will look into the nature of Q-factor curve of the $TM_{10\delta}$ mode excited inside an ETDRA. The Q-factor curves for ETDRA operated with $TM_{10\delta}$ mode are plotted by calculating the Q values for this DRA with different permittivity values and aspect ratio (a/h) of the dimensions. The Q-factor values can be calculated using equation 2.14. The maximum acceptable VSWR is assumed to be equal to 2 corresponding near to ∼10 dB return loss. The relative bandwidth and resonant frequency are obtained from simulations performed through HFSS. Every simulation to obtain antenna parameters corresponding to different aspect ratio and dielectric constant of an ETDRA is performed

after calculating the theoretical resonant frequency. The theoretical resonant frequency is calculated using the expression given by equation 2.11. The resonant frequency obtained through simulation is compared and verified with the theoretical resonant frequency before the calculation of Q. It is observed that the most typical range of dielectric constant values used in the design of ETDRA falls in two regions. Either the permittivity values are chosen with dielectric constant (ϵ_r) within $6.15 \leq \epsilon_r \leq 15$ or else with very high ϵ_r values around 82. The dielectric constants of very high values are used for low profile design ($h \ll a$) of the ETDRA, in which the extremely high operating resonant frequency of a small compact DRA is brought within the widely used frequency bands by using a very high dielectric constant material. The efficiency of such DRA can be maintained high by lowering the Q-factor even with very high ϵ_r value by choosing very very high aspect ratio (a/h).

We confine ourselves to the calculation of Q-factor for ETDRA with $6.15 \leq \epsilon_r \leq 15$, the most common range of permittivity values used in the design of ETDRA; with aspect ratios between $1 \leq a/h \leq 4$. Moreover, after performing several simulations with very high ϵ_r values of ETDRA having these aspect ratios, it is observed that the Q-factor values are very high and there is a considerable lowering of antenna efficiency. Hence, very high permittivity ETDRAs are not considered in the calculation of Q-factor. Figure 2.7 shows the nature of Q-factor curves for $TM_{10\delta}$ mode of operation of ETDRA with different values of ϵ_r and aspect ratios. It is to be noted that, for ϵ_r=6.15 the modes are not properly excited at some of the aspect ratios. Hence the calculation of Q-factor could not be performed precisely using equation 2.14. We therefore eliminated the Q values obtained for the ETDRA with ϵ_r=6.15. A closed form expression for the Q-factor (Q) is obtained by curve fitting approximation technique. The expression has two terms: (i) first term (Q_{10}) which gives quality factor value for different aspect ratio of ETDRA with ϵ_r=10 and (ii) second term ($\triangle Q$) which is a correction factor to calculate the Q with other dielectric constant values. So we express;

$$Q = Q_{10} + \triangle Q \tag{2.17}$$

where,

$$Q_{10} = \left[-71.48 + 104.7\left(\frac{a}{h}\right) - 12.44\left(\frac{a}{h}\right)^2\right] \times \left[5.62 + 2.02\left(\frac{a}{h}\right) + \left(\frac{a}{h}\right)^2\right]^{-1} \tag{2.18}$$

and

$$\triangle Q = 0.3922 \times \left[\frac{Q_{10} \times (\epsilon_r - 10)}{\sqrt{0.1\epsilon_r + \frac{a}{h}}}\right] \tag{2.19}$$

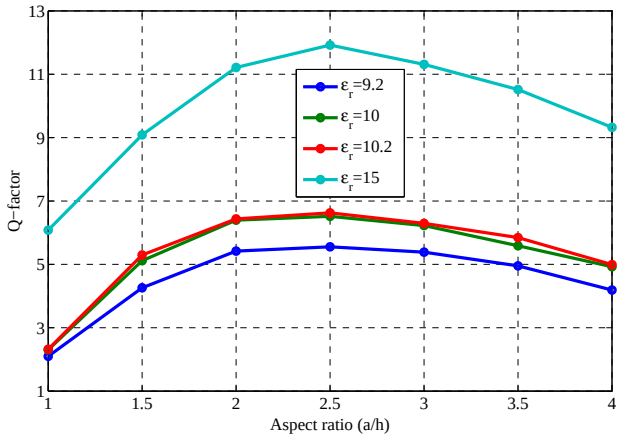

Figure 2.7: Q-factor curves for $TM_{10\delta}$ mode in ETDRA for varying aspect ratio and ϵ_r values.

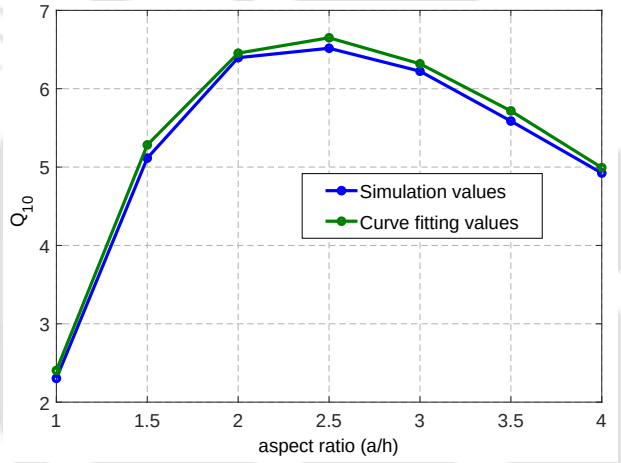

Figure 2.8: Approximate Q curve using eqaution 2.18 for varying aspect ratio with ϵ_r=10

Figure 2.8 shows the approximate curve for the quality factor with ϵ_r=10, which is expressed by equation 2.18. The value of $\triangle Q$ is the correction factor which vanishes for the cases when ϵ_r=10.

2.2.3 Q-factor comparison with the reported ETDRA in the literature

The expressions of equations 2.17 2.18 2.19 are validated by verifying with the practical Q values reported in the literature. The quality factor values of the $TM_{10\delta}$ mode in the ETDRA reported in the literature are very limited. However, two such values are available in [58] and [62]. An ETDRA of side a=66 mm and h =24 mm with ϵ_r=12 has experimental Q value of 11.21. The Q value for same ETDRA calculated using the closed form expression of equation 2.17 is 9.1081 and through simulation with HFSS, is obtained 9.02445. Another ETDRA of side a=36 mm and h =21 having ϵ_r=10 has experimental Q value of 7.85. The corresponding Q values from simulation and equation 2.17 are 6.142 and 5.9432 respectively. The comparison of the quality factor values are shown in Table 2.2.

The Q value obtained using HFSS simulation and equation 2.17 are very close for both the ETDRAs but, practical value in both the cases are slightly higher than the former values. Such small variation is because the bandwidth $\triangle f$ obtained from simulation and practical observation are not always equal but, only comparable. Moreover, it is also noted that for less than 1% change in the $\triangle f$, there is a change of more than 10% in the value of Q. Analytical methods of obtaining the Q value of the same DRA in [58] observed a percentage change in the quality factor with experimental value by more than 140%. However, the closed form expression of equation 2.17 for calculating the Q could obtain values close to the experimental observations. This formula, obtained through curve fitting approximation technique can be used to estimate the Q values more accurately than analytical values of ETDRA within the aspect ratio range $1 \leq a/h \leq 4$ and with dielectric constant values $9.2 \leq \epsilon_r \leq 15$. For better approximation, the curve fitting technique is restricted within this specified range of aspect ratio and dielectric constant values. Hence, the formula obtained for the calculation of Q-factor is limited to the ETDRAs having $1 \leq a/h \leq 4$ and $9.2 \leq \epsilon_r \leq 15$. Such limitations are avoided in analytical method in which Q-factor can be calculated for all possible values of aspect ratios and dielectric constant values of the ETDRA, but analytical Q values are reported to deviate significantly from the experimental values. The curve fitting technique based Q-factor calculation of the dominant mode can be adopted similarly for obtaining the corresponding expression for the higher order modes excited inside such DRAs. Similar curve fitting based expression can be developed for other ranges of aspect ratio and dielectric constant. However, we have restricted our investigation to those ranges of aspect ratio and dielectric constant which are commonly used for the design of practical ETDRAs.

2.3 Bandwidth Performance of $TM_{10\delta}$ mode in ETDRA

Now we look into the impedance bandwidth performance of this DRA excited with $TM_{10\delta}$ mode. Designing an antenna to operate with a specified bandwidth for a given resonant frequency is always a challenging task. However, in the case of ETDRA, excited with $TM_{10\delta}$ mode, we have developed a method to estimate the impedance bandwidth around the resonant frequency. The method makes use

Table 2.2: Comparison of quality factor values for practical ETDRA

Dimensions	**Q (Analytical)**	**Q (Practical)**	**Q (Simulation)**	**Q (from equation 2.17)**
a=66mm, h=24mm, ϵ_r=12 [62] [58]	27.624 [62]	11.21 [62]	9.02445	**9.1081**
a=36mm, h=21mm, ϵ_r=10 [62]	22.177 [62]	7.85 [62]	6.142	**5.9432**

of Q-factor of the ETDRA in estimating the impedance bandwidth.

We recall equation 2.15 discussed before, which expresses the fractional impedance bandwidth around the resonant frequency of an excited mode, in terms of Q-factor, VSWR and the degree of impedance matching (T). If we assume that, best impedance matching occurs around the resonant frequency of the DRA and neglect very small impedance mismatches, then we can choose T=1 and equation 2.15 reduces to equation 2.14. This assumption becomes valid only when a DRA is excited by suitable fine tuning of the feed, which could be a coaxial probe or a microstrip line, to attain maximum coupling with the antenna. For a VSWR=2, equation 2.14 further reduces to,

$$BW = \frac{\triangle f}{f_r} = \frac{1}{Q\sqrt{2}} \tag{2.20}$$

Therefore, the absolute bandwidth can be expressed as,

$$\triangle f = \frac{f_r}{Q\sqrt{2}} \tag{2.21}$$

Hence, for an ETDRA of specified dimension and permittivity value, having resonant frequency (f_r) and Q-factor (Q) can be used to calculate the impedance bandwidth using equation 2.21. The Q-factor of an ETDRA excited with fundamental $TM_{10\delta}$ mode can be calculated using equations 2.17 2.18 2.19. To verify the expression of equation 2.21, we compared with the practical bandwidths obtained by some of the reported ETDRA in the literature, excited with fundamental $TM_{10\delta}$ mode, which is shown in Table 2.3. It is to be noted that the bandwidth calculated using equation 2.21 can have some variation from the bandwidth observed through measurements due to following reason:

(1) The theoretical resonant frequency of $TM_{10\delta}$ mode can be slightly different from practical value. This is because while we use the modified expression for resonant frequency in [62], can have a maximum error of 4%.

(2) Some changes in the impedance bandwidth occur due to loading effect from the measuring instrument. This can effect the coupling between the source and the antenna.

The impedance bandwidth obtained using equation 2.21 may however be modified by applying a cor-

Table 2.3: Comparison of impedance bandwidth (in GHz) values for practical ETDRA

Dimensions	**Bandwidth (Simulation)**	**Bandwidth (Measured)**	**Bandwidth using equation 2.21**	**Bandwidth using equation 2.26**
a=66mm, h=24mm, ϵ_r=12 [58]	0.108 [58]	0.13 [58]	**0.1186**	**0.1562**
a=40mm, h=18mm, ϵ_r=9.8 [65]	0.282 [65]	0.45 [65]	**0.2903**	**0.4066**

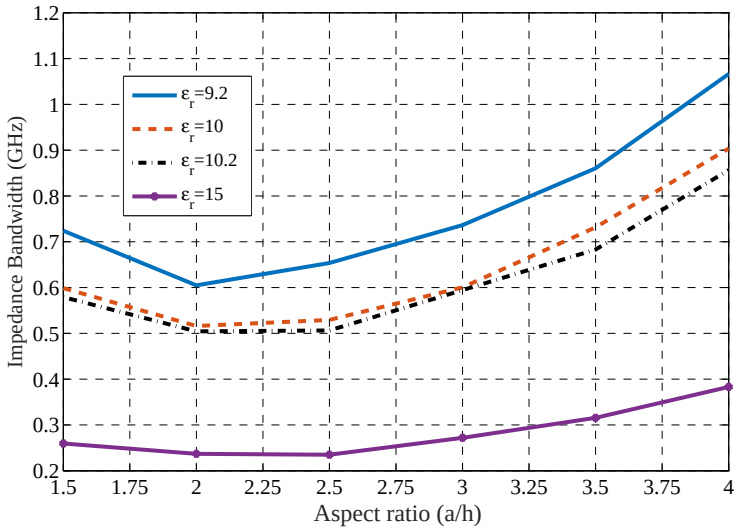

Figure 2.9: Variation of impedance bandwidth of an ETDRA for varying aspect ratio with a= 20 mm for various ϵ_r values at T=1

rection factor and can be made much closer to the measured value as can be seen from Table 2.3 (column 5). The details of the correction factor are presented later in this section.

The ETDRAs in [58] and [65] have aspect ratios of 2.75 and 2.22 respectively. We have very limited ETDRAs reported in the literature. Moreover, it is difficult to verify the practical bandwidths of several such DRAs belonging to wide ranges of aspect ratios. However, to know the nature of impedance bandwidth variation for varying aspect ratio, we present the case of an ETDRA having side a= 20 mm and the height h varied appropriately to change the aspect ratio from 1.5 to 4. The DRA is excited using a coaxial probe by properly fine tuning the probe height to achieve maximum impedance matching at the resonant frequency. The variation of the bandwidth is then plotted for different values of this ETDRA as shown in Figure 2.9. We observe that the impedance bandwidth reduces with increasing aspect ratio, reaches minimum and then gradually increases with further increase of the aspect ratio. This complies with the behaviour of Q-factor curves of Figure 2.7. Since bandwidth is inversely proportional to the Q-factor, wherever the value of Q-factor is more, for that aspect ratio the bandwidth is observed to be less, and vice versa. The Figure 2.9 is a demonstration for understanding the nature of impedance bandwidth variation with the variation in aspect ratio.

As stated before, the improper coupling between the source and the DRA could be a significant reason behind the difference observed in the practical impedance bandwidth and the corresponding value calculated using equation 2.21. Hence, we carried out investigation to know the effect on the impedance bandwidth with changes in source coupling. The source coupling is varied by exciting the

Table 2.4: Variation of impedance bandwidth with varying T for an ETDRA having a= 20 mm and h=8 mm and ϵ_r=10

T	Impedance bandwidth (GHz)	Resonant frequency (GHz)
1.0000	0.5294	5.1721
1.2623	0.6567	5.2258
1.3973	0.7173	5.2409
1.5352	0.7351	5.2525
1.7159	0.701	5.2581
1.8590	0.6656	5.2543

Table 2.5: Variation of impedance bandwidth with varying T for an ETDRA having a= 20 mm and h=6.66 mm and ϵ_r=10

T	Impedance bandwidth (GHz)	Resonant frequency (GHz)
1.0000	0.6006	5.6310
1.1878	0.7083	5.6585
1.3580	0.7495	5.6518
1.4935	0.7623	5.6371
1.6203	0.7435	5.6228
1.7561	0.7336	5.5995
1.9143	0.7263	5.5677

ETDRA using a coaxial probe and changing the probe height. Upon varying the probe height, we observed that the impedance matching gets gradually reduced around the resonant frequency. However, the impedance bandwidth is observed to be slightly increasing when compared to the bandwidth at best impedance matching. This increase in the impedance bandwidth attains a maximum value and then reduces with further variation of the height of excitation probe. This can be clear from Figure 2.10, which shows the variation of return loss and bandwidth for varying probe height for an ETDRA of a= 20 mm, h=8 mm and ϵ_r=10. While the impedance matching is reduced, now the value of T will not be unity ($T \neq 1$). It is to be noted that, the value of T can only vary between $0.5 < T < 2$. This can be clear when we substitute VSWR= 2 in equation 2.15 so that,

$$\triangle f = \frac{f_r}{Q}\sqrt{\frac{(2T-1)(2-T)}{2}} \tag{2.22}$$

To have positive $\triangle f$ we must have;

$$\sqrt{\frac{(2T-1)(2-T)}{2}} > 0 \tag{2.23}$$

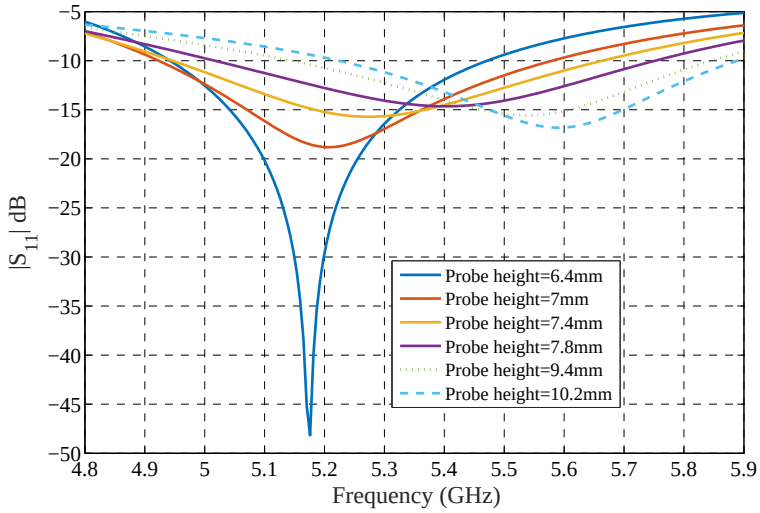

Figure 2.10: Variation of return loss for a=20 mm, h=8 mm and ϵ_r=10

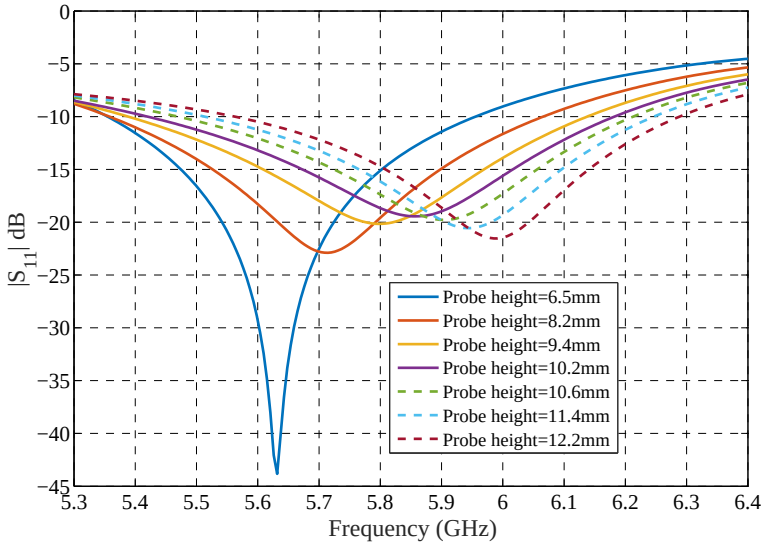

Figure 2.11: Variation of return loss for a=20 mm, h=6.66 mm and ϵ_r=10

and hence we obtain $0.5 < T < 2$. In order to explain this bound we consider two ETDRAs, each of ϵ_r =10 but having different aspect ratio (a/h), one with a/h=2.5 and other with a/h=3. We choose both the DRAs with a=20 mm and, height h=8 mm and h=6.66 mm corresponding to a/h=2.5 and a/h=3, respectively. The $TM_{10\delta}$ mode is excited in these DRAs through a coaxial cable. We vary the source coupling by changing the probe height of the coaxial excitation. When the probe height is varied, the impedance matching is effected and hence, the value of T will deviate away from unity. The Table 2.4 and Table 2.5 shows the variation of T and corresponding change in the bandwidth for both the ETDRAs, obtained through HFSS simulation. The variation of return loss for different T values for these DRAs with a/h=2.5 and a/h=3 are shown in Figure 2.10 and Figure 2.11,

respectively. From Table 2.4 and Table 2.5, we see that the impedance bandwidth increases gradually attains the peak value and then gradually reduces, with varying T. However, the percentage change in the impedance bandwidth depends on the dimension and dielectric value of the DRA. The ETDRA with a/h=2.5 achieves a maximum change in the bandwidth of nearly 38.85% and corresponding to the DRA of a/h=3 the change in bandwidth is only 26.92%. It is to be noted that, the resonant frequency (zero imaginary part of the impedance) of the excited $TM_{10\delta}$ mode in both the DRAs does not vary much, although the impedance matching is effected. However, the best impedance matching frequency gets shifted. Such behavior can be understood from the $|S_{11}|$ plot of these DRAs shown in Figure 2.10 and Figure 2.11. In Figure 2.10, the best impedance matching condition around the resonant frequency occurs at a probe height of 6.4 mm. However, when the probe height is kept at 7.4 mm, the matching is reduced significantly and the best matching frequency is also shifted. If we look at the variation of T (which is shown in Table 2.4 and represented in Figure 2.10), when it attains a value 1.859, the impedance matching gets degraded around the resonant frequency. This justifies the bound chosen for T which is deduced from equation 2.23 as $0.5 < T < 2$. A similar case applies with the behavior of impedance matching of the ETDRA in Figure 2.11. Deviation of the frequency of best matching from the resonant frequency (zero imaginary part of the impedance) with varying T values effect the performance of the antenna. Therefore, in the practical measurement of return loss, if a perfect impedance matching is not achieved ($T \neq 1$) around the resonant frequency of the operated mode, we observe a deviation in the best impedance matching frequency from their corresponding simulated value. Moreover, we also observed through simulations that, when such deviation in the best impedance matching frequency occurs, the impedance bandwidth is effected and is also different from the impedance bandwidth obtained with the case of T=1. At a particular value of T ($T \neq 1$), the impedance bandwidth is higher than the impedance bandwidth obtained with the case of T=1. Therefore, in the absolute bandwidth ($\triangle f$) calculation using equation 2.21 for the ETDRA excited with $TM_{10\delta}$ mode, we include a correction factor denoted by $\triangle f^{'}$. Now, the maximum achievable bandwidth for the excited $TM_{10\delta}$ mode around the resonant frequency denoted by B would be $\triangle f \leq B \leq \triangle f_{max}$, where

$$\triangle f_{max} = \triangle f + \triangle f^{'} \tag{2.24}$$

Table 2.6: Impedance bandwidth variation for ETDRA with a=20 mm and height chosen according to aspect ratio (a/h), for ϵ_r=10 and ϵ_r=15 cases

a/h	ϵ_r=10			ϵ_r=15		
	T	Impedance bandwidth at T=1	Impedance bandwidth for $T \neq 1$	T	Impedance bandwidth at T=1	Impedance bandwidth at $T \neq 1$
1.5	1.6650	0.5988	1.0690	1.8462	0.2596	0.2851
2.0	1.6920	0.5160	0.7729	1.7470	0.2371	0.2622
2.5	1.5352	0.5294	0.7351	1.6390	0.2350	0.2690
3.0	1.4935	0.6006	0.7623	1.4251	0.2720	0.3191
3.5	1.4853	0.7316	0.9500	1.5378	0.3157	0.4257
4.0	1.6800	0.9037	1.3019	1.5537	0.3831	0.6646

For the ETDRA of Table 2.4 and Table 2.5, $\triangle f_{max}$ will be 0.7351 GHz and 0.7623 GHz, respectively. However, for a general case, we obtained an expression for $\triangle f^{'}$ to calculate $\triangle f_{max}$. The expression for $\triangle f^{'}$ is obtained by carrying out further supporting HFSS simulation to obtain the variation of impedance bandwidth for varying T, for different aspect ratios and dielectric values of the ETDRA. As a representation of all those simulated data, the variation of maximum achievable bandwidth and their corresponding T value at different a/h ratios for ϵ_r=10 and ϵ_r=15 are shown in Table 2.6. The dimensions of these ETDRAs are chosen as a=20 mm and h is varied corresponding to different aspect ratio chosen. The variation of maximum impedance bandwidth achieved for these DRAs with respect to the increasing aspect ratio are shown in Figure 2.12. The variation of this curve for an ETDRA with same dimensions but having ϵ_r=10.2 and ϵ_r=9.2 are also included in Figure 2.12. These curves shown in Figure 2.12 corresponds to the variation of maximum impedance bandwidth obtained for the impedance bandwidth curves (for T=1) of Figure 2.9.

Although, in the calculation of Q-factor, aspect ratios are chosen between $1 \leq a/h \leq 4$, now in the case of bandwidth calculation we restrict the aspect ratios between $1.5 \leq a/h \leq 4$. This is because, for a large volume ETDRA with small aspect ratio, the dominant and higher order modes resonate at relatively nearby frequencies. While varying the impedance matching (for $T \neq 1$) by changing the probe height, the nearby mode gets excited and hence, the impedance bandwidth of $TM_{10\delta}$ mode cannot be precisely calculated around its resonant frequency. Based on this observation, we limited the aspect ratios in the interval $1.5 \leq a/h \leq 4$. We obtained an empirical formula for maximum change in the impedance bandwidth from the impedance bandwidth obtained at T=1, for the general case, through curve fitting technique, as given below;

$$\triangle f^{'} = \frac{1.732 \triangle f}{\sqrt{\epsilon_r}} \left[0.2377 + 1.023 \left(\frac{a}{h}\right) - 0.539 \left(\frac{a}{h}\right)^2 + 0.07973 \left(\frac{a}{h}\right)^3 \right] \tag{2.25}$$

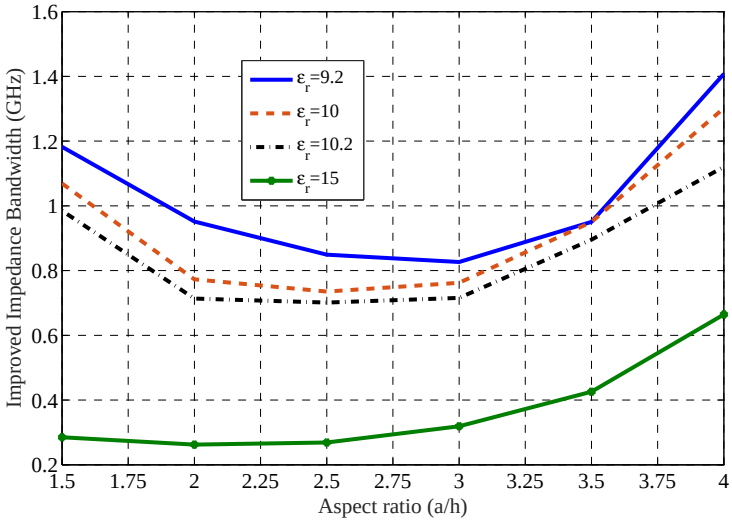

Figure 2.12: Variation of maximum impedance bandwidth of the ETDRA for varying aspect ratio with a= 20 mm for various ϵ_r values for $T \neq 1$

and the maximum possible impedance bandwidth can be expressed using equations 2.21 2.24 2.25 as;

$$\triangle f_{max} = \frac{f_r}{Q\sqrt{2}} + \frac{1.732\triangle f}{\sqrt{\epsilon_r}}\left[0.2377 + 1.023\left(\frac{a}{h}\right) - 0.539\left(\frac{a}{h}\right)^2 + 0.07973\left(\frac{a}{h}\right)^3\right] \quad (2.26)$$

This new expression for maximum achievable bandwidth can be used to calculate the impedance bandwidth of the reported ETDRAs mentioned in Table 2.3. Using equation 2.26, we obtain the impedance bandwidth of ETDRA of [58] and [65] in Table 2.3 as 0.1562 GHz and 0.4066 GHz respectively. For the ETDRA in [65], the practical bandwidth obtained is 0.45 GHz and it remains close with the bandwidth calculated using equation 2.26. Similarly, for the DRA in [58] the impedance bandwidth obtained is 0.13 GHz, which lies between the impedance bandwidth calculated using equation 2.21 and equation 2.26. The introduction of correction factor $\triangle f'$, improved the accuracy of the method for estimating the impedance bandwidth of the ETDRA excited with $TM_{10\delta}$ mode. The calculated impedance bandwidth will stay more close to $\triangle f$ and whenever the degree of impedance matching are effected, then the bandwidth is more likely to reach near $\triangle f_{max}$. The practical value of the bandwidth cannot go below $\triangle f$ significantly, because under such cases the practical Q-factor would increase compared to their theoretical value, which is less probable. The proposed method for calculating the impedance bandwidth of $TM_{10\delta}$ mode excited in an ETDRA will be very useful for the antenna designers to develop such DRAs of specified bandwidth. However, as the investigation is limited to only certain aspect ratios and dielectric values, this method can be only used in the bandwidth calculation corresponding to VSWR$\sim$2 for the ranges of $1.5 \leq a/h \leq 4$ and $9.2 \leq \epsilon_r \leq 15$.

Based on the investigation presented in this chapter on Q-factor and impedance bandwidth performance of an ETDRA operated in the dominant $TM_{10\delta}$ mode, the Antenna Engineers and Researchers might be curious to know the effect of shifting the frequency of best impedance matching (due to various degrees of impedance matching (for $T \neq 1$)) on the antenna parameters. The literature suggest that, it is more meaningful to compare antenna properties of the prototypes operating at same frequency. Therefore, the comparison of antenna properties for the case of different degrees of impedance matching (for $T \neq 1$) has not been included and the discussion in this chapter of the thesis is limited to only the Q-factor and impedance bandwidth performance of an ETDRA operated in the dominant $TM_{10\delta}$ mode.

2.4 Summary

In this chapter, we discusses about the $TM_{m,n,p}$ mode solutions of equilateral triangular dielectric resonator antennas and some of the factors effecting the practical resonant frequency of the excited modes inside such DRAs. The nature of Q-factor for various aspect ratios and material dielectric constant values are presented for the case of fundamental $TM_{10\delta}$ mode excited inside this DRA. A closed form expression for calculating the Q-factor for such modes excited in an ETDRA is developed by applying curve fitting approximation technique over the Q-factor curves. Further, an investigation on the impedance bandwidth performance of ETDRA is discussed and an expression for estimating the same is also presented for the dominant $TM_{10\delta}$ mode. The expression for calculating the Q-factor and the impedance bandwidth are verified for some of the practical ETDRAs reported in the literature. The proposed technique is expected to be very useful for the antenna engineers for estimating the impedance bandwidth of the practical ETDRA, excited with $TM_{10\delta}$ mode for the aspect ratio and dielectric constant values, ranging from $1.5 \leq a/h \leq 4$ and $9.2 \leq \epsilon_r \leq 15$.

3

Investigation on the Design of Dual-Band ETDRAs for WLAN Applications

Contents

In the previous chapter, we discussed the Q-factor and impedance bandwidth performance of an ETDRA operated in the fundamental $TM_{10\delta}$ mode. The expression for calculating the Q-factor and the achievable impedance bandwidth for an ETDRA excited with $TM_{10\delta}$ mode are also discussed. We now present how such ETDRAs can be designed for practical applications. In this chapter[1], we propose two ETDRA configurations which can be operated as a dual-band antenna. The proposed configurations of the dual-band ETDRA are excited by means of a conventional coaxial feed. The two configurations of the proposed dual-band ETDRAs are namely, configuration-I and configuration-II. The configuration-I use a single ETDRA for dual-band operation; whereas, configuration-II includes two ETDRAs to operate as a dual-band antenna. The design is well suited for applications in the WLAN frequency bands of 2.4-2.5 GHz and 5.75-5.85 GHz.

3.1 Introduction

A survey of dual-band DRAs available in the literature are discussed in Section 1.3.2.2 of this thesis. It is found that, the dual-band antennas using ETDRAs are a few [60,64], and a detailed investigation exploring the potential of such DRA geometry for dual-band application is not adequately reported. In this chapter, we initially present a preliminary investigation on the ETDRA to operate as a dual-band antenna. We refer this configuration as Design-I; which utilizes two ETDRAs, namely DRA-1 and DRA-2, each operated in the bands of 2.4-2.5 GHz and 5.75-5.85 GHz, respectively. Both the DRAs are operated in the fundamental $TM_{10\delta}$ mode of the ETDRA, which are excited by means of a coaxial feed. The DRAs use RT/ Duroid®6010 material having a dielectric constant of ϵ_r=10.2. The objective of this design is to obtain a similar radiation characteristic in both the operating bands. The design also aim at understanding the challenges and performance of this antenna configuration. The performance characteristic of this dual-band ETDRA is investigated by carrying out full wave electromagnetic (EM) simulations using Ansys High Frequency Structure Simulator (HFSS™) Version 15 [237]. Through careful understanding of the excited modes, it is observed that, a higher order mode excited in DRA-1 is affecting the desired radiation characteristics at the upper operating frequency. Therefore, this antenna configuration has been re-designed to improve the radiation characteristics

[1]The preliminary work reported in this chapter has been presented in the following conference publication:
P. Anoop and R. Bhattacharjee, "Design of Dual Band Triangular DRA for WLAN Application", *IEEE Applied Electromagnetics Conference (AEMC) 2015*, Guwahati, India, 2015, pp. 1-2.
The detailed investigation of the proposed DRA configurations are presented in the following journal publication:
Anoop P, Bhattacharjee R, " Investigation on Dual-band Equilateral Triangular shaped Dielectric Resonator Antennas for WLAN Applications," in *Int J RF Microw Comput Aided Eng.*, vol. 31, no. 7, e22672, July 2021. https://doi.org/10.1002/mmce.22672

at the desired operating frequencies, by using 99.7% Alumina material of ϵ_r=9.9. Here, a detailed investigation on the dual-band ETDRAs operating in the WLAN frequency bands of 2.4-2.5 GHz and 5.75-5.85 GHz is presented. We also propose two configurations of the dual-band ETDRA; (i) using single ETDRA and (ii) using two ETDRAs.

- In the first configuration, referred as configuration-I, we propose and present the design of a dual-band DRA using a single ETDRA excited by a conventional coaxial feed. The DRA utilizes 99.7% Alumina material of dielectric constant of ϵ_r=9.9. This simple yet effective design of a dual-band ETDRA is not reported in the literature so far. The proposed design excites the dominant $TM_{10\delta}$ mode and a higher order $TM_{3-3\delta}$ mode to achieve operational impedance bandwidths around 2.45 GHz and 5.8 GHz, respectively. The design demonstrates the potential of a simple ETDRA as a dual-band antenna. Further, this design also discusses the radiation characteristics and performance of the higher order $TM_{3-3\delta}$ mode excited inside ETDRAs, which are not discussed in the available literature.

- In the second confgiuration, namely configuration-II, we use two ETDRAs, which are excited by a common coaxial feed. Both the ETDRAs uses 99.7% Alumina material having a dielectric constant of ϵ_r=9.9. Each ETDRA is operated in its dominant $TM_{10\delta}$ mode, one in the lower operational band, around 2.45 GHz and the other in the upper operational band, around 5.8 GHz. The objective of this design is to maintain similar radiation characteristics at both the operating frequencies, using a simple excitation mechanism. As stated before, a preliminary investigation of this design configuration using full wave EM (Electromagnetic) simulation is demonstrated using Design-I, where RT/ Duroid®6010 material was used for the antenna elements. However, in Design-I, there is a significant contribution of higher order mode excited in one of the ETDRAs (namely, DRA-1) in the upper operating band near 5.8 GHz, which resulted in undesired radiation characteristics. In configuration-II, the antenna has been re-designed using 99.7% Alumina material having a dielectric constant of ϵ_r=9.9 and the antenna dimensions are chosen appropriately, so that, similar radiation patterns are maintained in both the operating bands.

This chapter is organized into five sections. The Section 3.2 discusses a preliminary investigation of a dual-band ETDRA configuration namely, Design-I. The return loss and the radiation performance of this antenna design are presented briefly with the supporting EM simulation results obtained using Ansys HFSS. The Section 3.3 discusses a detailed investigation of dual-band ETDRAs for WLAN

applications. Designs of both configuration-I and configuration-II are presented and their radiation performances are also discussed in this section. Further, the performance comparison of the proposed configurations of the dual-band ETDRA with other dual-band DRAs reported in the literature are also discussed in this section. Section 3.4 summarizes some of the challenges in the design of practical dual-band/ multi-band DRAs. Finally, the conclusions are drawn in Section 3.5.

3.2 Dual-band ETDRA: A preliminary investigation

3.2.1 Design of dual-band ETDRA for WLAN application: Design-I

In this section, we present a preliminary investigation of a dual-band ETDRA namely, Design-I. The theoretical background of an ETDRA is presented in the previous chapter. However, we will recall the relevant equation for calculating the resonant frequency of the excited modes of Design-I. For an ETDRA having side a and height h and material dielectric constant of ϵ_r, the resonant frequency of $TM_{m,n,p}$ modes excited inside such a DRA, is given by equation (2.7). In this design configuration, two ETDRAs, namely (i) DRA-1 operated in 2.4-2.5 GHz and (ii) DRA-2 operated in 5.75-5.85 GHz are placed close to the each other, which lie over a common ground plane as shown in Figure 3.1(a). Both the DRAs uses RT/ Duroid®6010 material of ϵ_r=10.2. The dimensions of the DRA-1 are: side a_1=40 mm and height h_1=18 mm. The DRA-2 has side a_2=14.6 mm and height h_2=6 mm. The ground plane dimension are chosen as 300 mm x 300 mm. The dimensions of DRA-1 and DRA-2 are suitably chosen to excite $TM_{10\delta}$ mode in both the DRAs. The objective of this design configuration is to obtain similar radiation characteristics in both the operating bands. The structure is excited using a conventional coaxial probe that protrude through the center of the ground plane touching one of the sides of both the DRAs. The simulations are then carried out to study the performance characteristics using electromagnetic (EM) simulation software, Ansys HFSS.

3.2.2 Results and discussions: Design-I

The characteristics of this coaxially excited dual-band ETDRA are studied through full-wave EM simulations using HFSS. The height of the coaxial probe is varied and appropriately fine tuned to obtain proper impedance matching as well as resonances near 2.45 GHz and 5.75 GHz. Impedance matching around the lower and upper operating frequencies are obtained at a probe height of 14 mm, as shown in the $|S_{11}|$ plot of Figure 3.1(b). The $TM_{10\delta}$ mode is excited in DRA-1 as well as in DRA-2 near 2.45 GHz and 5.75 GHz, respectively, as shown in the field distribution of Figure 3.2 and Figure 3.3.

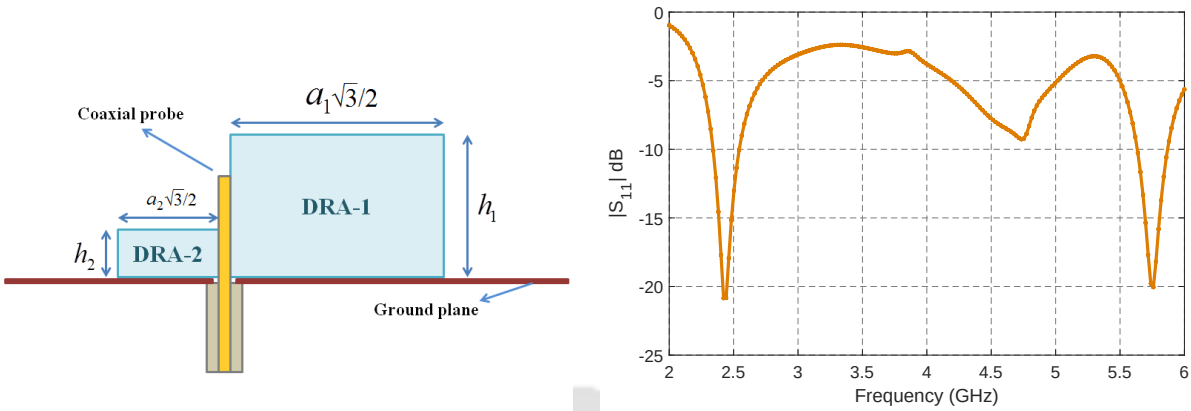

(a) (b)

Figure 3.1: Design-I ETDRA: (a) schematic diagram and (b) S_{11} plot.

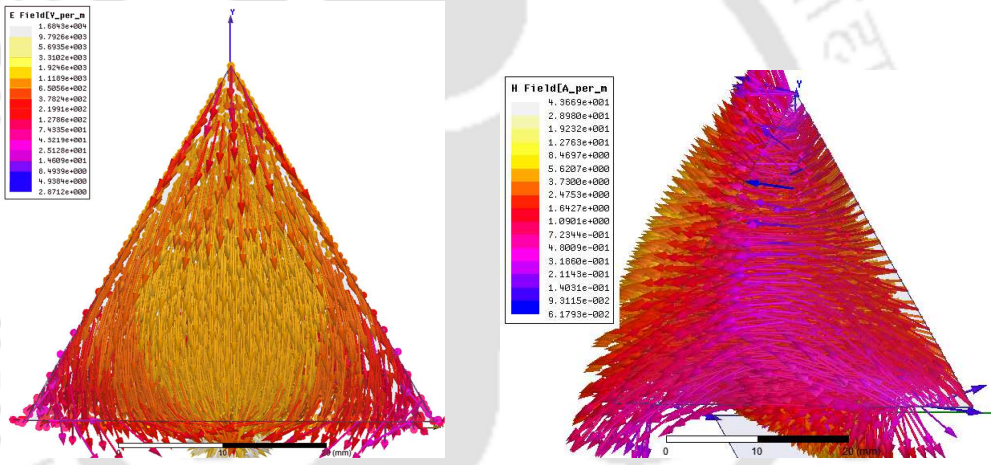

(a) (b)

Figure 3.2: Field distribution of $TM_{10\delta}$ excited in DRA-1 at 2.45 GHz: (a) E-field and (b) H-field.

The radiation pattern in the $\phi = 0^0$ and $\phi = 90^0$ planes, at 2.45 GHz and 5.75 GHz obtained through simulations, are shown in Figure 3.4(a) and Figure 3.4(b), respectively. The simulated gain of the antenna at 2.45 GHz and 5.75 GHz, respectively are 6.45 dBi and 9.05 dBi. The Table 3.1 shows variation of gain in the two operating bands of the Design-I. This configuration of the ETDRA can be used as a dual-band antenna for WLAN applications. Although, this configuration of the dual-band ETDRA aimed at achieving a similar radiation pattern at both the operating frequencies, it is observed that they are not similar. The radiation pattern at the lower operating frequency is broad. However, at the upper operating frequency the antenna exhibit an undesired radiation pattern. In a detailed investigation conducted on this antenna configuration, we observed that, the following issues

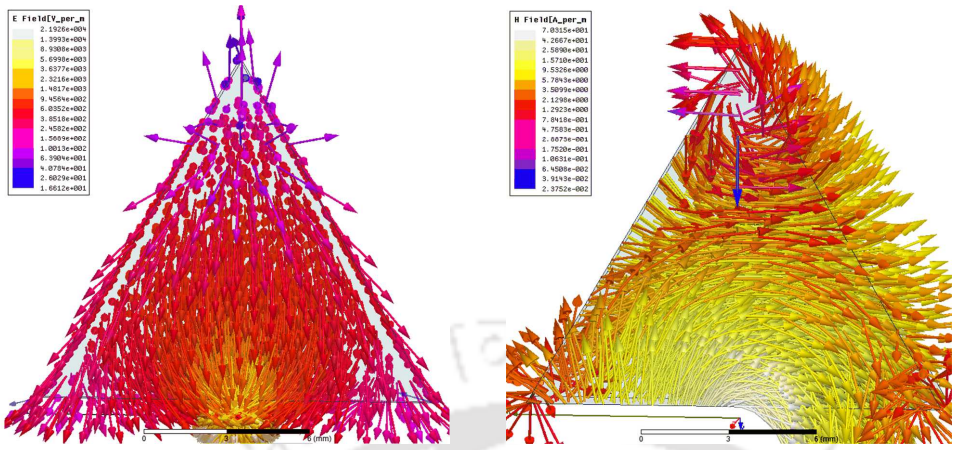

(a) (b)

Figure 3.3: Field distribution of $TM_{10\delta}$ excited in DRA-2 at 5.75 GHz: (a) E-field and (b) H-field.

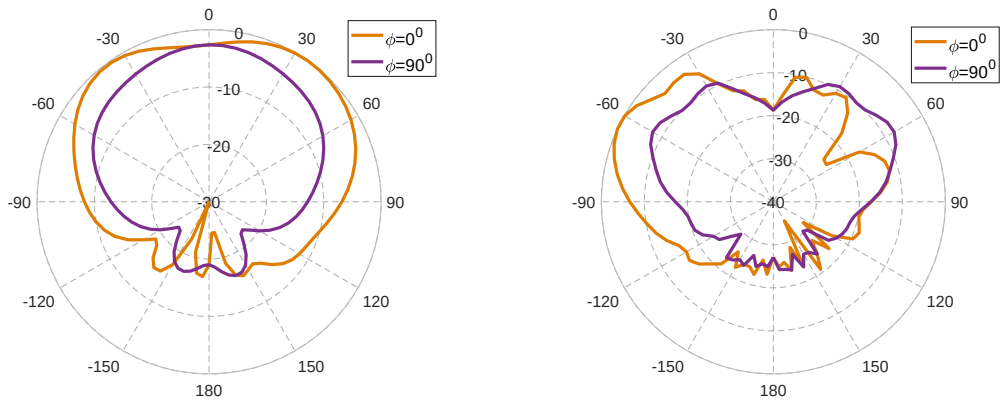

(a) (b)

Figure 3.4: Radiation pattern of Design-I dual-band ETDRA at (a) 2.45 GHz and (b) 5.75 GHz.

are effecting the performance of this DRA configuration;

(i) It is observed that the dimensions of the ETDRA which was calculated using expression (2.7) are inappropriate and these quantities are to be increased slightly to achieve appropriate impedance matching around the operating frequencies. In other words, the theoretically calculated resonant frequency and their corresponding simulated values are significantly different. This effect was reported later in [62], where a modified expression for the calculation of resonant frequency is presented, which is already discussed and given by (2.11) of chapter 2, in this thesis. However, we present these equations below;

$$f_{\text{modified}} = \frac{c}{2\pi\sqrt{\varepsilon_r}}\sqrt{\left(\frac{4\pi}{3a_e}\right)^2 (m^2+n^2+mn) + \left(\frac{p\pi}{2h_e}\right)^2} \tag{3.1}$$

Table 3.1: Variation of gain in the lower and upper operating bands of the dual-band ETDRA (Design-I)

Lower band		Upper band	
Frequency (GHz)	**Peak gain (dBi)**	**Frequency (GHz)**	**Peak gain (dBi)**
2.4	6.5	5.75	9.05
2.425	6.48	5.775	9.20
2.45	6.45	5.8	9.44
2.475	6.55	5.825	9.47
2.5	6.73	5.85	9.53

where,

$$a_e = a \times (1.003 \times e^{-0.0001747t} - 0.4172 \times e^{-0.4967t}) - 0.01 \times \left(\frac{h}{a}\right) \times \varepsilon_r^{-1.75}; t = |m| + |n| \quad (3.2)$$

$$h_e = h \times (1 - \varepsilon_r^{-1}) \quad (3.3)$$

are the effective values of side a and height h, respectively.

(ii) The design has a significant contribution of higher order mode excited in the DRA-1 which is appearing in the 5.75-5.85 GHz band, due to which the radiation characteristics of the antenna is effected in this operating bandwidth. Through full wave EM simulations, it is observed that $TM_{3-3\delta}$ mode of DRA-1 is excited in this operating band.

Considering the above mentioned issues, modifications are introduced in Design-I to improve the antenna performance in the upper operating band. The dimensions of the ETDRAs are chosen appropriately, to operate in the desired operating bands. Further, a detailed investigation on ETDRA is also conducted and their potential to operate as a dual-band antenna is presented in the following section.

3.3 Investigation on dual-band ETDRAs for WLAN applications

In this section, we present the investigation of dual-band ETDRA in a broader perspective. The resonant frequency of the $TM_{m,n,p}$ modes operated in the design are calculated using the modified expression given by (3.1). We present the dual-band ETDRA in two configurations; namely, configuration-I and configuration-II. Both the configurations use a conventional coaxial feed to have a simple excitation mechanism.

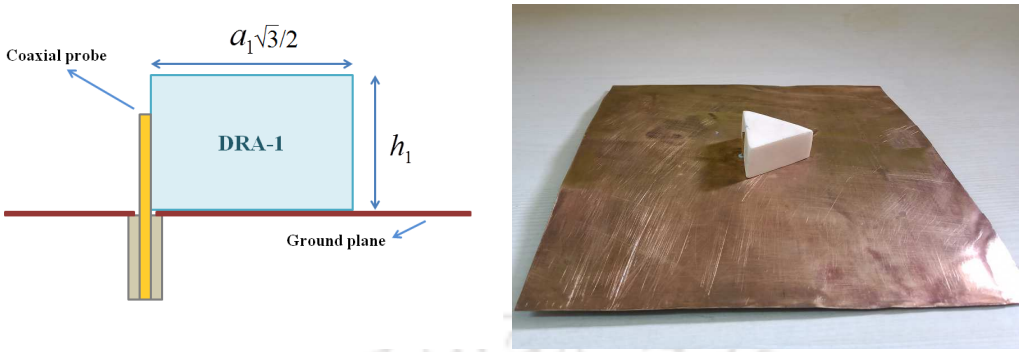

(a) (b)

Figure 3.5: The configuration-I (DRA-1) dual-band ETDRA: (a) schematic and (b) fabricated prototype

3.3.1 Dual-band ETDRA: Configuration-I

Configuration-I has a single ETDRA, referred here as DRA-1, which is excited by a conventional coaxial feed. The antenna arrangement in configuration-I dual-band ETDRA using DRA-1 is shown in Fig. 3.5(a). The coaxial probe is placed touching at the center of one of its sides and the DRA is placed over a groundplane. The dimensions of DRA-1 are: side a_1=40 mm and height h_1=18 mm. The DRA uses 99.7% alumina material of ϵ_r=9.9. Dominant $TM_{10\delta}$ mode is excited inside DRA-1 using coaxial feed by suitably varying the probe height. The impedance matching around the resonant frequency of 2.47 GHz is obtained at a probe height of 14 mm, using full wave EM simulations carried out using Ansys HFSS. However, the theoretically calculated resonant frequency is 2.58 GHz. The field distribution of $TM_{10\delta}$ mode excited inside the DRA-1 is shown in Fig. 3.6. It is observed that, by suitable choice of probe height, a higher order mode of this DRA is also excited near 5.8 GHz. By careful examination of the field distribution in the standing wave as shown in Fig. 3.7, it is found that, $TM_{3-3\delta}$ mode is excited at this frequency. The field distributions of $TM_{10\delta}$ and $TM_{3-3\delta}$ mode using analytical expressions are already shown in Fig. 2.2 and Fig. 2.6, presented in section 2.1 of chapter 2. From [238], it is noted that the Alumina material of more than 99% purity comes in different grades; and the tan δ values of these materials vary, from as low as of the order of 10^{-5} to as high as of the order of 10^{-2}, in the 10^9 Hz range of frequency. It is to be also noted that, in the case of standard Alumina material of 99.7% purity, which comes with a very low value of tan δ ($\sim 10^{-3}$) that is expected to vary if operated over a wide range of frequencies. This variation in the actual loss tangent value with the frequency makes the measured antenna parameters to differ from the simulation results obtained considering the fixed value of the dielectric loss tangent. Therefore,

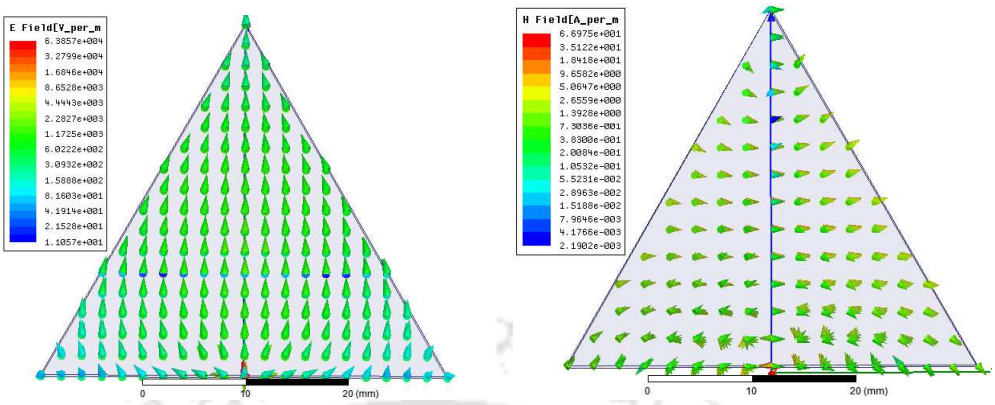

(a) (b)

Figure 3.6: Field distribution of configuration-I (DRA-1) at 2.45 GHz: (a) E-field and (b) H-field.

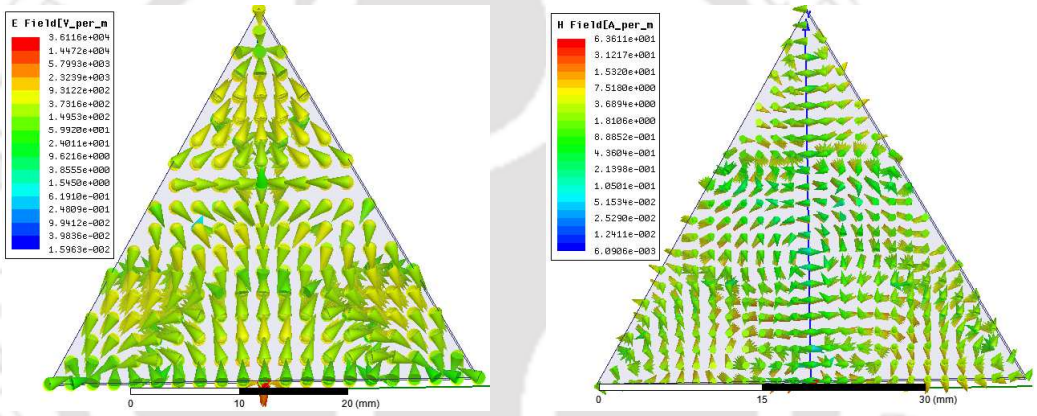

(a) (b)

Figure 3.7: Field distribution of configuration-I (DRA-1) at 5.8 GHz: (a) E-field and (b) H-field.

in simulations the loss tangent value for 99.7 % alumina material is varied from 10^{-3} to 10^{-2} in the sweep frequency by utilizing the standard piecewise linear dielectric loss tangent model available in Ansys HFSS.

3.3.1.1 Results and discussion: Configuration-I

Fig. 3.8(a) shows the variation in the return loss for different probe heights, obtained through full wave EM simulations carried out using Ansys HFSS. At a probe height of 13 mm, the best impedance matching is obtained around the operating frequency of 2.45 GHz and 5.8 GHz as shown in the $|S_{11}|$ plot of DRA-1 in Fig. 3.8(b). The simulations are also performed using CST Microwave Studio^{TM} and the $|S_{11}|$ plot for the same is included in Fig. 3.8(b). The measured result of the return loss is also included for comparison, for a fabricated prototype of DRA-1 shown in Fig. 3.5(b). If we closely observe the measured $|S_{11}|$ plot of the configuration-I, a resonance is occurring near 4.5 GHz. It is found that,

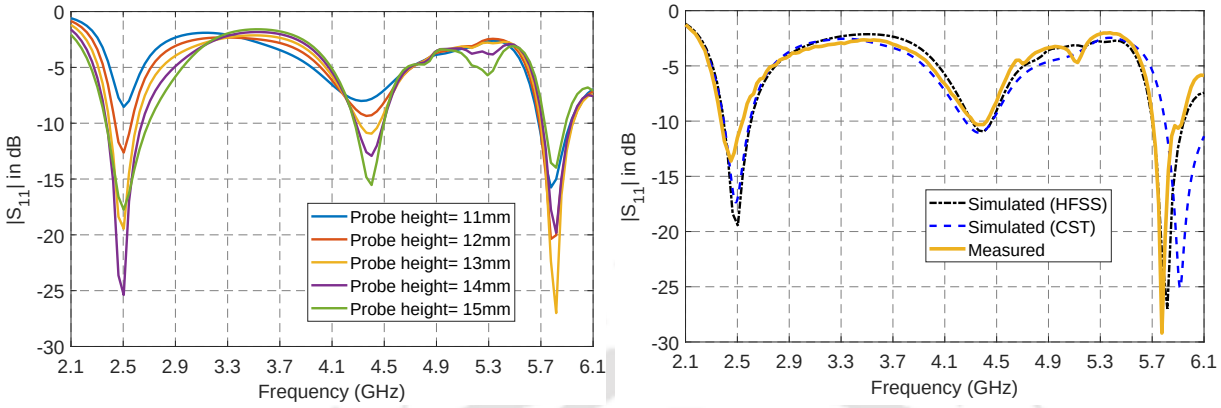

(a) (b)

Figure 3.8: $|S_{11}|$ plot of configuration-I (a) for different probe heights (using HFSS) and (b) at best impedance matching.

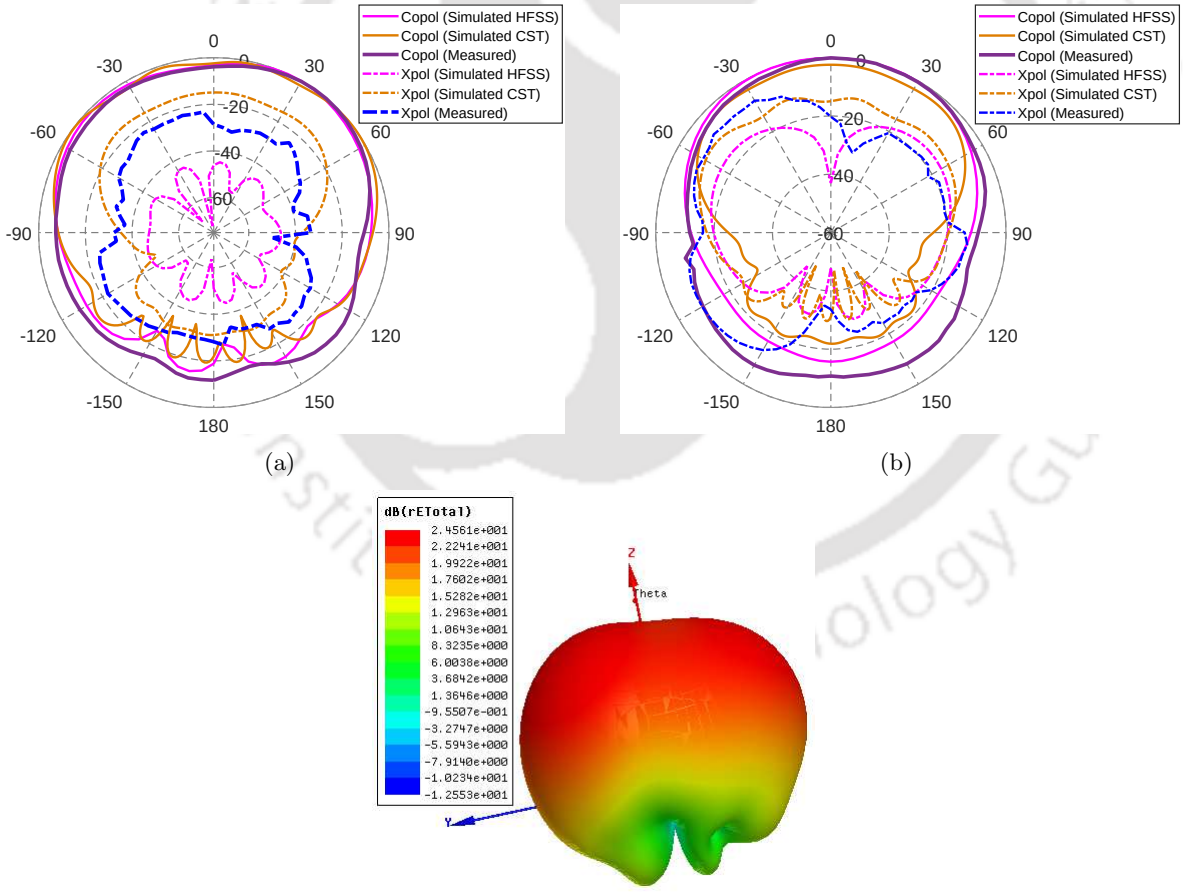

(a) (b)

(c)

Figure 3.9: Radiation pattern of configuration-I at 2.45 GHz: (a) ϕ=0^0 (E-plane)(b) ϕ=90^0 (H-plane) (c) 3-D pattern

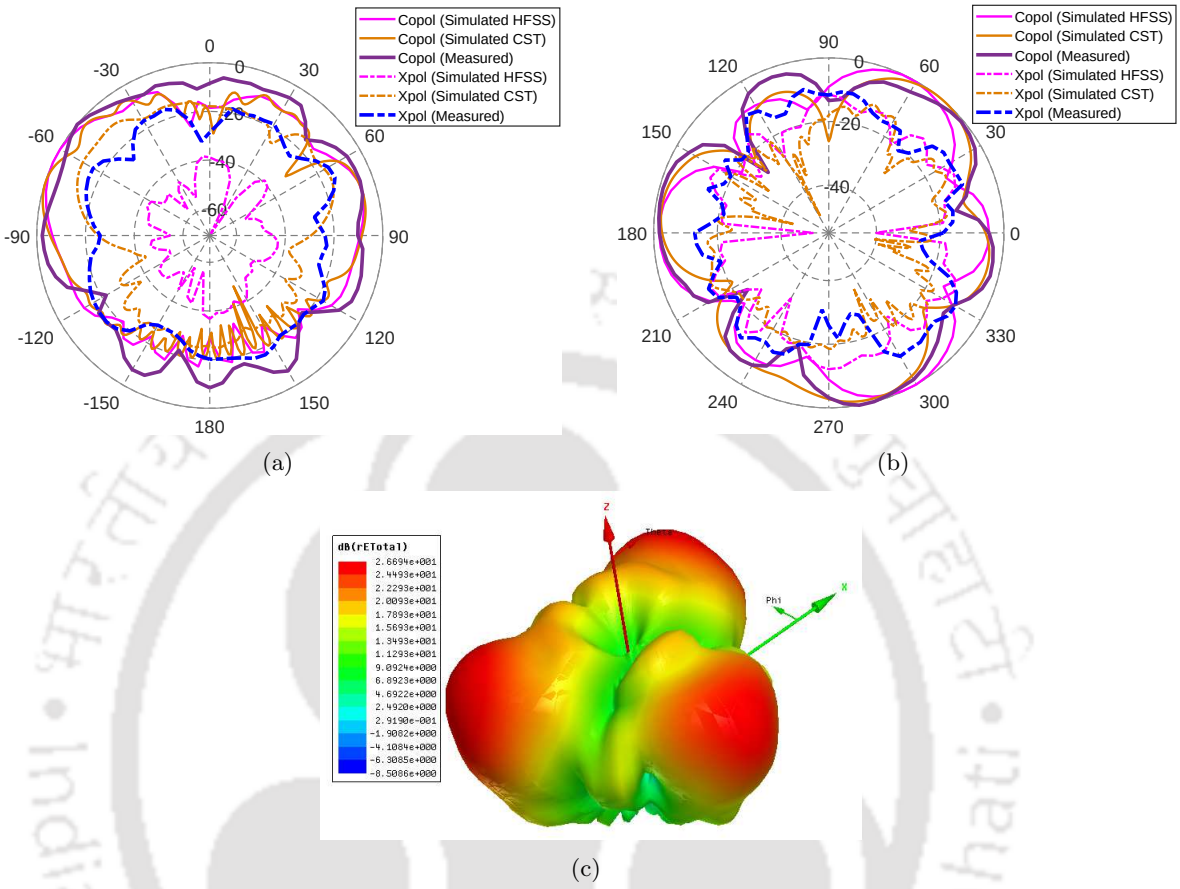

(a) (b)

(c)

Figure 3.10: Radiation pattern of configuration-I at 5.8 GHz: (a) ϕ=0^0 (E-plane) (b) θ=90^0 (H-plane) (c) 3-D pattern

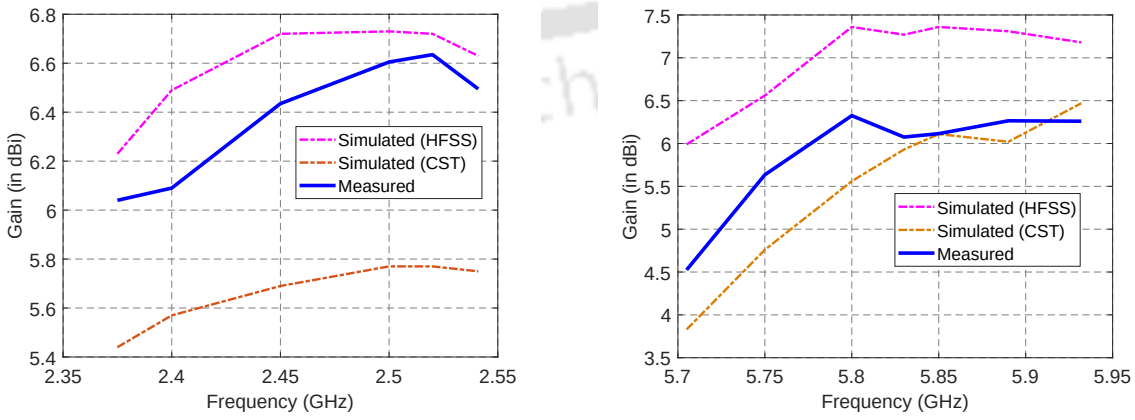

(a) (b)

Figure 3.11: Variation of the peak gain in the (a) lower and (b) upper operating bands for configuration-I.

this resonance is mainly due to a higher order $TM_{12\delta}$ mode excited inside this DRA. However, a weak coupling exist between the feed and the DRA around this frequency, due to poor impedance matching. For practical antennas, a return loss greater than 10 dB is acceptable for achieving an operational impedance bandwidth. Therefore, as a very low degree of impedance matching is existing around this frequency, they have not been included while considering the operational impedance bandwidth of the configuration-I.

The simulated radiation pattern obtained at 2.45 GHz and 5.8 GHz is shown in Fig. 3.9 and Fig. 3.10, respectively. Measured radiation pattern at both the operating frequencies is also included for comparison. The peak simulated gain at 2.45 GHz using HFSS is 6.72 dBi; whereas, the corresponding simulated gain using CST is 5.69 dBi. The measured gain is obtained 6.435 dBi. Similarly, at 5.8 GHz the simulated gain obtained using HFSS and CST are 7.36 dBi and 5.50 dBi, respectively. The corresponding measured gain is obtained 6.325 dBi. It is to be noted that, the antenna measurements are carried out in the normal laboratory conditions. The variation of the peak gain in the lower and upper operating bands of the Configuration-I are shown in Fig. 3.11(a) and Fig. 3.11(b), respectively. The Table 3.2 summarizes the simulated and measured gains of the configuration-I at the lower and the upper operating frequencies. It is observed that the peak measured antenna gain for configuration-I is close to the simulated value obtained using HFSS, at both the operating frequencies. The Table 3.3, compares the Q-factor and the efficiency at the operating frequencies of configuration-I. The simulated and measured gain values at the operating frequencies are also included in Table 3.3 for better comparison of the performances of the proposed configuration of the dual-band antenna. The simulated (using HFSS) gain and the Q-factor values are compared with their corresponding measured values. We already noted that, the practical gain performance of the configuration-I is almost comparable at both the operating frequencies. Both simulated and measured Q-factors are increasing, when operated in the upper operational frequency of 5.8 GHz. In contrast, the efficiency of the configuration-I drops at higher operating frequency of 5.8 GHz. The efficiency measurements requires a more practical antenna measurement facility and therefore, only simulation results are presented. From the values obtained for Q-factor and antenna efficiency, we observe that the antenna efficiency is inversely proportional to their Q-factor. A comparison of the Configuration-I dual-band ETDRA with other dual-band DRAs reported in the literature are presented in Section 3.3.3. As per IEEE standard (IEEE 802.11) specification for WLAN operation at 2.45 GHz and 5.8 GHz, are allotted

a bandwidth of 2.4-2.4835 GHz and 5.795-5.815 GHz. The proposed configuration of the dual-band ETDRA is linearly polarized with better gain performance and has practical operational impedance bandwidths of 2.375-2.541 GHz and 5.705-5.932 GHz, which covers the IEEE 802.11 standards for WLAN operation. Therefore, the proposed configuration-I antenna is suitable for use as a dual-band antenna for WLAN application. This configuration of the ETDRA which can be used for WLAN operation is an example of single DRA excited with multiple modes for dual-band applications.

3.3.2 Dual-band ETDRA: Configuration-II

The configuration-II of the dual-band antenna uses two ETDRAs, referred here as DRA-1 and DRA-2, each operated in the dominant $TM_{10\delta}$ mode. Both the DRAs are excited simultaneously using a coaxial feed. The coaxial probe is placed touching at the center of one of the sides of both the ETDRAs as shown in Fig. 3.12(a). The DRA-1 and DRA-2 are operated around 2.45 GHz and 5.8 GHz, respectively. A preliminary investigation of this configuration using full-wave EM simulation with Ansys HFSS is presented in Section 3.2, where both the ETDRAs uses RT/ Duroid®6010 material of ϵ_r=10.2. This configuration in its basic form in Design-I, has a significant contribution of higher order $TM_{3-3\delta}$ mode excited (in DRA-1) in the upper operating band, which effects the desired radiation characteristics. However, these effects are significantly reduced by re-designing it to configuration-II, so that, a similar radiation characteristic is maintained in both the operating bands. In the configuration-II, the two ETDRAs use 99.7% alumina material having ϵ_r=9.9. The DRA-1 has same dimensions as in Configuration-I. The DRA-2 has side a_2=17.4 mm and height h_2=8 mm, is independently studied before integrating into configuration-II. A fabricated prototype of configuration-II of the dual-band ETDRA is shown in Fig. 3.12(b). Full-wave EM simulations using Ansys HFSS are carried out to study the variation of return loss and radiation performance of the antenna. The standard piecewise linear dielectric loss tangent model available in Ansys HFSS is also included in the full wave simulations, so that variations in the loss tangent value of the alumina material over the frequency is taken into account.

3.3.2.1 Results and discussion: configuration-II

In the independent study of DRA-2 using full wave HFSS simulations, it is observed that, the $TM_{10\delta}$ mode is excited near 5.8 GHz. By varying the probe height, impedance matching is achieved around the resonant frequency of 5.75 GHz at a probe height of 6 mm. However, the theoretical

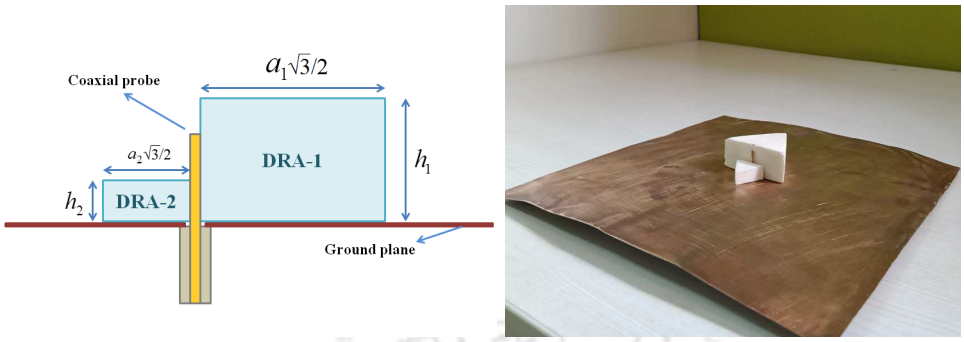

(a) (b)

Figure 3.12: The configuration-II dual-band ETDRA: (a) schematic and (b) fabricated prototype

resonant frequency of dominant $TM_{10\delta}$ mode is 5.92 GHz. The variation in $|S_{11}|$ parameter of DRA-2 for different probe heights of the SMA connector while exciting the fundamental $TM_{10\delta}$ mode through full-wave EM simulations using Ansys HFSS is shown in Fig. 3.13(a). The $|S_{11}|$ plot at a probe height of 6 mm, where best impedance matching is obtained is shown in Fig. 3.13(b). Measured result is also presented along with the simulated plot, for comparison. The radiation pattern at 5.8 GHz for DRA-2 is shown in Fig. 3.14, which includes the simulated pattern obtained using HFSS, compared with the corresponding measured pattern. A peak gain of 6.16 dBi obtained through simulation and 7.05 dBi through measurement.

In configuration-II, DRA-1 and DRA-2 are simultaneously excited to obtain impedance matching in the lower and the upper operating bands around 2.45 GHz and 5.8 GHz, respectively. The height of the coaxial probe is carefully adjusted while feeding the ETDRAs in this configuration, so that proper coupling (between the feed and the DRAs) as well as impedance matching around the desired operating frequencies are achieved. Fig. 3.15(a) shows variations in the return loss obtained through full-wave simulations performed using Ansys HFSS, for different probe heights for the configuration-II. Impedance matching around the operating frequencies of 2.45 GHz as well as 5.8 GHz is obtained at a coaxial probe height of 13 mm. It is also found during the investigation that the best matching at both the frequencies are obtained by keeping minimum difference between the values of height, while choosing the dimensions of DRA-1 and DRA-2. The comparison of simulated and measured return loss for the configuration-II dual-band ETDRA at the best impedance matching is shown in Fig. 3.15(b). The return loss obtained for the simulations performed using CST Microwave studio is also included in Fig. 3.15(b). The radiation pattern of the configuration-II at the frequencies of 2.45 GHz and 5.8 GHz are shown in Fig. 3.16 and Fig. 3.17, respectively. The simulated radiation pattern obtained

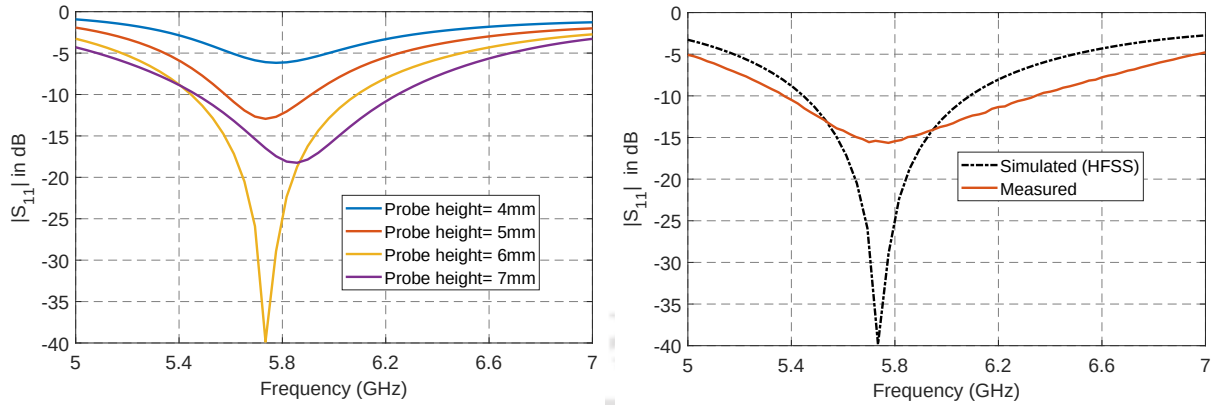

(a) (b)

Figure 3.13: $|S_{11}|$ plot of DRA-2 (a) for different probe heights and (b) at best impedance matching.

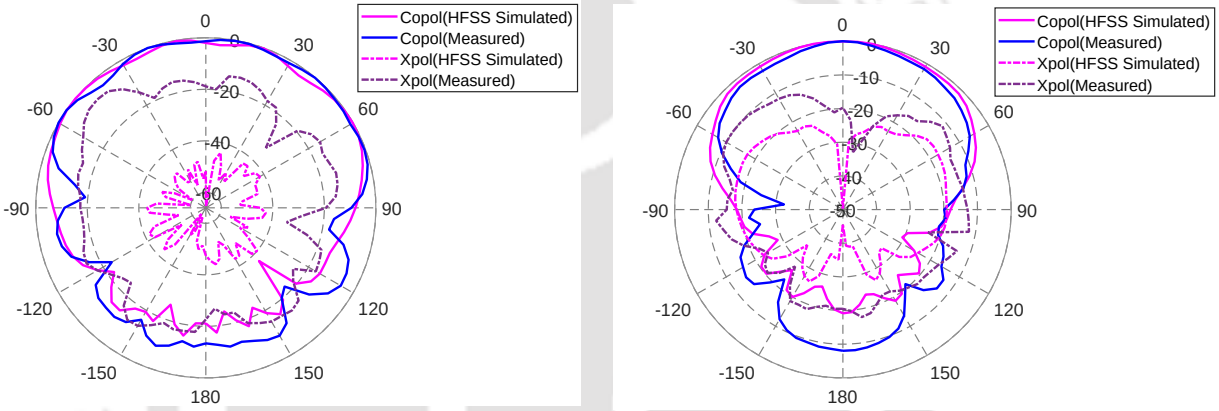

(a) (b)

Figure 3.14: Radiation pattern of $TM_{10\delta}$ mode of DRA-2 at 5.8 GHz: (a) ϕ=0^0 (E-plane) (b) ϕ=90^0 (H-plane)

using Ansys HFSS as well as CST are included. The measured radiation pattern is also included for comparison. At 2.45 GHz the antenna exhibits broad radiation characteristic which is similar to the characteristics shown by DRA-1 alone (Fig. 3.9). The radiation characteristic at 5.8 GHz is also obtained broad in nature. The modifications incorporated in the configuration-II improved the radiation performance at 5.8 GHz, when compared with the radiation characteristics obtained for Design-I. This improvement in the radiation pattern is due to reduction in the contribution of undesired higher order mode excited inside DRA-1 due to loading effect from the DRA-2, at the desired operating frequency. The peak simulated gains of the configuration-II dual-band ETDRA using Ansys HFSS are observed 6.30 dBi and 5.60 dBi at 2.45 GHz and 5.8 GHz, respectively, whereas the simulated gain at 2.45 GHz and 5.8 GHz using CST is obtained 5.62 dBi and 6.32 dBi, respectively. The gains obtained through measurements are 6.025 dBi and 6.185 dBi at 2.45 GHz and 5.8 GHz, respectively. The variation of the peak gain in the lower and upper operating bands of the Configuration-II are shown in

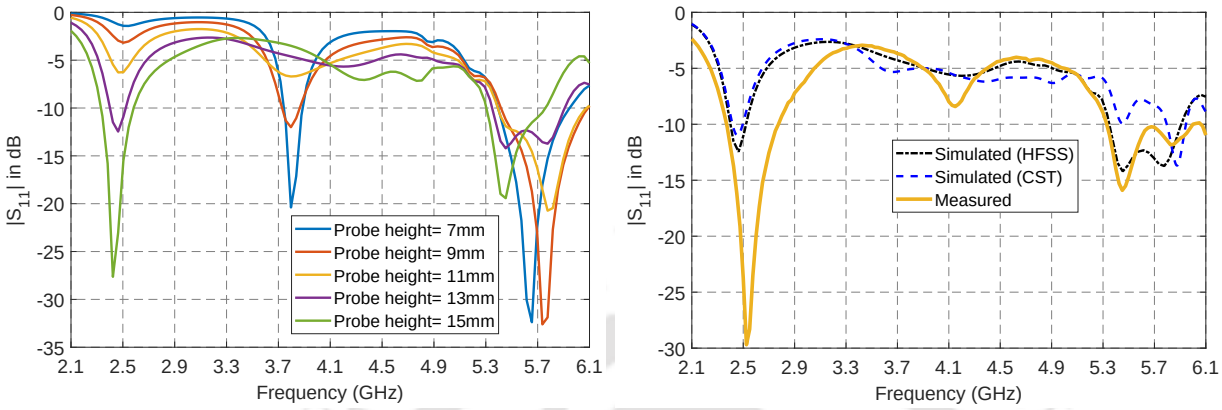

(a) (b)

Figure 3.15: $|S_{11}|$ plot of configuration-II dual-band ETDRA (a) for different probe heights (using HFSS) and (b) at best impedance matching.

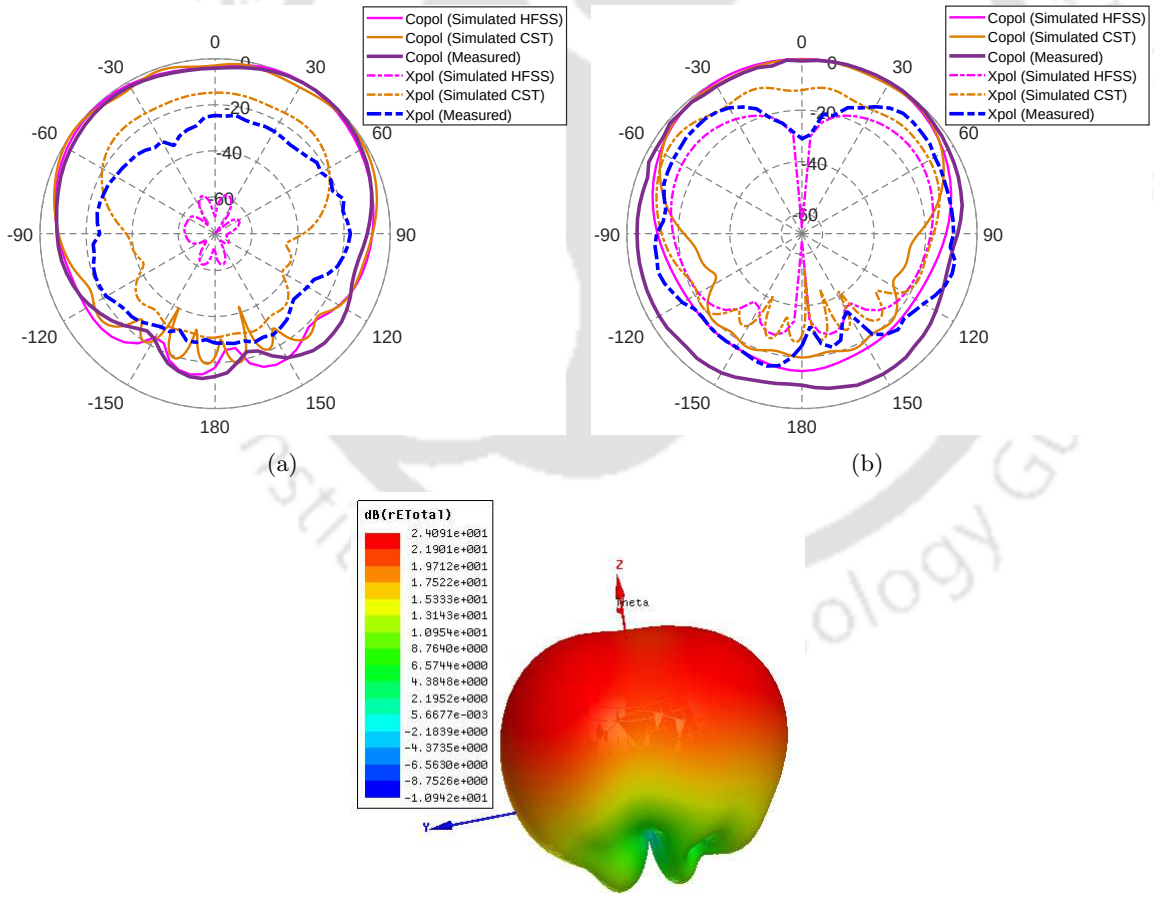

(a) (b)

(c)

Figure 3.16: Radiation pattern of Dual-band ETDRA (configuration-II) at 2.45 GHz: (a) ϕ=0^0 (E-plane) (b) ϕ=90^0 (H-plane) (c) 3-D pattern.

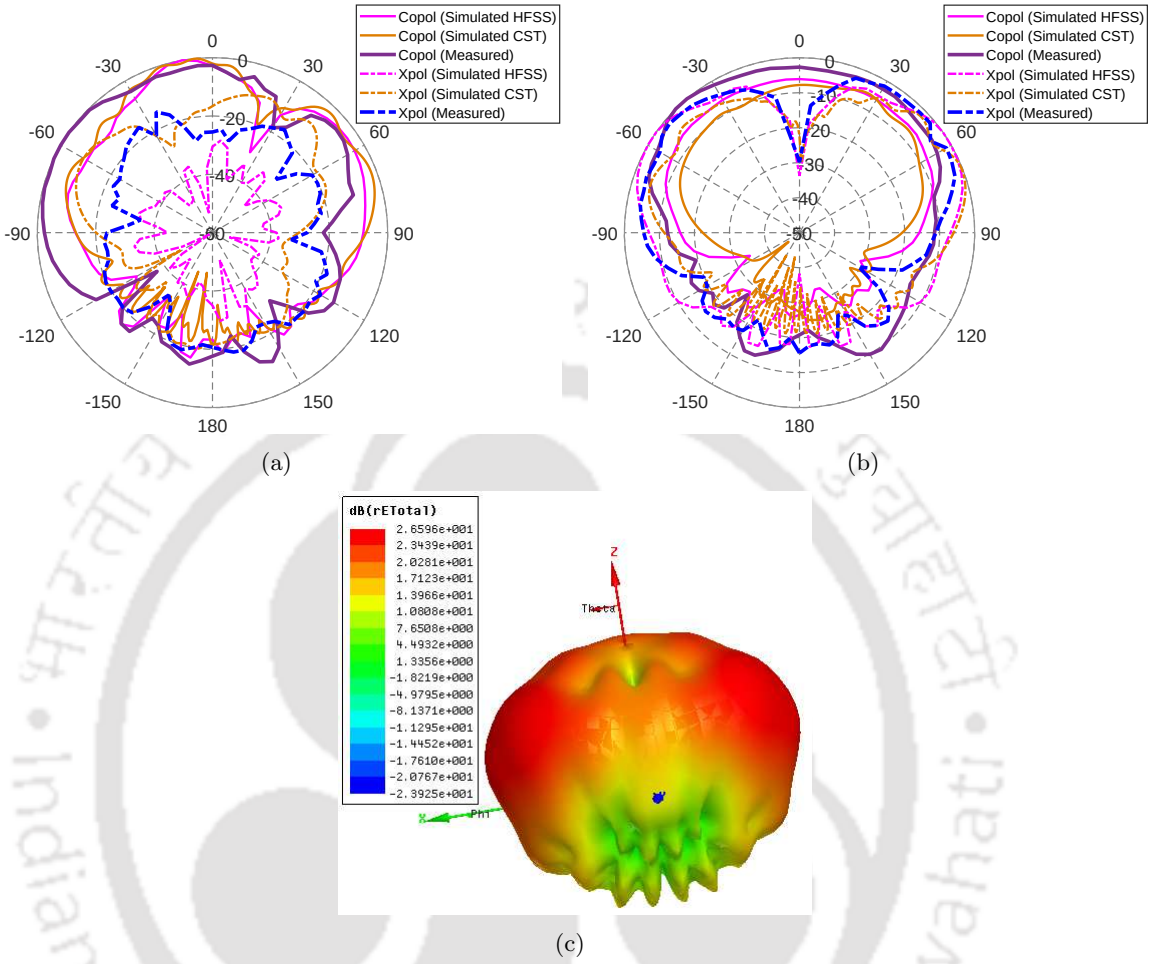

(a) (b)

(c)

Figure 3.17: Radiation pattern of Dual-band ETDRA (configuration-II) at 5.8 GHz: (a) ϕ=0^0 (E-plane) (b) ϕ=90^0 (H-plane) (c) 3-D pattern.

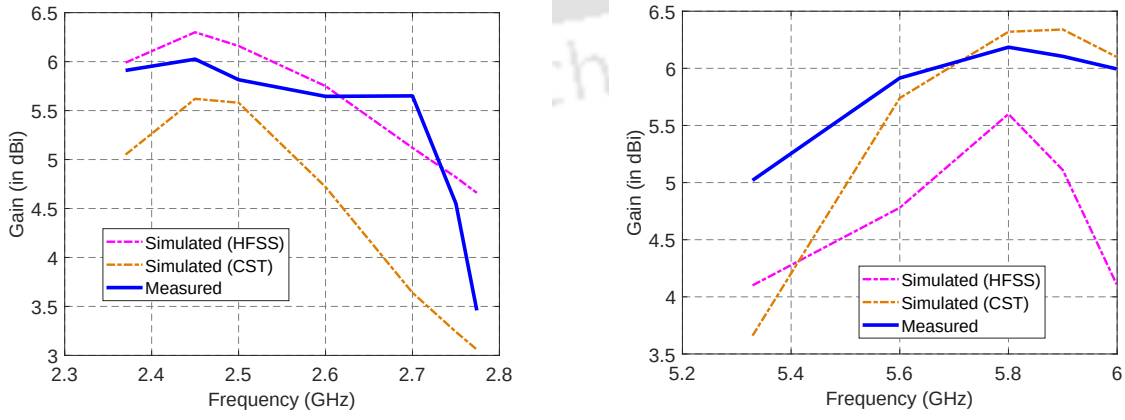

(a) (b)

Figure 3.18: Variation of the peak gain in the (a) lower and (b) upper operating bands for configuration-II.

Table 3.2: Antenna gains for configuration-I and configuration-II dual-band ETDRAs.

Design Configurations	Frequency (GHz)	Peak Gain (dBi)		
		Simulated		Measured
		HFSS	CST	
Configuration-I	2.45	6.720	5.690	6.435
	5.8	7.360	5.500	6.325
Configuration-II	2.45	6.300	5.620	6.025
	5.8	5.600	6.320	6.185

Fig. 3.18(a) and Fig. 3.18(b), respectively. The Table 3.2 also summarizes the simulated and measured gains of the configuration-II dual-band ETDRA at both the operating frequencies. It is observed that the peak measured antenna gain for configuration-II is close to the simulated value obtained using HFSS, at 2.45 GHz. However, at 5.8 GHz the peak measured gain is more close to the simulated gain obtained using CST. The Table 3.3, also compares the Q-factor and the efficiency at the operating frequencies of configuration-II. The simulated and measured gain values at the operating frequencies are also included in Table 3.3 for better comparison of the performances of the proposed configuration of the dual-band antenna. The simulated (using HFSS) gain and the Q-factor values are compared with their corresponding measured values. We already observed that, the practical gain values at the operating frequencies for the configuration-II are almost close. However, the measured Q-factor is slightly increasing at the higher operating frequency, when compared with the corresponding value at the lower operating frequency. The measured values are also obtained less than their corresponding simulated value at both the operating frequencies. In contrast, the efficiency of the configuration-II drops at higher operating frequency of 5.8 GHz. The efficiency measurements requires a more practical antenna measurement facility and therefore, only simulation results are presented. From the values obtained for Q-factor and antenna efficiency, we observe that the antenna efficiency is inversely proportional to their Q-factor. A comparison of configuration-II dual-band ETDRA with other dual-band DRAs reported in the literature is presented in the following section of this chapter. The proposed configuration of the dual-band ETDRA is linearly polarized with better gain performance and has practical operational impedance bandwidths of 2.370-2.774 GHz and 5.329-5.999 GHz, which covers the IEEE 802.11 standards for WLAN operation. Therefore, the proposed configuration-II antenna is suitable for use as a dual-band antenna for WLAN application.

Table 3.3: Comparison of gain, Q-factor and efficiency for the proposed configurations of dual-band ETDRAs.

Design Configurations	Frequency (GHz)	Peak gain (dBi)		Quality factor, Q		% Efficiency
		Simulated	Measured	Simulated	Measured	
Configuration-I	2.45	6.72	6.435	8.33	10.43	98.66
	5.8	7.36	6.325	16.69	18.00	83.70
Configuration-II	2.45	6.30	6.025	14.32	4.36	96.42
	5.8	5.6	6.185	12	6.19	82.89

Table 3.4: Comparison of gain and bandwidth of the proposed configuration-I and configuration-II dual-band ETDRAs with other dual-band DRAs reported in the literature

DRA shape	Ref.	Lower band			Upper band		
		Operating band/ frequency (GHz)	Bandwidth %	Peak gain (dBi)	Operating band/ frequency (GHz)	Bandwidth %	Peak gain (dBi)
CDRA	[150]	1.684-1.726	2.46 %	2.00	2.246-2.454	1.15 %	0.50
HDRA	[156]	2.430	-	3.75	3.630	-	5.75
RDRA	[157]	2.380-2.510	5.31 %	0.80	4.920-5.610	13.10 %	3.50
RDRA	[152]	2.210-2.855	28.00 %	5.23	4.835-5.455	11.90 %	6.26
CDRA	[239]	2.360-2.500	3.30 %	4.30	5.400-5.800	5.70 %	3.80
RDRA	[153]	3.250–3.780	15.00 %	4.02	5.030–5.470	8.30 %	7.52
C shaped	[154]	3.460-3.610	4.24 %	3.26	5.660-6.140	8.13 %	5.55
CDRA	[240]	1.700-2.000	15.50 %	6.32	2.390-2.480	3.70 %	7.99
Rectangular Ring	[159]	2.400-2.600	8.00 %	3.50	3.300-5.850	55.70 %	4.37
CDRA	[241]	3.400-3.600	5.71 %	1.54	5.530-5.990	7.99 %	4.06
Sierpinski Fractal Trapezium	[163]	2.250-2.600	14.46 %	5.58	3.100-4.100	27.78 %	5.51
Ring DRA	[162]	1.970-2.670	30.17 %	2.24	5.300-6.620	22.14 %	3.92
ETDRA (configuration-I)	Proposed	2.375-2.541	6.75 %	6.435	5.705-5.932	3.90 %	6.325
ETDRA (configuration-II)	Proposed	2.370-2.774	15.70 %	6.025	5.329-5.999	11.82 %	6.185

3.3.3 Comparison of the proposed antennas with existing dual-band DRAs in the literature

A comparison of the proposed configurations of the dual-band ETDRAs with other dual-band DRAs (having at least one of the operating frequencies in the frequency bands of the proposed antennas) reported in the literature are shown in Table 3.4. The proposed dual-band ETDRA configuration-I provides better gain in the lower as well as upper operating bands, compared with most of the other existing dual-band DRAs reported in the literature. It is to be noted that, by using the proposed DRA, drilling and cutting of dielectric material can be avoided, which makes the proposed DRA, very simple to realize. Moreover, in the case of dual-band CDRA reported in [239], having almost same lower and upper operational frequencies as in our proposed DRA, it is observed that configuration-I has higher gain and as well as better percentage bandwidth around the lower operating frequency. In the upper operational bandwidth, the gain of the proposed Configuration-I is higher; however, the percentage impedance bandwidth is slightly lower as compared with the CDRA in [239]. When we compare the Configuration-I with the RDRA in [157] having similar lower operating band, we observe that, the gain of the Configuration-I is significantly higher than the RDRA in [157] as well as bandwidth for

Configuration-I is also higher than the RDRA in [157].

The Configuration-II has almost close value of the measured gain, when compared with the configuration-I, in both the operating frequencies. Both the configurations therefore have similar distinction (in terms of gain performance) from other dual-band DRAs reported in the literature. In terms of bandwidth performance, configuration-II design is better compared with configuration-I. The configuration-II has percentage bandwidths of 15.7% and 11.82% in the lower and upper operating bands, respectively. The configuration-II also have higher gain and better percentage bandwidth with respect to the other dual-band DRAs [157, 159, 163, 239] (having almost same lower operating frequency) reported in the literature; except for RDRA in [152] and Ring DRA in [162] where, only the gain of proposed antenna is obtained higher. While comparing the performance of the configuration-II with other reported DRAs [154, 162, 239, 241] having almost same upper operating frequency, we observe that, the proposed DRA has higher gain. The configuration-II also has better percentage bandwidth, when compared with CDRA in [239, 241] and C-shaped DRA in [154].

Both configuration-I and configuration-II presents the potential of an ETDRA as a dual-band antenna in the operational frequency bands of 2.4-2.5 GHz and 5.75-5.85 GHz. Both the configurations use a conventional coaxial feed for the excitation of the antenna, which makes the proposed ETDRAs an easily realizable dual-band antenna. The performance of the proposed dual-band antenna configurations with existing material specifications, is better in terms of gain, when compared with most of the existing dual-band DRAs reported in the literature. However, in terms of bandwidth performance the proposed configurations of the dual-band ETDRA are either comparable or better than some of the dual-band DRAs reported in the literature. The proposed configurations of the ETDRAs can therefore be operated as a dual-band antenna and used for WLAN applications.

3.4 Challenges in the design of dual-band/ multi-band DRAs

The investigation on the design of dual-band ETDRAs for WLAN applications presented in this chapter, also serves as an insight into some of the challenges and advantages appearing in the design of DRAs for dual-band and multi-band applications, summarized below:

- A single DRA can be used to achieve multiple operating bands by properly exciting multi-modes of a DRA, at the appropriate frequencies, based on requirement and application. The radiation characteristics at the operating frequencies will be different in such DRA designs, as different

modes excited inside a DRA exhibit different radiation characteristic. However, if the radiation pattern is suitable for the application, the design reduces area, complexity and cost of the antenna. By appropriately fine tuning the bandwidth, same antenna can be used for wideband as well as UWB application. But, it is to be noted that for some frequency application the radiation pattern may not be suitable and such antennas cannot be recommended for multi-band applications. However, an additional benefit of using single DRA multiple band designs is that, no interference occur from the other excited modes within the DRA on the radiation pattern, unless degenerate modes are excited. The Configuration-I presented in Section 3.3.1 for WLAN operation is a very simple example of single DRA for multi-band application.

- Multiple operating bands can also be achieved by exciting multiple DRAs. Such configurations are suitable when a typical radiation characteristics are only permissible at desired frequencies of operation. This type of configurations are always accompanied by excitation of unwanted higher order modes that generally effects the impedance matching, radiation characteristics and gain of the design. The Design-I, presented in Section 3.2 is an example for such antenna design (however, this configuration of the dual-band antenna has been re-designed to configuration-II, and the radiation characteristics are significantly improved). Moreover, it is to be also noted that, the shifting of best impedance matching from the desired frequency of operation can also occur in this type of antenna configuration, which is a direct significance of the dielectric loading effect from the neighbouring DRA. A high amount of dielectric loading from one DRA over the other can also result in a high degree of impedance mismatch between the source and the DRA, around the operating frequencies. These effects therefore makes the multi-band DRA designs more sensitive and challenging. However, these effects does not impart much challenges to the antenna designers in the design of wideband antennas. Only the edge frequencies of the operational bandwidth are more of the concern, and shifting of the resonant frequency as well as frequencies of best impedance matching within the edge frequencies does not effect much on the antenna performance. In fact, in the wideband DRA designs, maintaining the impedance matching is much easier when compared with the cases of dual-band and multi-band designs.

- In the design of DRAs, impedance matching occurs in two ways: (1) dielectric resonance and (2) dielectric loading. Therefore, obtaining an impedance matching over a narrow range of frequencies while exciting a DRA will not always ensure a dielectric resonance. Dielectric resonance

happens at certain frequencies at which a radiating mode is excited inside a DRA, which can be TE or TM in nature, and the resonant frequency of this excited mode is decided by the dimensions of the DRA. Upon properly exciting the desired radiating mode using a suitable feed, a good degree of impedance matching can be obtained around the resonant frequency at which the DRA is operated. However, the presence of another DRA which if kept very close, can effect the impedance matching around the desired operating frequency. Hence, under such condition the DRA is very weakly coupled with the source, and the desired operating mode within the DRA may not be properly excited. This is an example of a dielectric resonance which is effected by dielectric loading. A similar effect is observed at 5.8 GHz of the configuration-II of the proposed dual-band ETDRAs. However, this phenomena has favourably affected the design configuration. Here, the effect of unwanted higher order $TM_{3,-3,\delta}$ mode excited in the DRA-1 in the upper operating band is significantly reduced by the loading effect from DRA-2. The dielectric loading phenomena can be investigated and favourably utilized in the design of dual-band antennas. An investigation on dielectric loaded antennas for dual-band application is presented in detail in chapter 5 of this thesis.

- The specification of the dielectric material used in the design of DRAs also has a significant contribution on the antenna performance. The two parameters of the dielectric materials are dielectric constant (ϵ_r) and the loss tangent ($\tan\delta$) values. It is of foremost concern that, in the practical design of DRAs, these parameters of the dielectric material are to be consistent with their standard values, around the operating frequency. In simulations, these values are assumed constant around the operating frequencies. However, in practice, a small tolerance value of these parameters can reduce the practical DRA performance as compared with their corresponding simulated results. These effects are noted in the antenna gain performance in the upper operating band of the Configuration-I and Configuration-II designs of the dual-band ETDRAs presented in this chapter. Therefore, in simulations, the loss tangent value of the Alumina material is not assumed constant and a standard piecewise linear dielectric loss tangent model available in Ansys HFSS is included while performing full wave EM simulations, so that variations in the loss tangent value of the Alumina material over the frequency band are taken into account. It is to be noted that, the effect of practical loss tangent value on the antenna performance is important in understanding the behaviour of practical antennas.

3.5 Summary

In this chapter an investigation on ETDRA for dual-band application is presented. A preliminary investigation of a dual-band antenna configuration using two ETDRAs is presented, namely Design-I, to obtain a similar radiation characteristic in both the operating bands. This design configuration, which use RT/ Duroid®6010 material having ϵ_r=10.2, is investigated to understand the challenges as well as antenna performance, when excited using a conventional coaxial feed and operated in the WLAN frequency bands of 2.4-2.5 GHz and 5.75-5.85 GHz configuration. It is observed that, a higher order $TM_{3-3\delta}$ mode excited in the upper operating band has effected the radiation performance of this antenna configuration. Through proper understanding of the excited modes, the potential of the ETDRA as a dual-band antenna is investigated in detail; based on which two configurations of dual-band ETDRA are proposed, namely Configuration-I and Configuration-II. Both the configurations uses 99.7% Alumina material having ϵ_r=9.9, and the dimensions of the DRAs are appropriately chosen to operate in the bands of 2.4-2.5 GHz and 5.75-5.85 GHz. The configuration-I is a single ETDRA dual-band antenna. This antenna operates in the dominant $TM_{10\delta}$ mode in the lower band and in higher order $TM_{3-3\delta}$ mode for the upper band. The configuration-II presents a dual-band antenna using two ETDRAs with similar radiation characteristics, by exciting $TM_{10\delta}$ mode for each ETDRA at one of the operating frequencies. Both the configuration-I and configuration-II of the proposed dual-band ETDRAs are excited by means of a conventional coaxial feed. Prototypes of both the DRA configurations are fabricated and their practical radiation characteristics are presented. Further, the performance of the proposed configurations of the dual-band ETDRAs are also compared with other dual-band DRAs reported in the literature. The performance of the proposed DRAs is either better or similar to most of the dual-band DRAs reported in the literature. The proposed configurations of ETDRAs are easily realizable and can be used for WLAN applications in the bands of 2.4-2.5 GHz and 5.75-5.85 GHz. Further, based on various observations in the investigation of the proposed configurations of the ETDRAs, some of the challenges in the design of dual-band DRAs are also summarized.

4

Investigation on a New Rhombic Dielectric Resonator Antenna

Contents

In the previous chapter we discussed how ETDRAs can be designed to operate as a dual-band antenna. We also discussed, how the performance of such antennas are effected in a practical design by presenting the performance characteristics of a fabricated prototype of the same antenna. The challenges in the design of dual-band DRAs are also presented which will be useful in the initial design of such antennas. However, some of these challenges are not present in the design of wideband DRAs, as such the wideband DRAs are much easier to realize. A detailed survey of wideband DRAs presented in the literature are discussed in Section 1.3.2.2. The wide impedance bandwidth using DRAs are achieved by exciting multiple resonating modes in the operating bands [107–113]. The available literature presents wideband DRAs with a simple conventional excitation scheme [48,49,91,92] to some of the modified novel feeding techniques [98–106] to achieve multiple resonances in the realization of DRAs for wideband applications. In this chapter we present a DRA, which is a suitable candidate to operate as a wideband antenna and which requires only a conventional coaxial probe to achieve such characteristics. The proposed DRA which can be classified among the DRAs having basic geometry, is very compact at its operating frequency, when compared to the other DRAs in this classification.

This chapter[1], introduces a novel Rhombic shaped DRA formed by joining two ETDRAs at one of their sides. The dimensions and shape of this new geometry is different from an ETDRA. Therefore, the excited modes and their corresponding resonant frequency, in this new DRA will be different from the excited modes and their corresponding resonant frequency values of an ETDRA. Hence, the initial discussion on this DRA will be on the excited modes and the calculation of resonant frequency of these excited modes. Some of the techniques to excite these modes and their radiation characteristics are discussed and the realization of this DRA as a wideband antenna is also presented in this chapter.

4.1 Introduction to the new Rhombic DRA

We are familiar with the geometry of an ETDRA which has side 'a', and height 'h'. We join two such ETDRAs at one of their sides to develop a new DRA shape which has a Rhombic cross-section, and can be classified among the DRAs having basic geometry. We name this new DRA as Rhombic DRA, whose schematic diagram is shown in Figure 4.1. The proposed Rhombic DRA geometry has four sides each of length, 'a'. It has two diagonals 'd_1' and 'd_2' with $d_1 > d_2$. The length of the diagonals d_1 and d_1 are respectively '$\sqrt{3}a$' and 'a'. The DRA has height of 'h' above the ground plane. The DRA is

[1]The work reported in this chapter has been presented in the following journal publication:
Anoop, P, Bhattacharjee, R., "Investigation on a new compact wideband rhombic dielectric resonator antenna", *Int J RF Microw Comput Aided Eng.* 2019;e21864. https://doi.org/10.1002/mmce.21864.

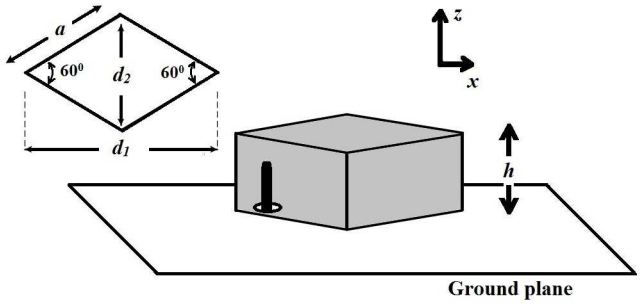

Figure 4.1: Geometry of the proposed Rhombic DRA

placed in such a fashion that the diagonal d_1 lies along the x-axis. The Rhombic DRA is excited along one of its diagonals to get the desired mode of operation. The proposed DRA geometry can be excited using conventional excitation methods such as probe feeding, aperture coupling or using striplines. We use the conventional coaxial probe technique to excite some of the possible modes, which will be discussed in the subsequent sections of this chapter. While exciting, the probe is placed at the end of any of the diagonals of the DRA. Drilling of the DRA can be avoided by placing the probe just outside the periphery, in the vicinity of the corner of the Rhombic shaped antenna. Such feeding methods are followed in Rectangular DRA to excite orthogonal modes to produce circular polarization [195]. A survey of literature shows that, a Rhombic shaped DRA is reported by Sayantan Dhar in [233]. It is to be noted that, this DRA is a rotated version of the basic square shaped DRA.

This chapter is organized into 8 sections. Section 4.2 discusses the resonant modes excited in the proposed rhombic-shaped DRA. Expressions for the resonant frequencies of the x and y polarized TE fields in rhombic DRA are provided in Section 4.3. The feeding techniques for such DRAs are presented in Section 4.4. Section 4.6 presents discussion on the resonant frequency and radiation characteristics of the Rhombic DRA having low profile geometry. Section 4.5 discusses the radiation characteristics of the proposed DRA. Measured results are also presented in this section and compared with simulation results. Section 7 deals with the design of wideband rhombic DRAs. Simulations as well as measured results are also presented in this section. Finally, conclusions are drawn in Section 4.8.

4.2 Introduction to the modes of Rhombic DRA

The various modes excited inside the new Rhombic DRA are identified by performing eigen mode simulations of this DRA geometry using commercial EM simulation software, CST Microwave studio.

The investigation on some of the modes identified using CST reveals that, the field distribution of the excited modes in such DRA are, similar to the modes excited inside a Rectangular DRA as detailed in [40] and [39]. This does not infer that both the DRAs have same field distribution, but dissimilarities exist as our proposed Rhombic DRA and a rectangular DRA are excited at different locations. The point of feeding a DRA by convention is the position where maximum coupling between the excitation source and the DRA exists. By convention, modes of a rectangular DRA are excited using a coaxial probe from any of the sides of such DRA. However, in our proposed Rhombic DRA the modes are excited using a coaxial probe placed at any of the corresponding corners and not at the sides of the DRA. The previously reported Rhombic DRA in [233] is also excited from the corner. But, as the geometry is formed by rotation of a square DRA, orthogonal modes get excited. However, in our proposed Rhombic DRA, upon feeding with a coaxial probe at the corner, only a particular mode is excited at a single frequency and such feeding will not excite orthogonal modes. This makes our proposed Rhombic DRA different from Rectangular DRA, Square DRA and other variant of the Rectangular DRA reported in the literature.

The dominant mode and a few of the higher order modes of the proposed Rhombic DRA are identified through eigen mode analysis using CST simulation. Further investigations on these identified modes are performed through CST as well as using HFSS simulation. Feeding technique used in the simulation is the conventional coaxial probe method which excites only TE modes. We therefore confine the investigation on the proposed DRA within such modes only. The E-fields of these modes are distributed either along diagonal d_1 or d_2. Accordingly we classify them as either $(\mathrm{TE}_n)^y$ (x-polarized) or $(\mathrm{TE}_n)^x$ (y-polarized) mode respectively, where 'n' represents the order of the mode. The mapping of the modes excited inside the Rhombic DRA with similar modes of Rectangular DRA is shown in Table 4.1. The purpose of this mapping is only to allow a better visualization and understanding of the fields distributed inside the Rhombic DRA.

4.2.1 Dominant $(\mathrm{TE}_1)^y$ mode

The dominant mode excited in the new Rhombic shaped DRA is the $(\mathrm{TE}_1)^y$ mode. The field distributions of $(\mathrm{TE}_1)^y$ mode are shown in Figure 4.2. The E-field is characterized by a single half cycle along the x-axis. This mode is similar to $\mathrm{TE}^y_{1\delta 1}$ mode excited inside a Rectangular DRA. This mode can be easily excited inside the proposed Rhombic DRA by corner feeding technique, i.e. by using a coaxial probe placed near the corner along the diagonal d_1, where maximum field is coupled

Table 4.1: Modes of the Rhombic DRA

Modes of Rhombic DRA	Similar modes of Rectangular DRA
$(\mathrm{TE}_1)^y$	$\mathrm{TE}^y_{1\delta 1}$
$(\mathrm{TE}_1)^x$	$\mathrm{TE}^x_{\delta 11}$
$(\mathrm{TE}_2)^y$	$\mathrm{TE}^y_{2\delta 1}$
$(\mathrm{TE}_2)^x$	$\mathrm{TE}^x_{\delta 21}$
$(\mathrm{TE}_3)^y$	$\mathrm{TE}^y_{3\delta 1}$
$(\mathrm{TE}_3)^x$	$\mathrm{TE}^x_{\delta 31}$

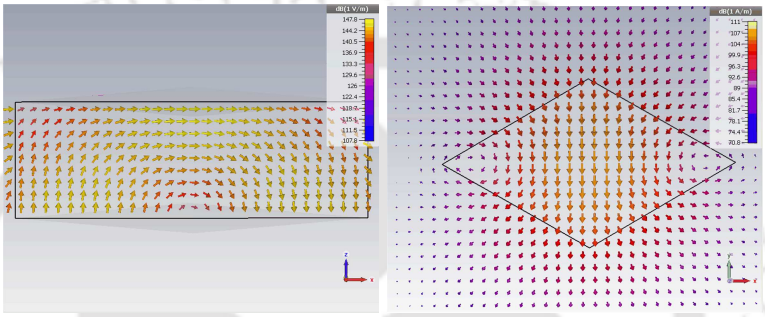

(a) (b)

Figure 4.2: Field distributions of $(\mathrm{TE}_1)^y$ mode: (a) E-fields and (b) H-fields.

between the source and the DRA. Henceforth, this feeding technique will be referred to as *corner* feeding or *Type-I* feeding.

4.2.2 $(\mathrm{TE}_1)^x$ mode

Next higher mode excited inside a Rhombic DRA is the $(\mathrm{TE}_1)^x$ mode. The field distributions of $(\mathrm{TE}_1)^x$ mode are shown in Figure 4.3. The E-field is characterized by a single half cycle along y-axis. This mode has the smallest resonant frequency among the set of y-polarized modes excited in the DRA. The field distributions of mode are similar to $\mathrm{TE}^x_{\delta 11}$ mode excited inside the Rectangular DRA. This mode can be excited using *Type-I* feeding by placing the coaxial probe near the corner along the diagonal d_2.

4.2.3 Higher order TE modes

The field distribution of $(\mathrm{TE}_1)^y$ and $(\mathrm{TE}_1)^x$ modes are discussed in the previous subsections. We referred Type-*I* feeding as a suitable technique for exciting such modes. We now introduce a few of the higher order TE modes excited in the proposed Rhombic DRA. Such modes can also be excited using conventional *Type-I* feeding technique. However, the field distribution of such modes excited in

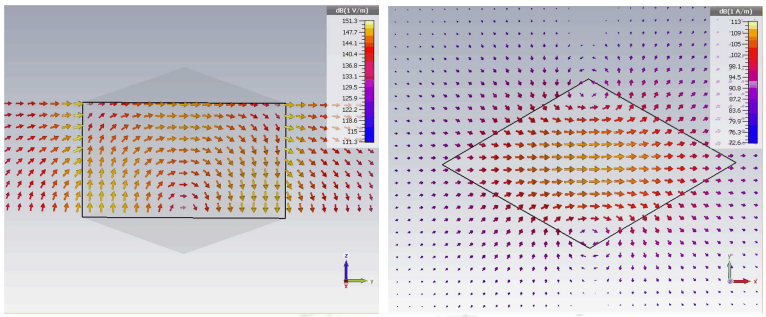

(a) (b)

Figure 4.3: Field distributions of $(TE_1)^y$ mode: (a) E-fields and (b) H-fields.

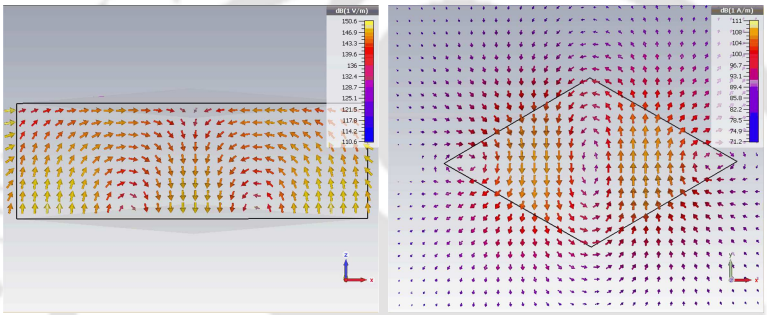

(a) (b)

Figure 4.4: Field distributions of $(TE_2)^y$ mode: (a) E-fields and (b) H-fields.

the new Rhombic DRA allows different feeding schemes, that allows flexibility in positioning the feed. Various techniques for exciting the TE modes of the Rhombic DRA are discussed later, in Section 4.4. However, we will initially discuss the field distribution of higher order TE modes excited inside the proposed DRA geometry before presenting the technique of exciting such modes.

4.2.3.1 $(TE_2)^y$ mode

The $(TE_2)^y$ mode is the next higher mode among the set of x-polarized modes after $(TE_1)^y$. The field distributions of $(TE_2)^y$ mode are shown in Figure 4.4. The E-field distribution has two half cycles along the diagonal d_1. This field distribution is similar to $TE^y_{2\delta1}$ mode excited inside Rectangular DRA. Such modes can be excited through conventional coaxial probe from any of the two positions: (1) from one of the corners along the diagonal d_1 using *Type-I* feeding or (2) from the geometric center of the DRA, referred as '*Center feeding*'.

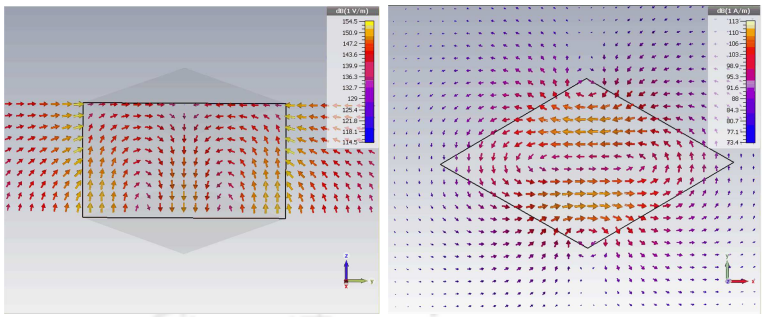

(a) (b)

Figure 4.5: Field distributions of $(TE_2)^x$ mode: (a) E-fields and (b) H-fields.

4.2.3.2 $(TE_2)^x$ mode

The $(TE_2)^x$ mode is the next higher mode among the set of y-polarized modes after $(TE_1)^x$. The field distribution of $(TE_2)^x$ mode are similar to $TE^x_{\delta 21}$ mode in the Rectangular DRA. Other than corner feeding technique, they can be excited by center feeding, a similar technique which are used in the excitation of $(TE_2)^y$ mode. The field distribution of $(TE_2)^x$ mode are shown in Figure 4.5.

4.2.3.3 $(TE_3)^y$ mode

The field distributions of $(TE_3)^y$ mode are shown in Figure 4.6. They can be excited by *Type-I* feeding technique like other lower order modes excited in Rhombic DRA. The E-field distribution of $(TE_3)^y$ mode has three half cycles along the diagonal d_1, which allows a different point of excitation where the feed is placed at $\sim d_1/3$ from the corner of the DRA along x-axis. We refer such feeding techniques as *Type-II* feeding technique. This mode can have resonant frequency close to that of $(TE_2)^x$ mode depending on the dimensions and material properties of the DRA. Hence feed should be properly placed while exciting this mode as it may allow a reason for the excitation of $(TE_2)^x$ mode as well.

4.2.3.4 $(TE_3)^x$ mode

The $(TE_3)^x$ mode is similar to $(TE_3)^y$ mode excited within the Rhombic DRA. They have similar field distributions and the E-fields are directed along diagonal d_2. The field distributions of $(TE_3)^x$ mode are shown in Figure 4.7. The $(TE_3)^x$ mode can be excited inside the Rhombic DRA using corner feeding/ *Type-I* feeding technique. Such mode can also be excited using *Type-II* feeding technique by placing the feed at a distance of $\sim d_2/3$ from one of the corner of such DRA, along diagonal d_2.

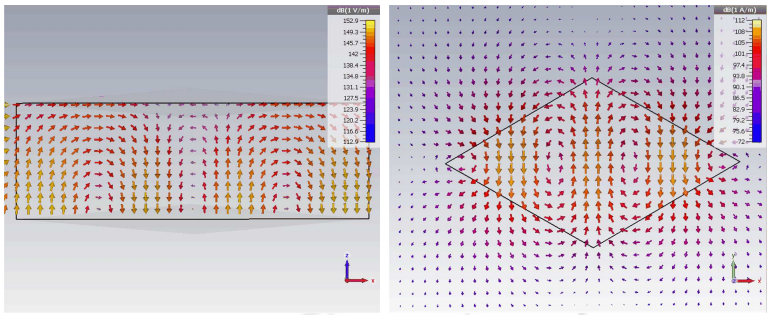

(a) (b)

Figure 4.6: Field distributions of $(TE_3)^y$ mode: (a) E-fields and (b) H-fields.

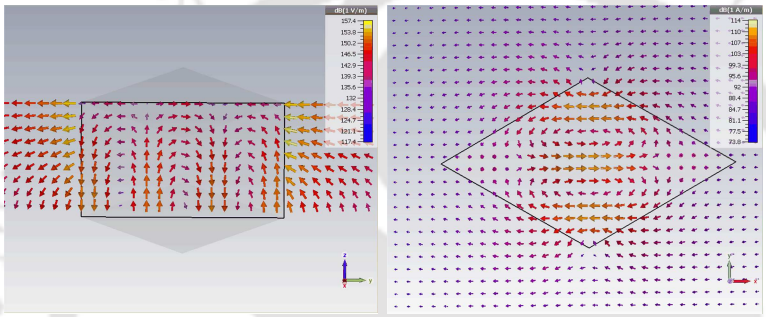

(a) (b)

Figure 4.7: Field distributions of $(TE_3)^x$ mode: (a) E-fields and (b) H-fields.

4.3 Resonant frequency calculation of the new Rhombic DRA

The resonant frequencies of $(TE_n)^y$ and $(TE_n)^x$ modes are determined by the dimensions of the Rhombic DRA. The E-fields of the modes excited inside this DRA are distributed along the diagonals d_1 and d_2 for $(TE_n)^y$ and $(TE_n)^x$ modes, respectively. Hence, the resonant frequency of the modes are defined in the manner that $(TE_n)^y$ modes depends on dimensions d_1, a and h of the DRA and $(TE_n)^x$ modes depend d_2, a and h of the same DRA. It is to be noted that when the geometry of the DRA is having sharp corners, the absence of fields in those regions is more probable. This makes the effective dimensions of the DRA smaller than their actual values and hence, the practically observed resonant frequency of a mode would be considerably higher than the theoretically calculated value of resonant frequency. Such cases are reported for Triangular DRA in [62]. The fields excited inside the Rhombic DRA also exhibit similar effects and hence, we have used effective values for the diagonals d_1 and d_2 and height h of the DRA. After performing several eigen mode analysis on our new Rhombic DRA with various dimensions and dielectric values, closed form expressions have been obtained for effective

dimension of larger diagonal 'd_{1eff}', smaller diagonal 'd_{2eff}' and height 'h_{eff}'. Figure 4.8 shows how these effective dimensions of the new Rhombic DRA vary with different values of permittivity ϵ_r and aspect ratio 'd_1/h' of the DRA geometry. The curves are plotted accordingly to fit with empirical formulae deciding the resonant frequency of the identified modes, which are expressed separately for $(\mathrm{TE}_n)^y$ and $(\mathrm{TE}_n)^x$ modes as;

$$f_{(TE_n)^y} = \frac{c}{2\pi\sqrt{\epsilon_r}}\sqrt{\left(\frac{n\pi}{d_{1eff}}\right)^2 + \left(\frac{\pi}{a}\right)^2 + \left(\frac{\pi}{2h_{eff}}\right)^2} \tag{4.1}$$

$$f_{(TE_n)^x} = \frac{c}{2\pi\sqrt{\epsilon_r}}\sqrt{\left(\frac{\pi}{a}\right)^2 + \left(\frac{n\pi}{d_{2eff}}\right)^2 + \left(\frac{\pi}{2h_{eff}}\right)^2} \tag{4.2}$$

where 'n' is the order of $(\mathrm{TE}_n)^y$ and $(\mathrm{TE}_n)^x$ modes.

The curves of effective dimensions provide information about how the effective values change and fit to their best to the behavior of Rhombic DRA. To obtain the value at each point on these curves, a procedure has been followed. As d_{1eff} and h_{eff} are simultaneously varying for $f_{(TE_n)^y}$, the d_{1eff}/d_1 value is appropriately found for corresponding value of h_{eff}/h, for a particular value of ϵ_r and corresponding resonant frequency of the Rhombic DRA, which is identified through Eigen mode as well as fullwave EM simulations. This procedure has been repeated for different ϵ_r values and d_1/h ratios of the Rhombic DRA, to know the variation of d_{1eff}/d_1 and corresponding variation of h_{eff}/h. Considering these variations, the method is extended to identify the variation of d_{2eff}/d_2 for such DRAs, with different values of ϵ_r and d_1/h ratios. The effective values d_{1eff} and d_{2eff} can be expressed as a function of ϵ_r only, whereas the height h_{eff} is found to rely both on ϵ_r and d_1/h ratio. The closed form expressions for the effective values of the dimensions are found through curve fitting approximation, as follows:

$$d_{1eff} = d_1 \times 0.2671e^{-0.1736\epsilon_r}(1 + 2.7466e^{0.18316\epsilon_r}) \tag{4.3}$$

$$d_{2eff} = d_2 \times 0.1863e^{-0.1724\epsilon_r}(1 + 4.7037e^{0.17734\epsilon_r}) \tag{4.4}$$

$$h_{eff} = h \times [0.998 + (3.686 \times 10^{-5}\epsilon_r^{1.399} - 0.04923) \times e^{\frac{d_1}{h}(2.234-0.435\epsilon_r)(3.759+\epsilon_r)^{-1}}] \tag{4.5}$$

The resonant frequencies of $(\mathrm{TE}_n)^y$ and $(\mathrm{TE}_n)^x$ modes can be calculated by substituting d_{1eff}, d_{1eff} and h_{eff} values calculated from Equations (4.3) (4.4) (4.5) in Equation (4.1) and Equation (4.2). Since the calculated resonant frequencies are close to the resonant frequencies obtained through full

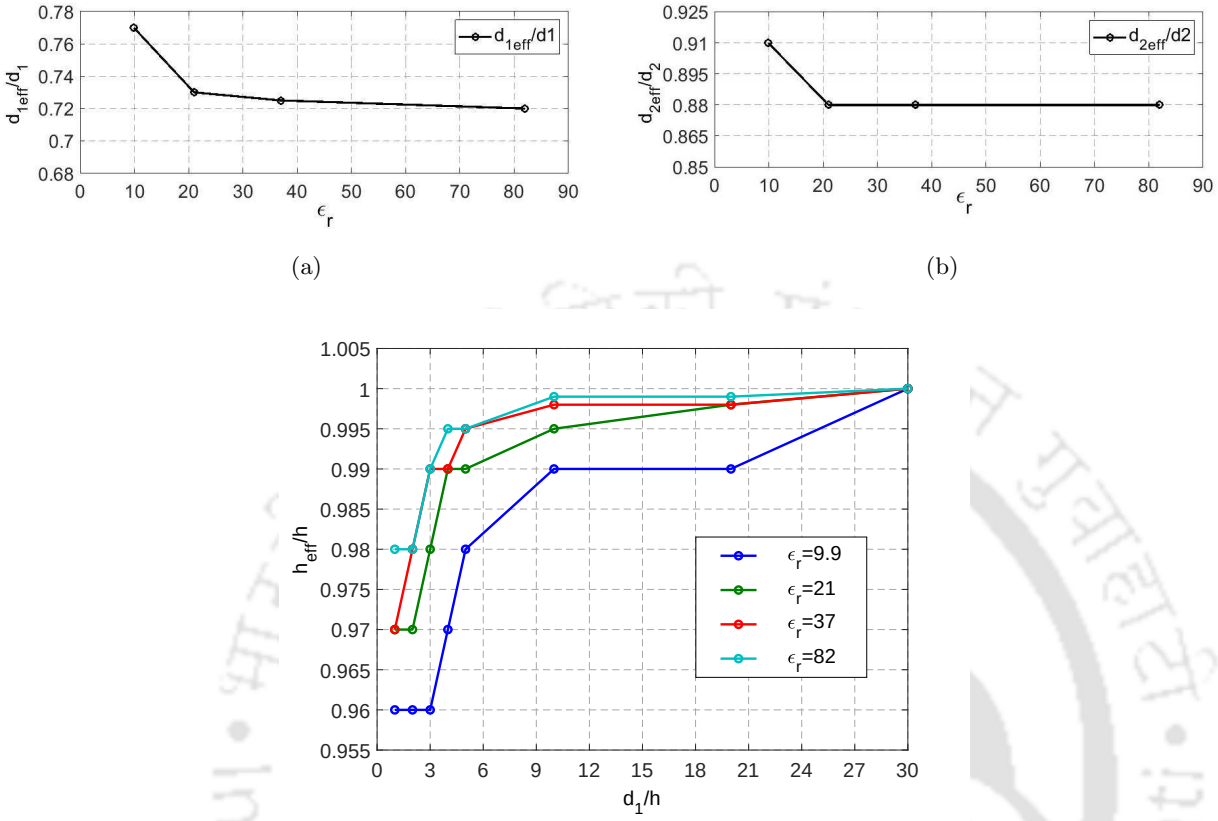

Figure 4.8: (a) Variation of d_{1eff}/d_1 with respect to ϵ_r, (b) variation of d_{2eff}/d_2 with respect to ϵ_r and (c) variation of h_{eff}/h with d_1/h ratio for different ϵ_r values.

wave simulation of the DRAs, the Equations (4.1) (4.2) (4.3) (4.4) (4.5) will be very useful for initial design of such Rhombic DRAs for wide range of d_1/h ratios ($1 \leq d_1/h < 30$) and dielectric values ($9 < \epsilon_r \leq 82$). This approximate expression can predict the resonant frequency of TE modes excited inside a Rhombic DRA upto n=3 and within 6% error from the simulated values. The Table 4.2 shows comparison of empirical value of resonant frequency of the dominant and a few of the higher order TE modes excited inside our proposed Rhombic DRA, having dimensions a=25 mm, h=14.43 mm and ϵ_r=9.9, along with their simulated and measured resonant frequencies. All the empirical resonant frequency values of the excited modes are within 6% error from the simulated value. However, in the case of measured resonant frequency value of $(TE_2)^y$ mode, a small deviation is observed. This is because of the small error introduced in the empirical formulae as well as the small shift in measured resonant frequency due to fabrication tolerances.

Table 4.2: Resonant frequency of various modes of the Rhombic DRA with a=25 mm, h=14.43 mm and ϵ_r=9.9

Excited modes	Resonant frequency				% Error between empirical and simulated resonant frequency		% Error between measured and empirical resonant frequency
	Simulations		Empirical formula (GHz)	Measured (GHz)	HFSS	CST	
	HFSS (GHz)	CST (GHz)					
$(TE_1)^y$	2.78	2.7926	2.86	2.88	2.87	2.41	0.699
$(TE_1)^x$	3.18	3.16	3.24	3.196	1.88	2.53	-1.3
$(TE_2)^y$	3.8093	3.806	3.632	3.89	-4.65	-4.57	7.1
$(TE_3)^y$	4.7911	4.8116	4.6365	4.83	-3.22	-3.63	4.17
$(TE_2)^x$	5.0134	5.025	4.7468	5.03	-5.31	-5.53	5.96
$(TE_3)^x$	6.3164	6.3775	6.5198	6.20	3.22	2.23	-4.9

4.4 Feeding techniques

Now we will look into the feeding techniques that can be used to excite the possible modes inside Rhombic DRA. The Rhombic DRA can be excited using a conventional coaxial probe feed. The feed is placed at the corner of one of diagonal of the DRA. The dominant $(TE_1)^y$ mode is excited by *Type-I* feeding technique, where the coaxial feed is placed at the corner of larger diagonal d_1 as shown in Figure 4.9(a) below. All the set of $(TE_n)^y$ and $(TE_n)^x$ modes can be excited inside the Rhombic DRA using the *Type-I* feeding technique. However, drilling inside the DRA at appropriate position is required to place the feed to bring enough coupling with the fields inside the DRA. The drilling can be avoided by using aperture coupling, stripline feeding and other conventional methods used in the literature for the excitation of DRAs. It is to be noted that, the drilling in case of *Type-I* feeding can be avoided by placing the probe just outside the periphery, in the vicinity of the corner of the Rhombic shaped DRA, as shown in Figure 4.10(b).

Apart from *Type-I* feeding, two other feeding techniques can be used to excite selected modes inside the DRA. Feeding at the geometric center of the DRA which we referred as *center feeding* as shown in Figure 4.9(b) can be used to excite $(TE_2)^y$ and $(TE_2)^x$ modes. It is to be noted that the *center feeding* will excite both $(TE_2)^y$ as well $(TE_2)^x$ modes; however, their corresponding *Type-I* feeding will excite either $(TE_2)^y$ or $(TE_2)^x$ mode based on the feed position. Another feeding technique that we referred to as *Type-II* feeding excites the DRA along the diagonals at a distance of $\sim d_1/3$ or $\sim d_2/3$ to generate $(TE_3)^y$ and $(TE_3)^x$x modes, respectively. The schematic diagram of *Type-II* feeding to excite $(TE_3)^y$ mode is shown in Figure 4.9(c).

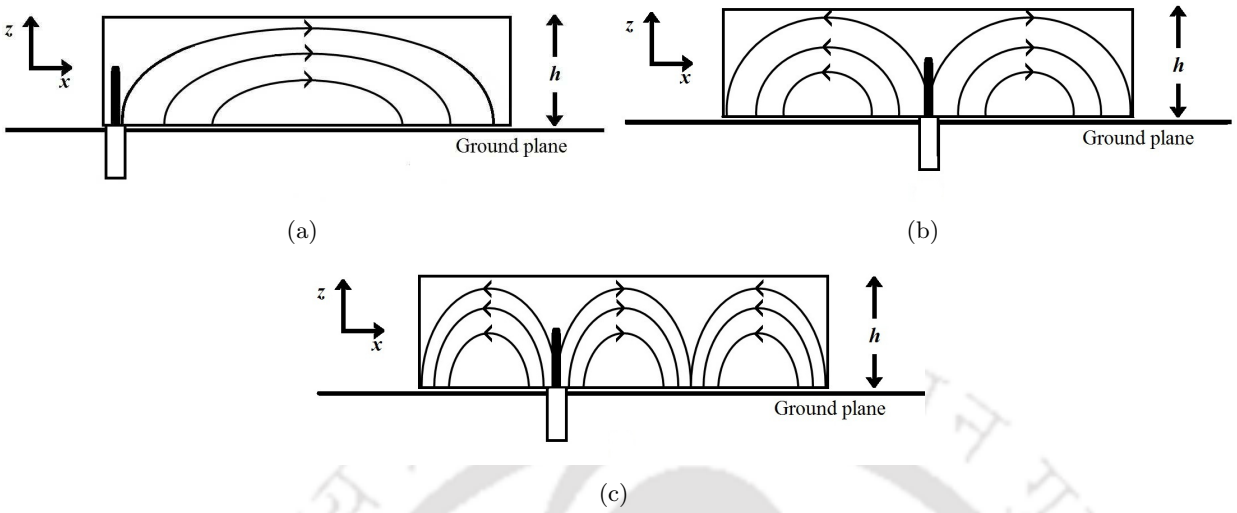

Figure 4.9: Feeding techniques: (a) *Type-I* feeding (b) *center* feeding and (c) *Type-II* feeding.

4.5 Practical radiation characteristics of $(TE_n)^y$ and $(TE_n)^x$ modes of Rhombic DRA

Now, we discuss the practical radiation characteristics of these excited modes inside the Rhombic DRA. We consider a Rhombic DRA of side a=25 mm. An aspect ratio of d_1/h=3 is assumed for convenience, so that height of the DRA becomes h=14.43 mm. A dielectric material of 99.7% alumina having dielectric constant value ϵ_r=9.9 is chosen. The resonant frequency of the dominant mode and a few of the higher order TE modes which are excited in this Rhombic DRA are calculated using Equations (4.1) (4.2) (4.3) (4.4) (4.5). This is summarized and shown in Table 4.2. These modes are excited using the corner feeding technique as shown in Figure 4.10. The nature of radiation patterns of the excited modes are studied by performing simulations using commercial EM simulation software, HFSS and CST Microwave Studio. However, as a representative plot we present only the simulated radiation patterns using HFSS. Measured radiation patterns are also presented for a fabricated prototype of the proposed Rhombic DRA and compared with their corresponding simulated data.

4.5.1 Characteristics of $(TE_1)^y$ mode operation

The resonant frequency of $(TE_1)^y$ mode using CST and HFSS simulations are found as 2.7926 GHz and 2.78 GHz, while theoretically calculated resonant frequency is 2.86 GHz. Pattern of H-field distributed in the DRA is similar to $TE^y_{1\delta1}$ mode in the Rectangular DRA. This field distribution is equivalent to an horizontal magnetic dipole that exhibit radiation characteristics which are broad in

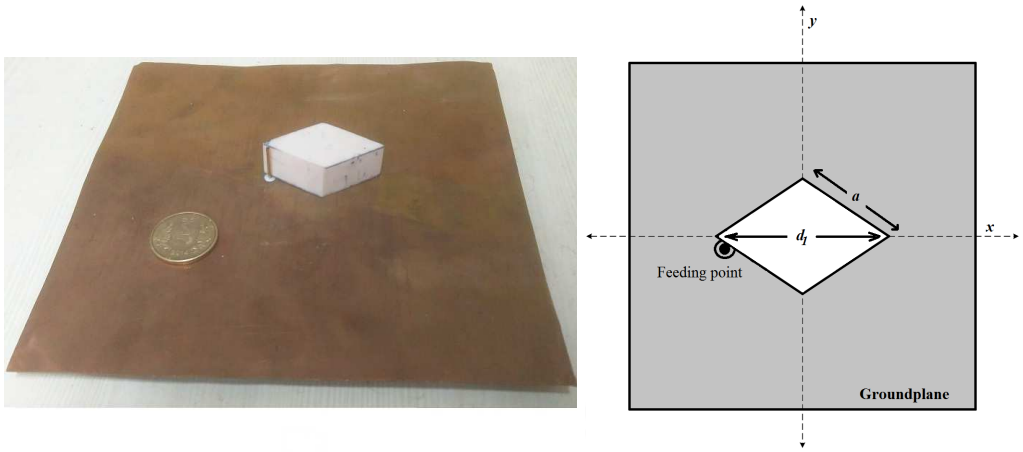

(a) (b)

Figure 4.10: (a) Fabricated prototype of the Rhombic DRA and (b) schematic diagram of the feeding method to excite $(TE_1)^y$ mode in a Rhombic DRA.

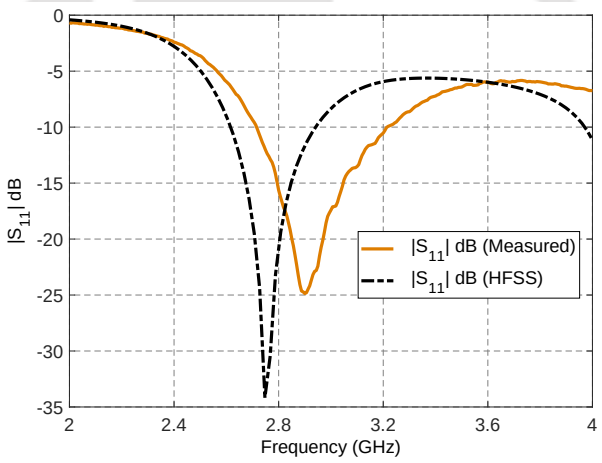

Figure 4.11: $|S_{11}|$ of the proposed Rhombic DRA excited with $(TE_1)^y$ mode.

nature, as mentioned in [39]. Similar radiation characteristics are obtained through CST as well as HFSS simulations. A maximum gain of 7.1 dB and 7.36 dB are obtained respectively from CST and HFSS simulations. The prototype of the proposed Rhombic DRA is fabricated and the same is shown in Figure 4.10(a). The DRA is excited at the vicinity of one of the corners of the DRA containing the diagonal d_1 (as shown in Figure 4.10(b)). The feed is placed outside the DRA as it is difficult to practically drill at the sharp corner of the DRA geometry. The measured resonant frequency occurs near to 2.88 GHz, which remain close to the theoretically calculated value of 2.86 GHz. The $|S_{11}|$ plot of the Rhombic DRA excited with this mode is presented in Figure 4.11. The radiation pattern obtained through measurements at different azimuth planes are shown in Figure 4.12. Both measured and simulated radiation characteristics have similar pattern. The measured gain is obtained as 6.735 dB.

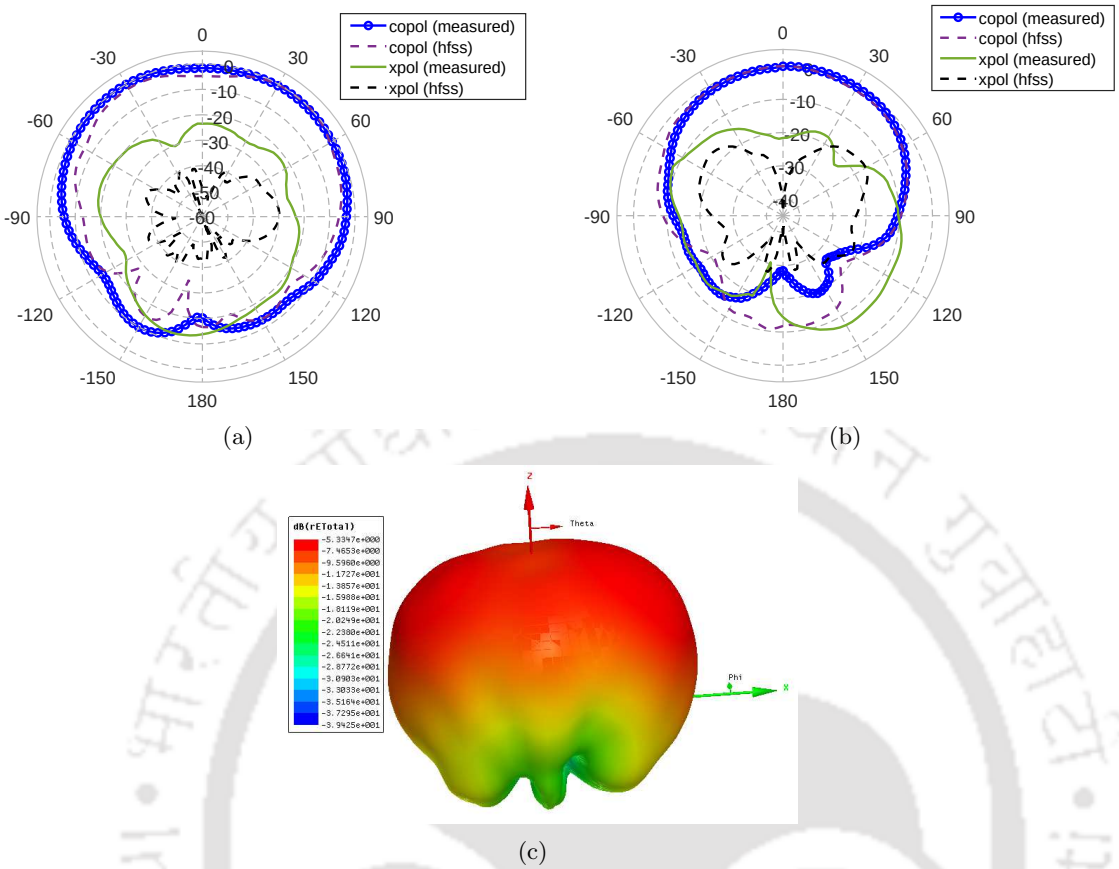

Figure 4.12: Radiation patterns of $(TE_1)^y$ mode at (a) $\phi = 0^0$ (E-plane) and (b) $\phi = 90^0$ (H-plane) (c) 3-D pattern.

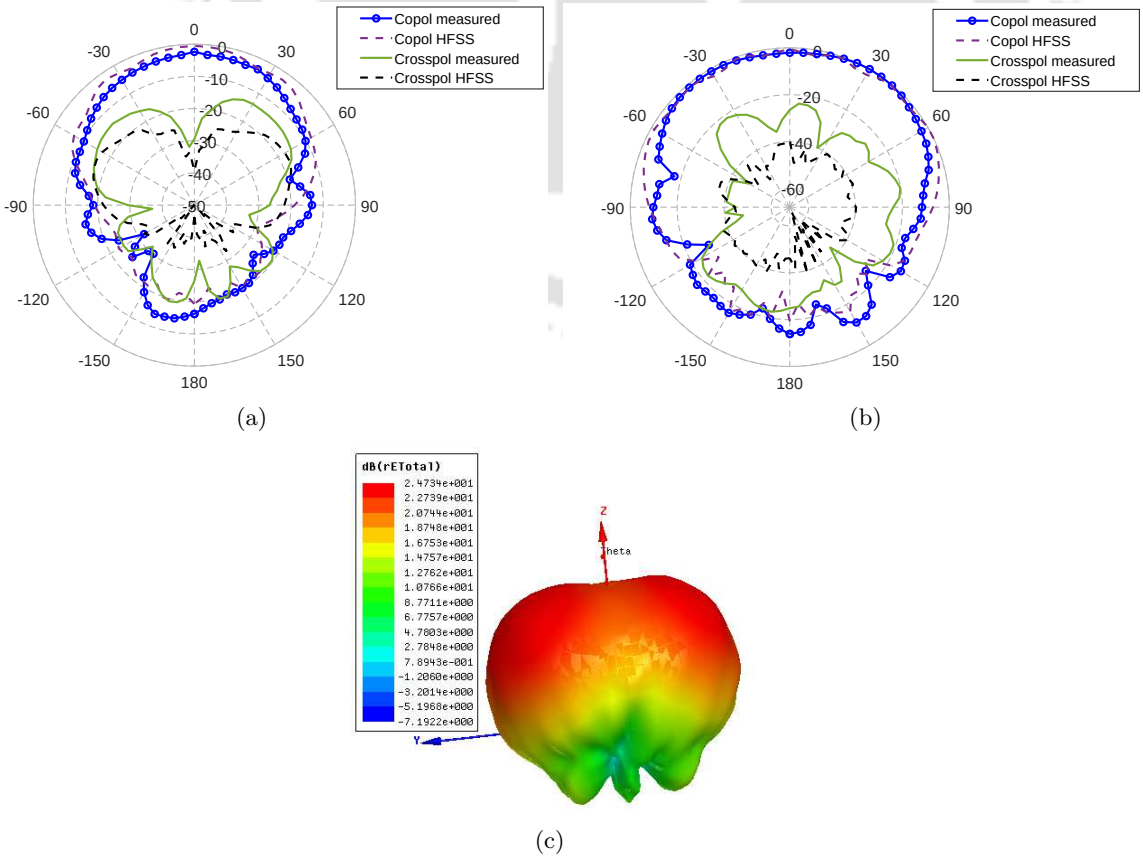

Figure 4.13: Radiation patterns of $(TE_1)^x$ mode at (a) $\phi = 0^0$ (H-plane) and (b) $\phi = 90^0$ (E-plane) (c) 3-D pattern.

4.5.2 Characteristics of $(TE_1)^x$ mode operation

The $(TE_1)^x$ mode is excited by placing the feed at the corner of a Rhombic DRA containing the diagonal d_2. The resonant frequency of this excited mode using CST and HFSS simulations are found to occur at 3.16 GHz and 3.18 GHz as compared to theoretically calculated value of 3.24 GHz. The measured resonant frequency is obtained 3.196 GHz. The radiation characteristics of $(TE_1)^x$ will be similar to $TE^x_{\delta 11}$ mode excited inside a Rectangular DRA. They exhibit broad radiation characteristics like the dominant mode, which are shown in Figure 4.13 for different azimuth planes. A comparison of measured radiation pattern with the HFSS simulated pattern is also included in Figure 4.13. Similar patterns are observed through CST simulations as well; however, as a representative plot only HFSS simulated patterns are shown. Maximum gains of 6.43 dB and 6.426 dB are observed from the patterns obtained through CST and HFSS simulations, respectively. The measured gain is obtained 5.91 dB.

4.5.3 Radiation characteristics of higher order TE modes of Rhombic DRA.

4.5.3.1 Characteristics of $(TE_2)^y$ mode operation

The resonant frequencies of $(TE_2)^y$ mode are found to occur at 3.8093 GHz and 3.806 GHz using HFSS and CST simulations respectively. The theoretically calculated resonant frequency is found to occur around 3.632 GHz. The measured resonant frequency is obtained 3.89 GHz. The $(TE_2)^y$ mode is similar to $TE^y_{2\delta 1}$ mode in the Rectangular DRA which exhibit radiation characteristics that are omni-directional in nature. The simulated radiation pattern of the $(TE_2)^y$ mode also exhibit similar radiation characteristics. This is shown in Figure 4.14. The measured pattern is also included in the same figure, which follows the simulated pattern. The peak gain is obtained as 7.18 dB and 7.78 dB through HFSS and CST simulations, respectively. A gain of 6.96 dB is obtained through measurements.

4.5.3.2 Characteristics of $(TE_2)^x$ mode operation

The nature of radiation pattern of $(TE_2)^x$ mode is similar to $TE^x_{\delta 21}$ mode excited in rectangular DRA. The theoretically calculated resonant frequency of $(TE_2)^x$ mode is obtained 4.7468 GHz. The resonant frequencies are obtained 5.0134 GHz and 5.025 GHz through HFSS and CST simulation are summarized in Table 4.2. Resonant frequency is obtained 5.03 GHz through measurements. The radiation patterns of $(TE_2)^x$ mode are similar to that of $(TE_2)^y$ mode. Therefore, as a representative plot only the simulated patterns of $(TE_2)^x$ mode obtained using HFSS are presented, as shown in

Figure 4.15. The radiation pattern obtained using CST simulation are also observed in agreement with the corresponding simulated pattern using HFSS, for the two azimuth planes. The simulated peak gain is obtained 10.037 dB and 8.87 dB through HFSS and CST simulations, respectively.

4.5.3.3 Characteristics of $(TE_3)^y$ mode operation

For the fabricated Rhombic DRA of Figure 4.10(a), the resonant frequency of $(TE_3)^y$ mode is obtained 4.83 GHz, through measurements. The corresponding theoretical value is obtained 4.6365 GHz and through simulations, the resonant frequencies are obtained 4.7911 GHz and 4.8116 GHz using HFSS and CST, respectively. The radiation patterns of $(TE_3)^y$ mode in the two azimuth planes are shown in Figure 4.16. The measured patterns are also presented along with the simulated radiation pattern, for comparison. It is observed that the measured radiation pattern follows the corresponding simulated pattern. A peak gain of 7.68 dB and 6.62 dB are obtained through simulations using HFSS and CST, respectively. The measured gain is obtained 6.09 dB.

4.5.3.4 Characteristics of $(TE_3)^x$ mode operation

The theoretically calculated resonant frequency of $(TE_3)^x$ mode excited inside the fabricated prototype of the proposed Rhombic DRA is obtained 6.5198 GHz. A resonant frequency of 6.3164 GHz and 6.3775 GHz are obtained, respectively through simulations performed using HFSS and CST. The $(TE_3)^x$ mode exhibit similar radiation characteristics as that of $(TE_3)^y$ mode excited in a Rhombic DRA. Therefore, as a representative plot we present only the simulated radiation patterns of this excited mode obtained through HFSS. However, it is observed that the radiation pattern of the $(TE_3)^x$ mode obtained through CST simulation are in agreement with the corresponding pattern obtained through HFSS simulation. The simulated radiation pattern using HFSS in the two azimuth planes are shown in Figure 4.17. A peak gain of 10.44 dB and 11.3 dB are obtained using HFSS and CST simulation, respectively.

4.6 Low profile Rhombic DRA: Resonant frequency and Radiation characteristics

In the previous section we presented the dominant and few of the higher order TE modes that are excited inside a Rhombic DRA. Closed form expressions for calculating the resonant frequency of such modes are obtained separately for x- and y-polarized fields. The radiation characteristics of these

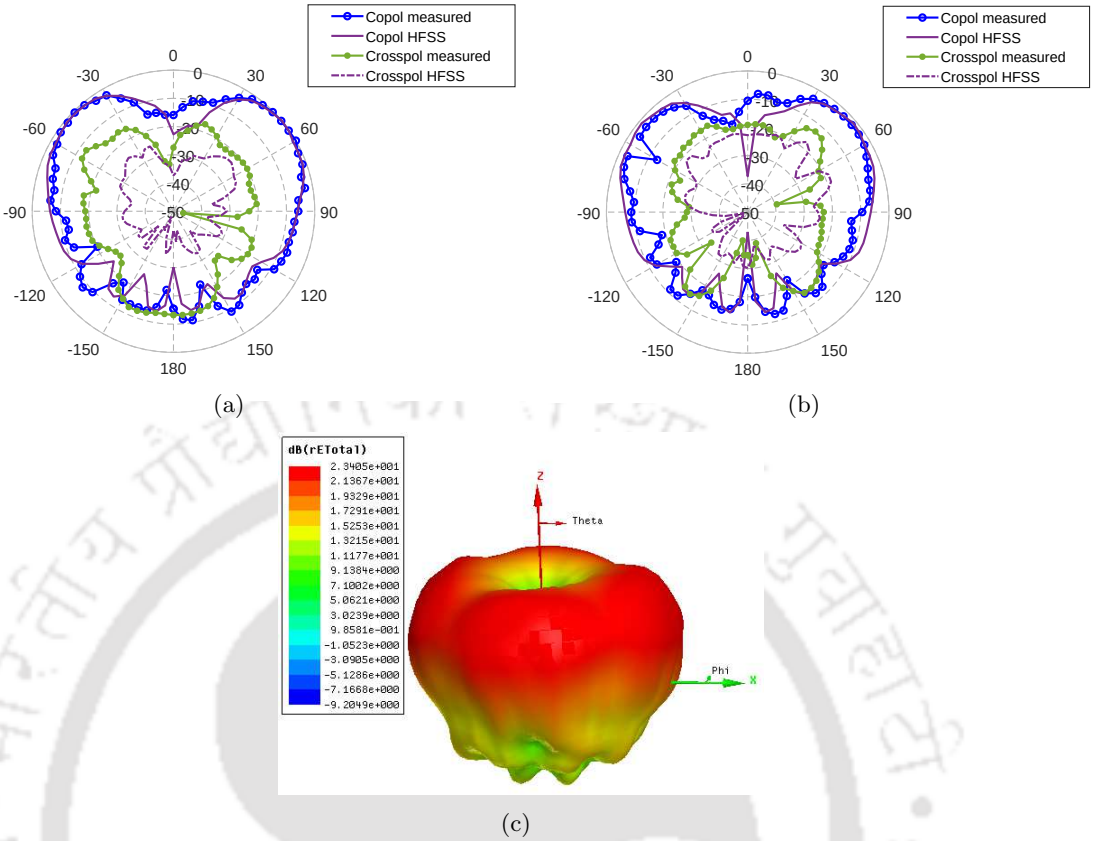

Figure 4.14: Radiation patterns of $(TE_2)^y$ mode at (a) $\phi = 0^0$ (E-plane) and (b) $\phi = 90^0$ (E-plane) (c) 3-D pattern.

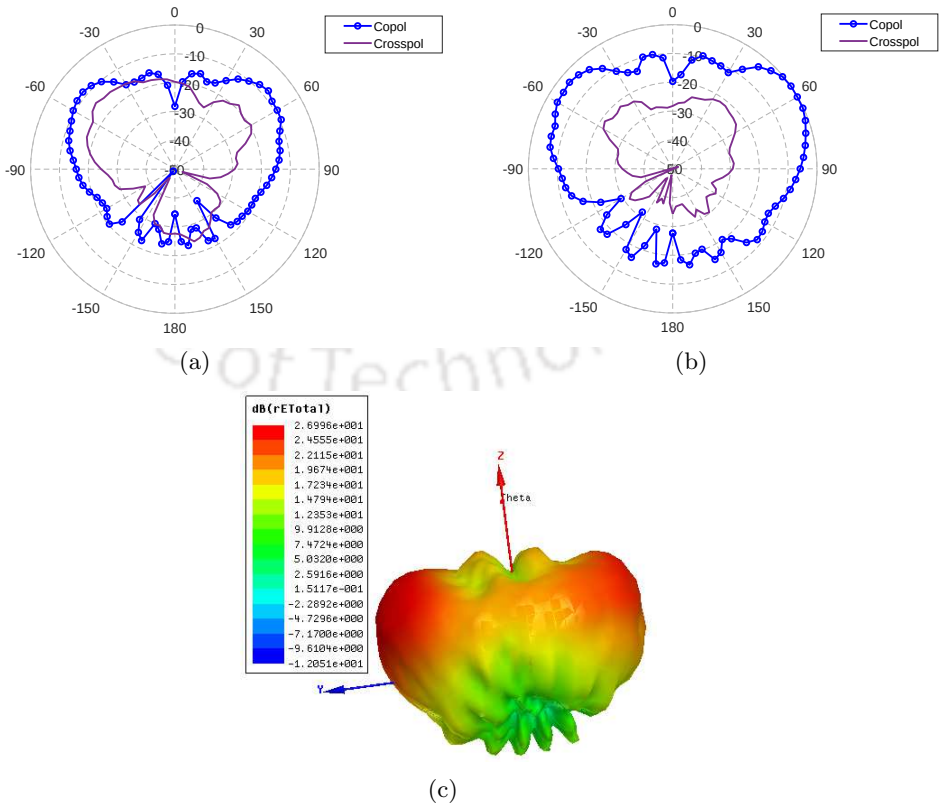

Figure 4.15: Radiation patterns of $(TE_2)^x$ mode obtained using HFSS simulation at (a) $\phi = 0^0$ (E-plane) and (b) $\phi = 90^0$ (E-plane) (c) 3-D pattern.

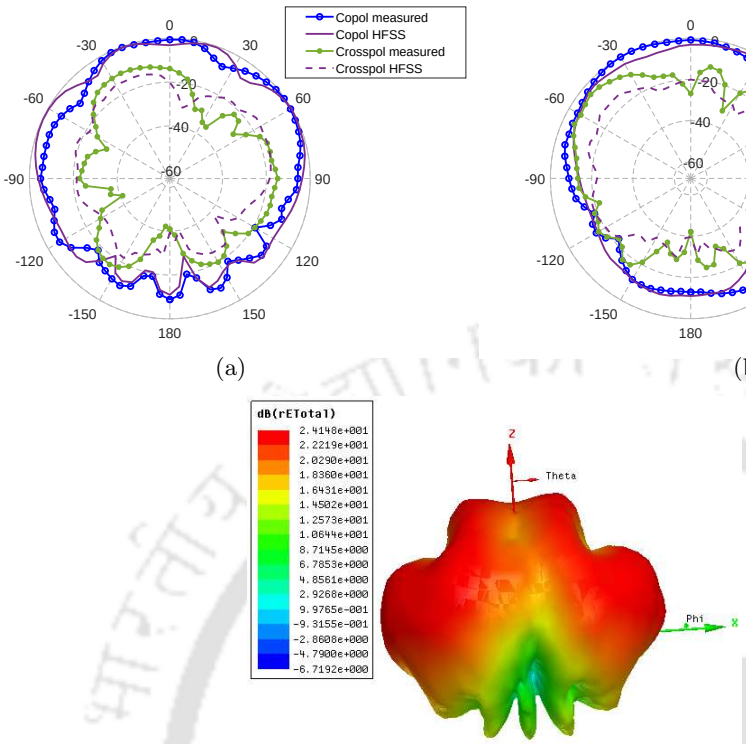

Figure 4.16: Radiation patterns of $(TE_3)^y$ mode at (a) $\phi = 0^0$ (E-plane) and (b) $\phi = 90^0$ (H-plane) (c) 3-D pattern..

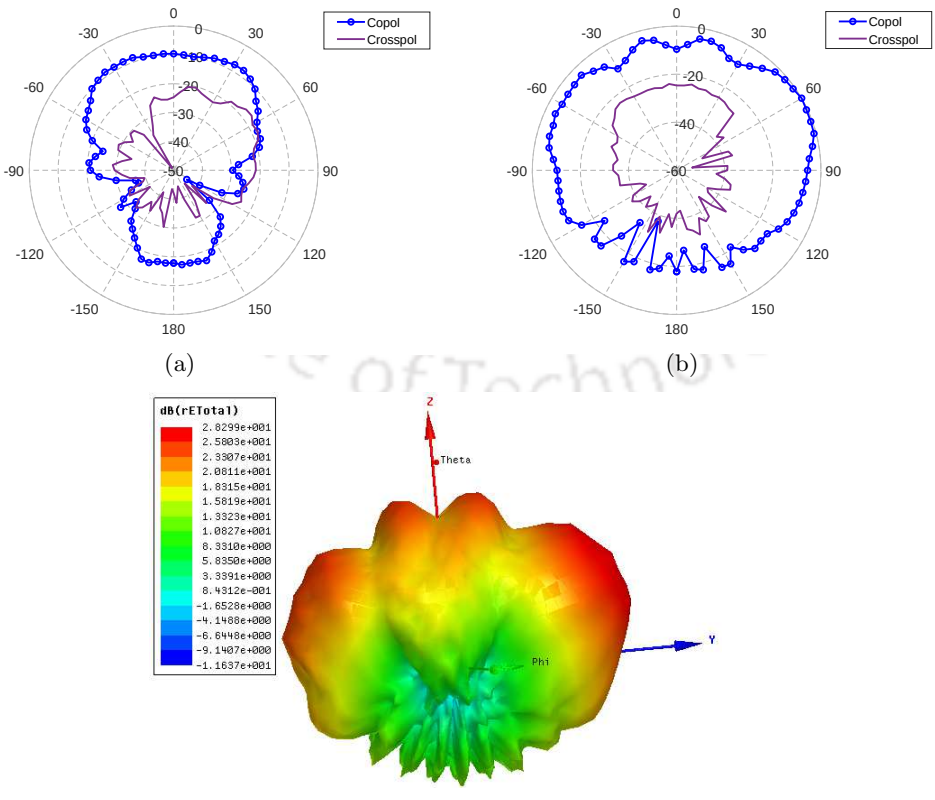

Figure 4.17: Radiation patterns of $(TE_3)^x$ mode obtained using HFSS simulation at (a) $\phi = 0^0$ (H-plane) and (b) $\phi = 90^0$ (E-plane)(c) 3-D pattern.

excited TE modes are also discussed and the corresponding practical observations are presented for a prototype of the fabricated Rhombic DRA. Now, we will discuss a special case of this DRA geometry, where the height h is very small compared to the diagonals d_1 and d_2(or $h << d_1$ and $h << d_2$).

We recall Equations (4.1) (4.2), given by;

$$f_{(TE_n)^y} = \frac{c}{2\pi\sqrt{\epsilon_r}}\sqrt{\left(\frac{n\pi}{d_{1eff}}\right)^2 + \left(\frac{\pi}{a}\right)^2 + \left(\frac{\pi}{2h_{eff}}\right)^2} \tag{4.6}$$

$$f_{(TE_n)^x} = \frac{c}{2\pi\sqrt{\epsilon_r}}\sqrt{\left(\frac{\pi}{a}\right)^2 + \left(\frac{n\pi}{d_{2eff}}\right)^2 + \left(\frac{\pi}{2h_{eff}}\right)^2} \tag{4.7}$$

For very small values of height h, the effective value of height for such DRA will be h_{eff}= h. In this configuration, the resonant frequency of the dominant and the higher order TE modes, becomes very close. This is because, the $(1/2h_{eff})$ term in the Equations (4.6) (4.7) dominates over the other terms in the expression. Therefore, in the case of $(TE_1)^y$ and $(TE_1)^x$ modes, the Equations (4.6) (4.7) can be further simplified to a single expression as;

$$f_{(TE_1)} = \frac{c}{2\pi\sqrt{\epsilon_r}}\left(\frac{\pi}{2h}\right) \tag{4.8}$$

Which means both $(TE_1)^y$ and $(TE_1)^x$ modes are expected to have same resonant frequency. This equation remains same and is valid for the calculation of resonant frequency of dominant mode of a low profile DRA of any cross section. The Equation (4.8), which is deduced from Equations (4.6) (4.7) is same as expression discussed in the literatures and presented in [40], for calculation of resonant frequency of the dominant mode excited in a low profile DRA.

For further clarity of the excited $(TE_1)^y$ and $(TE_1)^x$ modes in a low profile Rhombic DRA, a simulation study of a low profile Rhombic DRA is presented, which has a side a=35 mm, height h=2.5 mm and having ϵ_r=82. The full wave EM simulation study are carried out using Ansys HFSS software. The DRA is excited using microstrip line for both $(TE_1)^y$ and $(TE_1)^x$ modes. The resonant frequency of $(TE_1)^y$ and $(TE_1)^x$ modes are calculated using Equation (4.8). The theoretical resonant frequency is obtained 3.3 GHz for both $(TE_1)^y$ and $(TE_1)^x$ mode. The $|S_{11}|$ plot for both $(TE_1)^y$ and $(TE_1)^x$ modes are shown in Figure 4.18(a) and Figure 4.18(b), respectively. It is observed that, the simulated values of the resonant frequency for both the modes are observed below their corresponding theoretical value. The lowering of simulated value of the resonant frequency from their corresponding theoretical value is due to fringing fields which makes the effective height of the DRA slightly higher (of

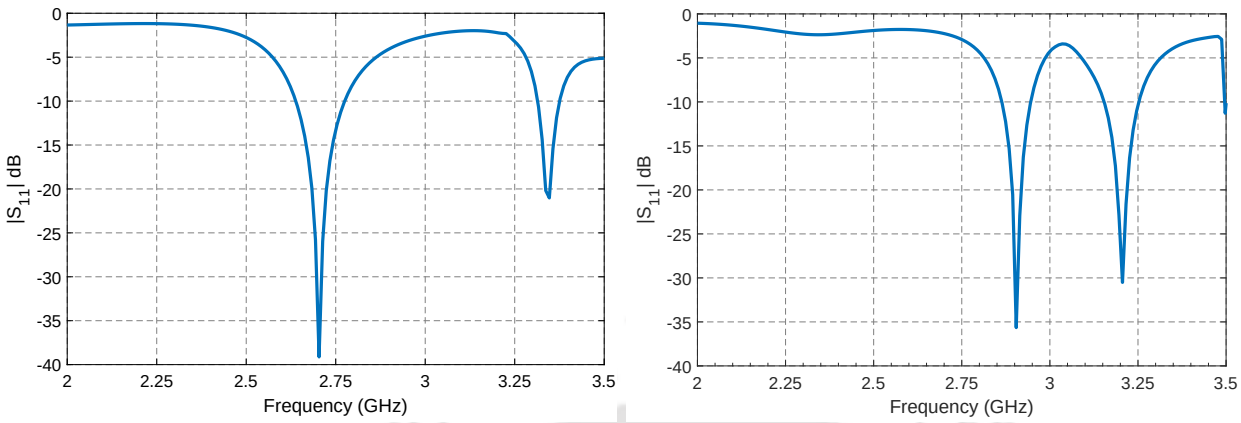

Figure 4.18: $|S_{11}|$ of (a) $(TE_1)^y$ and (b) $(TE_1)^x$ mode for a low profile Rhombic DRA of a=35 mm, h=2.5 mm and ϵ_r=82.

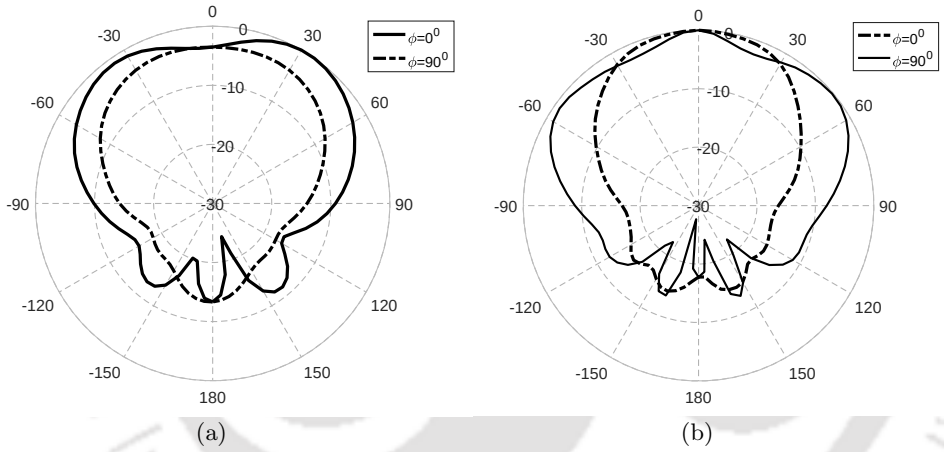

Figure 4.19: Radiation pattern of (a) $(TE_1)^y$ and (b) $(TE_1)^x$ mode for a low profile Rhombic DRA of a=35 mm, h=2.5 mm and ϵ_r=82.

the order of a fraction of millimeter) than their actual value of height. The radiation characteristics of both the modes are found broad in nature, as shown in Figure 4.19(a) and Figure 4.19(b) for $(TE_1)^y$ and $(TE_1)^x$ modes, respectively. Both the modes are providing nearly same peak realized gain of 4.22 dB, through simulations.

A preliminary investigation on a low profile Rhombic DRA is presented in this chapter. However, a detailed investigation on the performance characteristics of this geometry of the DRA, is kept as a future scope for the research carried out and presented in this thesis.

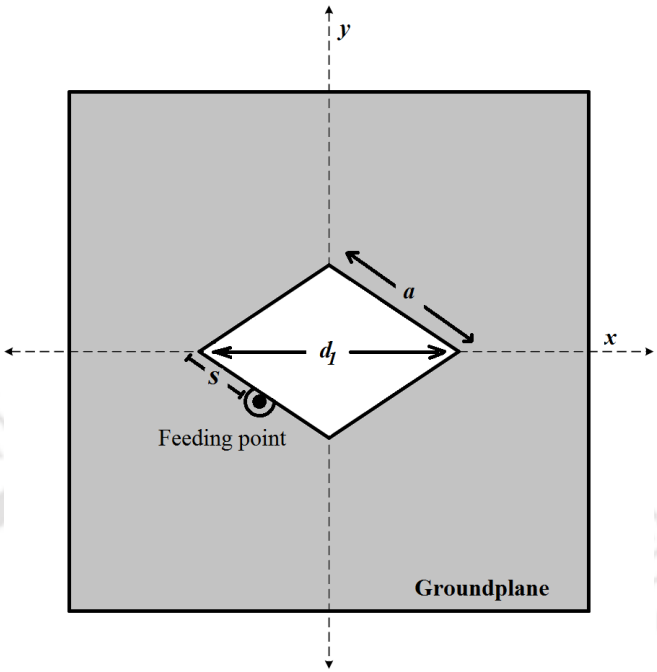

Figure 4.20: Feed configuration for exciting wideband Rhombic DRA

4.7 Design and Excitation of wideband Rhombic DRA

We observed that placing the feed at one end of either of the diagonals of a Rhombic DRA gives linearly polarized $(\mathrm{TE}_n)^y$ or $(\mathrm{TE}_n)^x$ mode. For wideband operation of the Rhombic DRA, the basic idea is to excite both $(\mathrm{TE}_1)^y$ and $(\mathrm{TE}_1)^x$ modes using a single feed, which is achieved by placing the feed near any side of the DRA. We therefore place the feed near (but not at) the center of one of the sides of the Rhombic DRA as shown in Figure 4.20, so that both these modes get excited. It may be noted that by adopting this feeding technique, drilling of hole inside the DRA is avoided. Further, separation of the resonant frequencies of the two modes are determined mainly by the corresponding diagonal distances d_1 and d_2. We keep the dimensions of the DRA and ε_r same as before so that the resonant frequency of $(\mathrm{TE}_1)^y$ and $(\mathrm{TE}_1)^x$ modes does not change. The feed position and the feed height are optimized through HFSS as well as CST simulations. The optimized position and height of the probe feed are identified through varying the feed position 's' along the sides of the DRA, and at each different position s, the height of the probe is fine-tuned to identify the best impedance matching for a wide range of frequencies.

4.7.1 Results and discussions

A wide impedance matching is observed, when the feed is placed at a distance of s= 13.5 mm along one of the sides, from the corner containing the diagonal d_1 of the Rhombic DRA. The variation of impedance matching at different probe heights for s= 13.5 mm obtained through HFSS simulation is shown in Figure 4.21. However, for the probe height of 14 mm, we achieved the best impedance matching over a wide range of frequencies; hence, we choose this feed height as the optimized value. The broad impedance bandwidth obtained with this configuration of the proposed Rhombic DRA is shown in the $|S_{11}|$ plot of Figure 4.22. It can be observed that the bandwidth obtained in actual measurement for this prototype is higher than the bandwidth observed through HFSS and CST simulations. The difference in the bandwidth may be due to the change in material properties at higher frequencies, which has not been accounted in the simulation, as in the simulation study dielectric constant and the loss tangent values are assumed constant. This may be one of the reasons for the observed change along with other factors such as dimensional accuracy of the fabricated device, effect of conducting plate where the antenna is mounted, and fixing of probe. However, both simulation and measurement results reflect the nature of response that was expected from the proposed antenna for this feeding condition. Similar effects are observed in the return loss around the resonant frequency of $(TE_1)^y$ mode, as shown in Figure 4.11. The measured impedance bandwidth of the fabricated prototype of the proposed DRA is nearly 1 GHz. The bandwidth obtained through commercial simulators is approximately 760 MHz. The nature of radiation characteristics of the antenna at two frequencies (2.9 GHz and 3.45 GHz) within the impedance bandwidth, where measured results show better matching are shown in Figure 4.23. The radiation patterns are broad in nature at both the frequencies. The measured and simulated radiation plots follow similar patterns however, backlobe radiations are slightly higher in the measured patterns. It may be noted that the measurements are carried out under normal laboratory conditions. The gain measured at 2.9 GHz and 3.45 GHz are respectively, 4.3 dB and 6.3 dB, and their corresponding simulated values using HFSS are obtained 6.01 dB and 7.22 dB, respectively. An empirical formula for finding the gain from the radiation pattern described in [242] and detailed in Appendix B, is also used to validate the simulated and measured gain values at these frequencies. The calculated values of gain are 4.77 dB and 6.642 dB, respectively at 2.9 GHz and 3.45 GHz, when -3 dB beamwidth values are taken from the measured pattern. The Figure 4.24 shows the variation of gain along the impedance bandwidth for both the simulations and measurements.

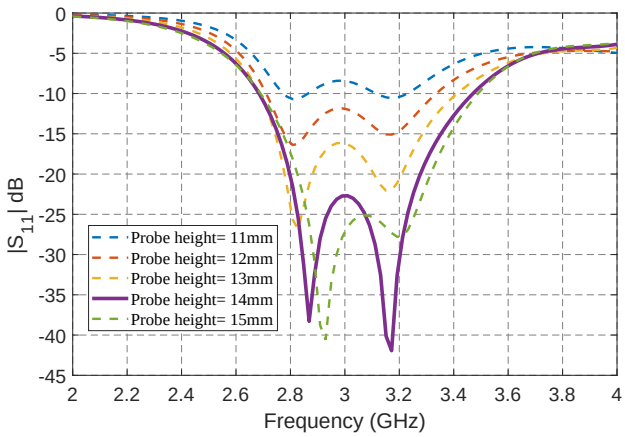

Figure 4.21: Variation of $|S_{11}|$ of wideband Rhombic DRA for different probe heights.

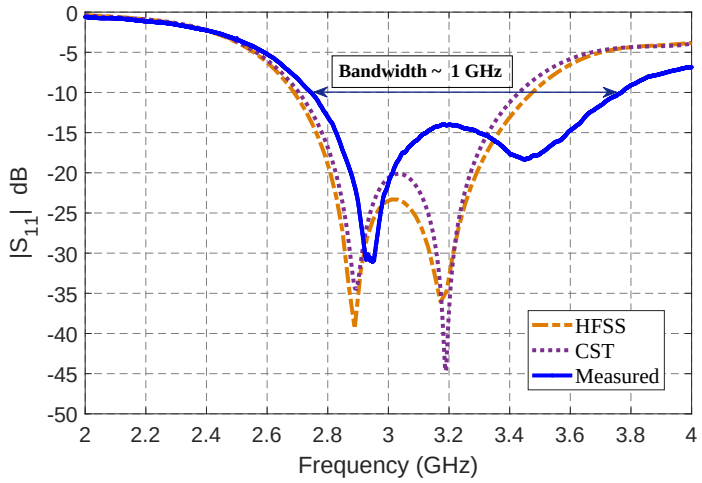

Figure 4.22: $|S_{11}|$ of wideband Rhombic DRA

4.7.2 Performance comparison with existing DRAs in the literature

A comparison of the proposed DRA with some of the reported simple wideband DRAs in the literature are shown in Table 4.3. The proposed Rhombic DRA has either slightly improved or comparable percentage bandwidth with these reported DRAs in the literature. Moreover, the highlight of our proposed DRA is its compact design covering significantly smaller volume. Further, the proposed DRA is well compact compared to hemispherical DRA in [243] and rectangular DRA in [244] which are having higher dielectric values and even operated at slightly higher frequency with respect to the operating frequency of our proposed antenna. In [233], a rhombic DRA, which a variant of square DRA, formed by rotation of square DRA, has a percentage bandwidth of 26.8%. However, our proposed Rhombic DRA is geometrically different, providing a percentage impedance bandwidth of 31.64%.

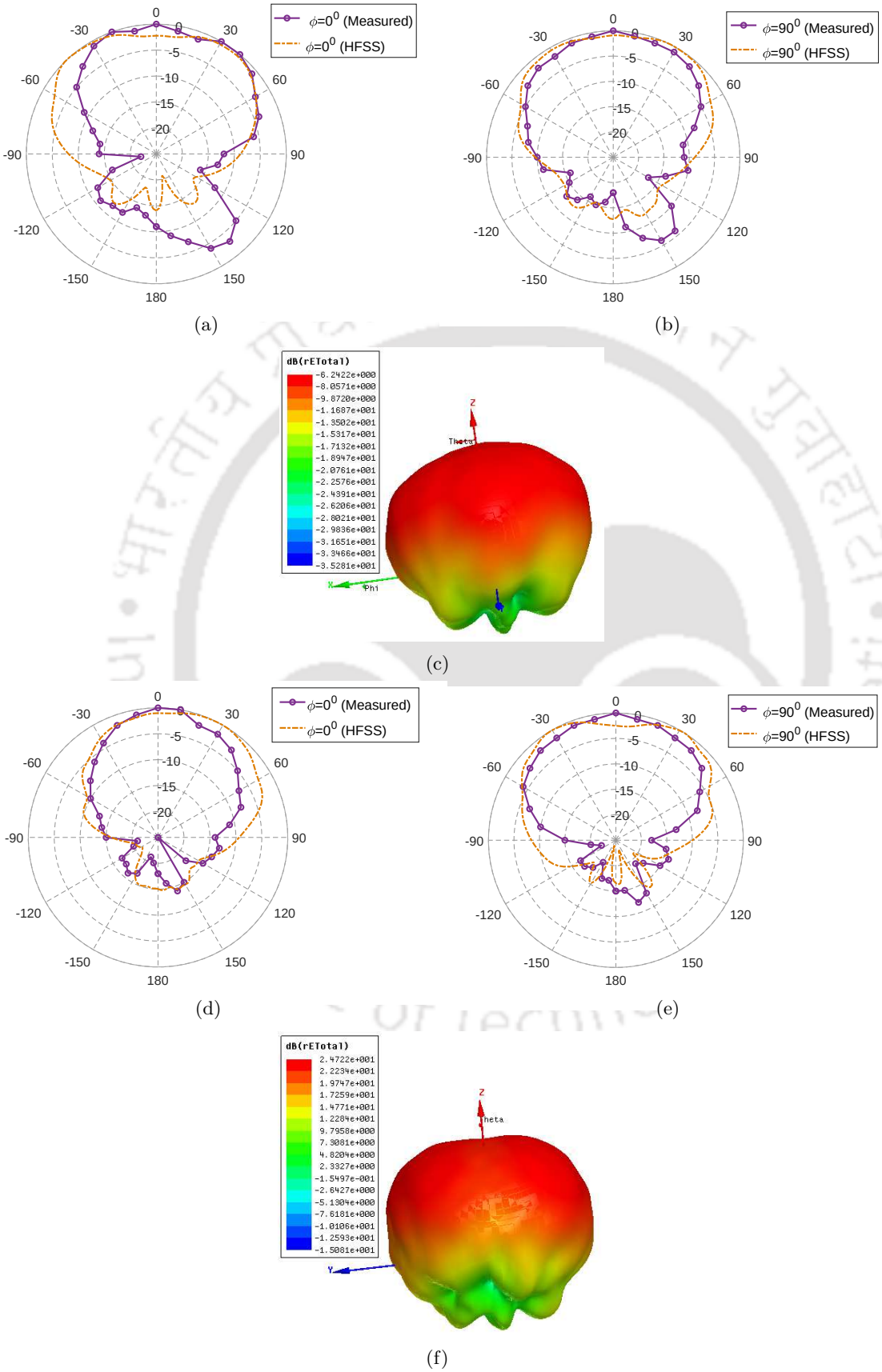

Figure 4.23: Radiation patterns of the wideband Rhombic DRA at (a) $\phi = 0^0$ (E-plane) at 2.9 GHz, (b) $\phi = 90^0$ (H-plane) at 2.9 GHz, (c) 3-D pattern at 2.9 GHz (d) $\phi = 0^0$ (H-plane) at 3.45 GHz and (e) $\phi = 90^0$ (E-plane) at 3.45 GHz (f) 3-D pattern at 3.45 GHz

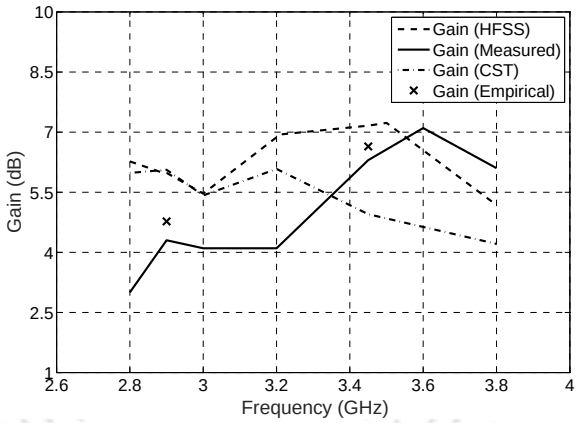

Figure 4.24: Variation of gain over the bandwidth

Table 4.3: Comparison of percentage bandwidth and size of the proposed DRA with reported wideband DRAs in the literature

Ref.	ϵ_r	DRA shape	Modes	Volume (cm^3)	% Bandwidth	Center frequency (GHz)
[233]	10	Rectangular	TE^x_{111}, TE^y_{111}	3.125	26.8%	5.89
[243]	10	Hemisphere	$HEM_{11\delta}$, $TM_{10\delta}$	16.75	30%	3.5
[244]	12	Rectangular	TE^x_{121}, TE^y_{211}	21.6	28.73%	3.55
[72]	12	Conical	$HEM_{11\delta}$, $TM_{01\delta}$	40.63	21%	1.54
[125]	4.5	Frustum	-	91.63	34%	2.94
Proposed	**9.9**	**New Rhombic**	**$(TE_1)^y$, $(TE_1)^x$**	**7.8124**	**31.64%**	**3.255**

The Table 4.4 shows comparison of the proposed Rhombic DRA with a recently reported wideband design using equilateral triangular DRA [65]. The percentage bandwidths are almost comparable however, the new Rhombic DRA achieved better gain in the overlapping operational bandwidth when compared with the wideband equilateral triangular DRA. Both the DRAs overlap at an operational band of frequencies from 2.74 GHz to 3.1 GHz, in which the triangular DRA has a peak measured gain of 3.55 dB and the proposed wideband Rhombic DRA provides a peak measured gain of 4.3 dB. However, the Rhombic DRA can be operated within a wide impedance bandwidth from 2.74 GHz to 3.77 GHz, in which it provides a peak measured gain of 7.3 dB. The proposed design uses a simple coaxial probe excitation method and covers lesser volume compared to other reported DRAs operated at the nearby frequencies, which makes the design of this new wideband Rhombic DRA very simple and compact. The geometry of this proposed DRA is novel and to the best of knowledge of the authors, is not been reported so far.

4.8 Summary

In this chapter, we have presented a new rhombic DRA geometry. A few of the possible TE modes that are excited inside this DRA geometry are identified through eigen mode analysis with

Table 4.4: Comparison of gain of the proposed DRA with reported wideband DRA in the literature

Ref	ϵ_r	**DRA shape**	**volume (cubic mm)**	**bandwidth coverage**	**% bandwidth**	**Peak gain in the band (dBi)**
[65]	9.8	Triangular	12.47	2.23-3.1	32.64%	3.55
Proposed	9.9	New Rhombic	7.8124	2.74-3.77	31.64%	4.3

the aid of CST simulation. Suitable feeding techniques that can be used for exciting these modes are discussed. The identified TE modes were classified into $(TE_n)^y$ and $(TE_n)^x$ modes, and the empirical formulae for calculating the resonant frequencies of these modes are developed through curve-fitting approximation. The nature of radiation characteristics of these modes are also identified, and are presented to give insight on the behavior of these modes excited inside this proposed DRA. A prototype of the DRA is fabricated to verify the measured resonant frequency and radiation characteristics of $(TE_n)^y$ and $(TE_n)^x$ modes with the simulated results obtained through HFSS. Appropriate position of the feed is also identified by proper fine-tuning, with the aid of HFSS simulation, to achieve a broad impedance bandwidth. The impedance bandwidth is obtained nearly 1 GHz through measurements. The variations of gain and nature of radiation patterns within the measured bandwidth are compared with the results obtained through HFSS simulations. The performance characteristics of the proposed wideband Rhombic DRA is also compared with the performance of other basic DRA geometries presented in the literature. A preliminary investigation on the special case of this DRA geometry with low profile configuration is also discussed, and the radiation characteristics of lowest x- and y-polarized TE modes are presented.

5

Investigation on Some Aspects of Dielectric Loaded Antennas

Contents

In the previous chapters, we discussed the application of ETDRAs and Rhombic DRAs as a dual-band and wideband antennas, respectively. The performance characteristics of these antennas are presented with a fabricated prototype and the practical observations are compared against their simulated results which are obtained through fullwave EM simulations carried out using Ansys HFSS. The performances of these proposed antennas are also compared with some of the practical DRAs which are reported in the literature. In the design of dual-band ETDRA presented in chapter 3, we noticed that, the performance of a DRA is effected by placing an adjust DRA which is operated at a different frequency. Such configuration introduces dielectric loading effect on the DRA from an adjacently placed DRA. Moreover, such effects also introduced many other challenges in various DRA designs that further degrades the overall antenna performance. However, the dielectric loading phenomena can also be utilized in the design of antennas favourably. As per literature, the phenomena of dielectric loading is basically utilized in reducing the antenna size [234]. However, we here present a detailed investigation on the concept of dielectric loading effect and how such a phenomenon is used to design a dual-band antenna.

This chapter presents[1] the investigation on some of the aspects of dielectric loaded antennas. The investigation focus on the effect of dielectric loading in the form of various geometry, size, volume and dielectric permittivity values over a rectangular monopole strip to operate as a dual-band antenna. A closed form expression is obtained relating the volume of the dielectric block and its dielectric constant for a specific upper operating band, when loaded over the rectangular monopole which is operated within the lower operating band of 2.4-2.5 GHz. The applicability of the relation is also demonstrated for different dielectric geometries and the cases where the deviations are observed are also highlighted.

5.1 Introduction

The research community have widely studied and thoroughly investigated the dielectric loading effect on the monopole antennas, for the last several decades. The survey on such antennas reveals that, even for the last two decades they remain as an active areas of research. The electromagnetic characteristics of a thick monopole antenna with dielectric loading are investigated and reported by W. Huang and A. Kishk in [234]. Improving the efficiency-bandwidth product in small dielectric monopole antenna is studied and reported by I. Ida ans Sato in [245]. The dependance of the

[1]The work reported in this chapter has been presented in the following conference publication:
P. Anoop and R. Bhattacharjee, "Investigation on Dielectric Loaded Monopole Antennas for Dual Band Application", *National Conference on Communications (NCC) 2016*, Guwahati, India, 2016.

efficiency-bandwidth product on the volume of the dielectric is also investigated in detail, which are later presented in [235]. However, in the meantime printed monopole antennas have also become very popular and their investigation were reported in the literature [246–248]. Among the popular investigations, the design of various shapes of monopole and methods to improve the bandwidth were studied by Girish Kumar and discussed in [249,250]. In the case of DRAs, we have already seen that the combination of monopole and DRA [49,91,92] have been used to improve the impedance bandwidth. Such wideband antennas were designed by achieving multiple resonances. Similar techniques are followed in the case of dielectric loaded antennas to achieve multi-band as well as wideband designs.

In this chapter, we investigate on the dielectric loading effect on a monopole strip, to obtain a dual-band antenna operating in the bands of 2.4-2.5 GHz and 5.75-5.85 GHz. The dielectric loading effect has been used in the literature to achieve dual-band operation using PMAs, some of which are reported in [251]. However, apart from an application oriented design, in this chapter we will present a more detailed investigation on the geometry and the size of the load, and the effect of the same on the impedance matching as well as on the radiation characteristics around the operating bandwidths. A relation involving the volume of the dielectric block and dielectric constant which can be used for the design of dielectric loaded strip antennas for dual-band operation is also presented. This chapter is organized into seven sections. The design of dual-band dielectric loaded antenna with variation on dielectric constant (ϵ_r) and volume of the dielectric materials are discussed in Section 5.2. Modeling of the dielectric loaded antenna design is discussed in Section 5.3. Behaviour and performance characteristics with dielectric materials of different ϵ_r values and geometrical shapes loaded on metal strip, their radiation characteristics are discussed in Section 5.4. Section 5.5 discusses the case studies on the design, where the deviations are observed. The practical radiation characteristics and the performance of the dielectric loaded dual-band antenna are presented in Section 5.6, followed by conclusion in Section 5.7.

5.2 Design of dielectric loaded monopole dual-band antenna

A quarter wave monopole is designed using a coaxial probe to resonate at 2.45 GHz. The matching is improved by replacing the coaxial probe of circular cross-section by a metal strip of rectangular cross section that protrudes into the air, as a radiator [250], as shown in Figure 5.1(a). The rectangular strip improves the matching as compared to the conventional coaxial probe, as shown in the $|S_{11}|$

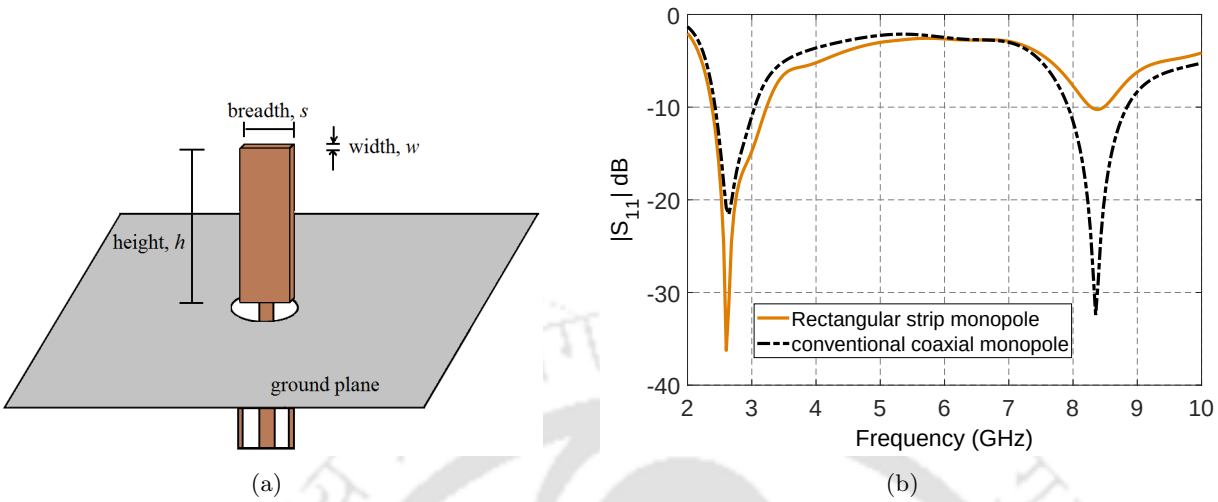

Figure 5.1: Metal Monopole strip of rectangular cross section: (a) schematic diagram and (b) corresponding $|S_{11}|$ plot.

plot of Figure 5.1(a). In order to study the effect of dielectric loading on this radiator, a dielectric block of rectangular cross section having dielectric constant of ϵ_r=4.1 is kept, touching the metal strip (as shown in Figure 5.2(a)) and simulations were performed using Ansys HFSS- V15 software. The dimensions of the block are fine tuned to obtain an upper operational impedance bandwidth in the range of 5.75-5.85 GHz, without effecting the impedance matching in the lower operating band of 2.4-2.5 GHz.. The dimensions of the rectangular dielectric block are 26 mm x 13 mm x 10.2 mm. The rectangular dielectric block provides three degrees of freedom and hence the height of the structure is kept comparable to the height of metal strip and the other two dimensions are varied to bring proper impedance bandwidth as well as resonance around the upper operating frequency of 5.8 GHz. The $|S_{11}|$ plot for the configuration is shown in the Figure 5.2(b). The ground plane size is adjusted until the resonances are not effected and remain within the band of operation. The impedance matching and the resonance seen in the 5.75-5.85 GHz band is because of the presence of the dielectric, which allows higher harmonics to appear due to dielectric loading effect. To understand the effect on dielectric loading with a different value of dielectric constant and volume of material, the metal strip is loaded with chosen values of ϵ_r and appropriate volume of material to bring impedance matching as well as resonances in the operating bands 2.4-2.5 GHz and 5.75-5.85 GHz, as before. Figure 5.3 shows the $|S_{11}|$ plot of the loaded monopole metal strip with dielectric material having ϵ_r=4.1, 4.5, 5.7 6.8, 8.3, 9.2 and 10.2 and corresponding appropriate volumes of the block determined from a relationship described in the next section.

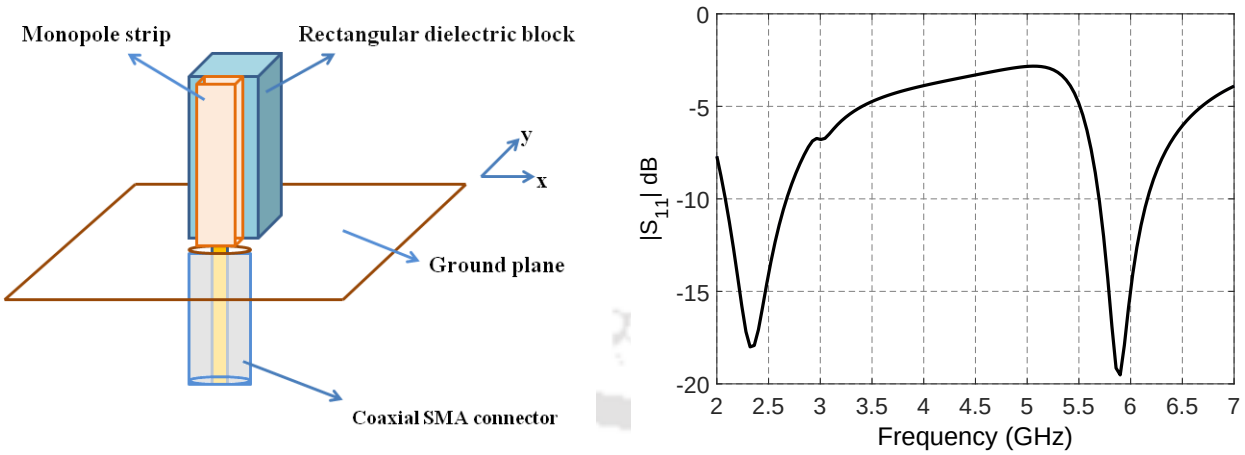

(a) (b)

Figure 5.2: Rectangular volume dielectric loaded monopole: (a) schematic diagram and (b) $|S_{11}|$ plot for the cases of dielectric load with ϵ_r=4.1

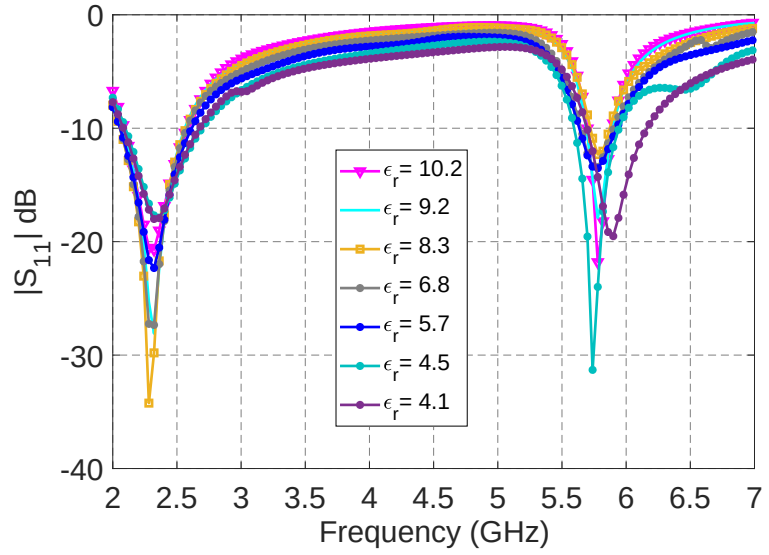

Figure 5.3: $|S_{11}|$ of the rectangular dielectric loaded monopole strip for the cases of dielectric load with various ϵ_r values.

5.3 Modeling of dielectric loaded monopole dual-band antenna

The effect of variation of the volume of the dielectric block having rectangular cross-section and corresponding ϵ_r values are studied through HFSS simulation and the same is plotted as in Figure 5.4. A curve fitting tool is used to determine the relation involving ϵ_r and dielectric volume for a given upper operating frequency, which is expressed as;

$$(volume^{1/3})(\varepsilon_r^{1/2}) = k \tag{5.1}$$

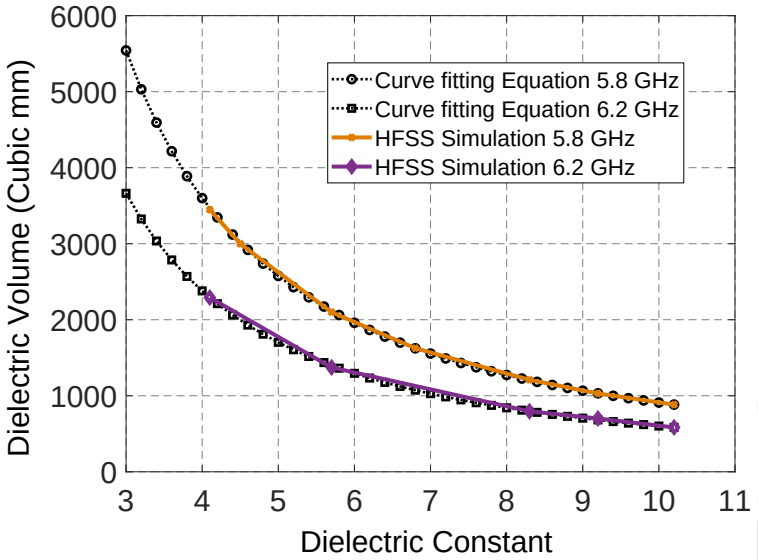

Figure 5.4: Variation of dielectric volume loaded on the metal strip with corresponding ϵ_r around 5.8 GHz and 6.2 GHz.

where 'k' is a constant. For a resonant frequency of 5.8 GHz, the value of k is 30.65. For other resonant frequencies, Equation (5.1) applies with different values of k. For example, when the simulations are performed for resonance around 6.2 GHz and impedance matching in the 6.15-6.25 GHz band, the curve follows Equation (5.1) with k value of 26.7. The variation of dielectric volume with ϵ_r for both the bands are shown in Figure 5.4.

5.4 Dielectric loading with different geometries

The study on dielectric loading are also performed with other structures like triangular prism (Figure 5.5(a)), axially cut cone (Figure 5.5(b)), axially cut cylinder (Figure 5.5(c)). A detailed investigation is carried out to understand the effect of shape, size, volume and dielectric constant of the dielectric load on the impedance matching around the lower as well as upper operating frequencies.

5.4.1 Effect of choosing different volume and dielectric constant for different shapes

All the four shapes of dielectric load of different ϵ_r values are studied using HFSS simulation. For a chosen ϵ_r value, the volume of the dielectric load is adjusted until resonances and impedance matching is achieved around both the operating bands. It is to be noted that, while varying the dielectric volume, the height of the dielectric load is kept almost comparable to the height of the rectangular monopole strip. The k values are then calculated by substituting the required amount of volume

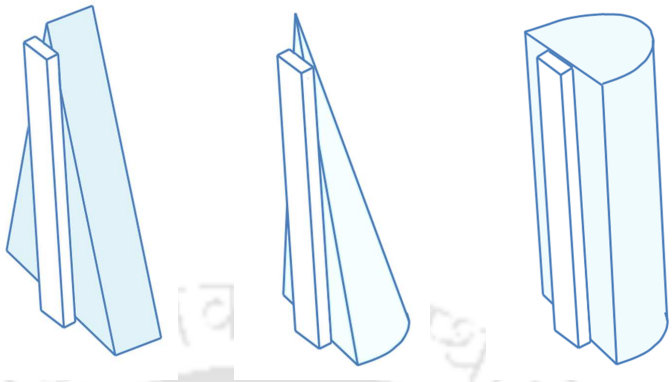

Figure 5.5: Schematic diagram of dielectric loading with other geometries over the rectangular monopole strip: (a) triangular shape, (b) axially cut cone shape and (c) axially cut cylinder shape.

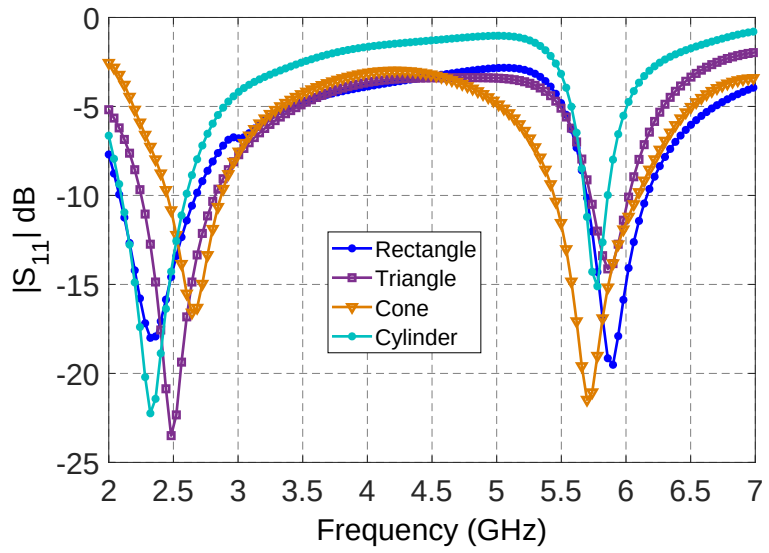

Figure 5.6: $|S_{11}|$ plot for various structures for different volume and dielectric constant.

and the ϵ_r value of the dielectric load, in Equation (5.1). Through simulations it is noted that, the resonance and the impedance matching in the 5.75-5.85 GHz band is exhibited by all the structures with almost same k values which is summarized in Table 5.1. The comparison of $|S_{11}|$ plots of all the geometries considered for loading the monopole are shown in Figure 5.6.

5.4.2 Effect of different loading element having same dielectric constant and volume

Investigation is also carried out using HFSS simulation to determine whether shape of the loading element effects the impedance matching at both the operating frequencies, when the volume as well as

Table 5.1: Constant 'k' calculated for various structures.

Dielectric shape	Volume (mm^3)	ϵ_r	k value
Rectangle	3447.60	4.1	30.58
Triangle	1927.80	6.15	30.86
Half cylinder	1020.50	9.2	30.53
Axially cut cone	883.125	10.2	30.64

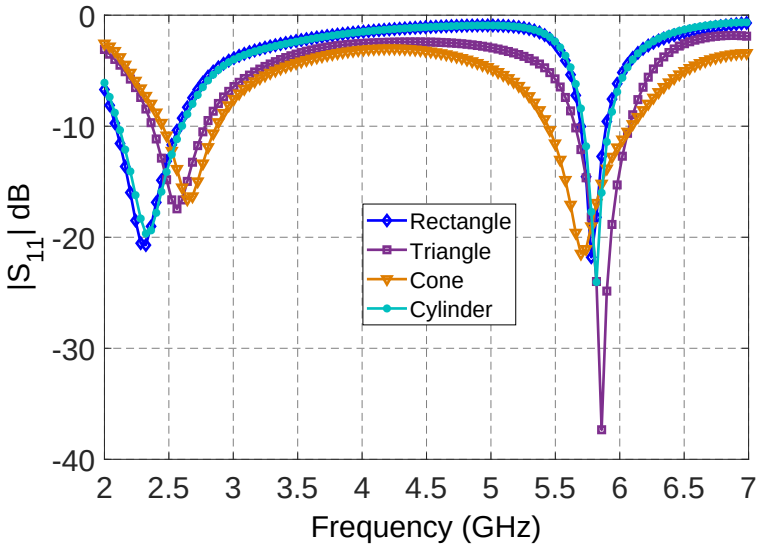

Figure 5.7: $|S_{11}|$ plot for various structures studied for ϵ_r=10.2 and constant volume.

dielectric constant of all the dielectric shape are kept constant. The plots of the impedance bandwidth performance for the case of different dielectric geometries are shown in Figure 5.7. A similar impedance matching characteristic is shown by all the four cases of the dielectric loads, when k is kept constant $\sim$ 30.65 and ϵ_r=10.2.

5.4.3 Radiation Plots

Now we will look into the radiation characteristics of this dielectric loaded dual-band antenna in both the operating bands. Representative plots for the following cases are presented: (a) radiation plots for rectangular shaped volume dielectric (ϵ_r=4.1) loaded monopole as shown in Figure 5.8, (b) radiation plots for triangle prism shaped volume dielectric (ϵ_r=6.15) loaded monopole as shown in Figure 5.9, (c) radiation plots for half cylinder shaped volume dielectric (ϵ_r=9.2) loaded monopole as shown in Figure 5.10 and (d) radiation plots for axially cut cone shaped volume dielectric (ϵ_r=10.2) loaded monopole as shown in Figure 5.11. For all the cases we observe that the radiation characteristics

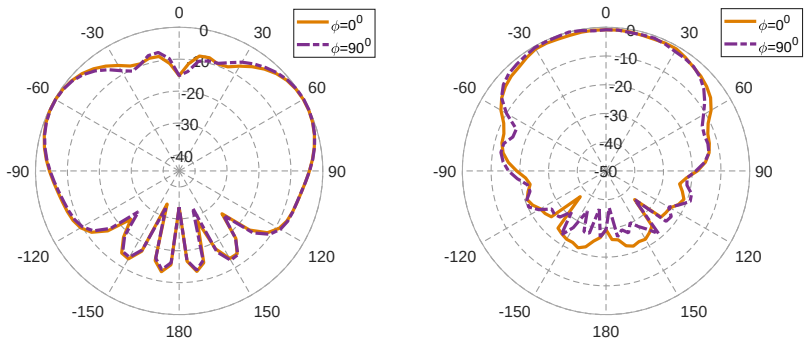

(a) (b)

Figure 5.8: Radiation plot of rectangular dielectric volume loaded monopole at (a) 2.45 GHz and (b) 5.8 GHz.

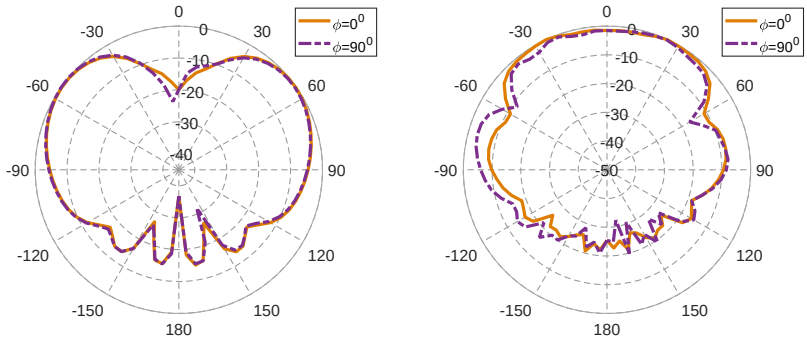

(a) (b)

Figure 5.9: Radiation plot of triangle prism dielectric volume loaded monopole at (a) 2.45 GHz and (b) 5.8 GHz.

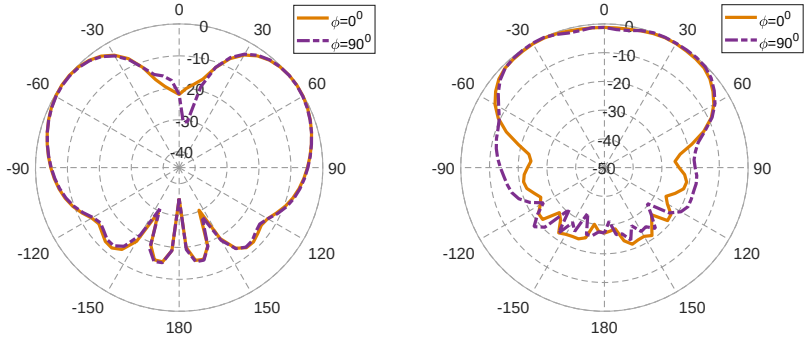

(a) (b)

Figure 5.10: Radiation plot of half cylindrical dielectric volume loaded monopole at (a) 2.45 GHz and (b) 5.8 GHz.

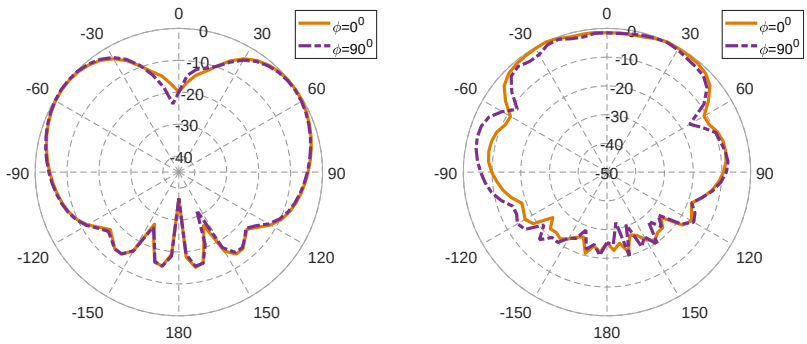

(a) (b)

Figure 5.11: Radiation plot of axially cut cone dielectric volume loaded monopole at (a) 2.45 GHz and (b) 5.8 GHz.

Table 5.2: Gain of the dielectric loaded monopole dual-band antenna for some of the dielectric shape

Shape of the dielectric load	Dimensions	Gain at 2.45 GHz	Gain at 5.8 GHz
Rectangular cross section	length=26mm, breadth=13mm, thickness=10.2 mm, er=4.1	4.10 dB	8.17 dB
Triangular Prism	base=27mm, height=28mm, thickness=5.1 mm, er=6.15	4.20 dB	7.91 dB
Half Cylinder	radius=5mm, height=26 mm, er=9.2	3.70 dB	6.83 dB
Axially cut Cone	radius=7.5mm, height=30mm, er=10.2	3.78 dB	6.54 dB

Table 5.3: Dimensions chosen maintaining constant dielectric volume.

WIDTH (mm)	LENGTH (mm)	HEIGHT (mm)	VOLUME (mm^3)
10	3.4	26	VOLUME-1 = 884
26	3.4	10	VOLUME-2 = 884
3.4	26	10	VOLUME-3 = 884

are similar. The antenna exhibit omni-directional radiation pattern at 2.45 GHz. At 5.8 GHz, the radiation patterns are broad for all the shapes of dielectric load. The simulated realized gain of the dielectric loaded monopole strip at 2.45 GHz and 5.8 GHz, for some of the dielectric shapes are shown in Table 5.2 We observe that at 2.45 GHz, the realized gain do not vary much. However, at 5.8 GHz a small variation in the gain is observed for different shapes of the dielectric load.

5.5 Cases where deviations are observed

In the studies presented so far, it is assumed that the height of the dielectric loading block is comparable to that of the strip. Moreover, the geometries included in the investigation has multiple degrees of freedom while adjusting the dielectric volume to maintain k=constant for a given choice of ϵ_r. Here, case studies are presented where the relation given in Equation (5.1) does not apply.

5.5.1 Height of the geometries not comparable to the height of metal strip monopole

In this investigation, we choose three dielectric blocks of rectangular cross section all having same volume but height of only one of the block (VOLUME-1) is kept comparable to the height of the metal strip and other two blocks (VOLUME-2 and VOLUME-3) are chosen with heights different than the height of the metal strip. Simulations are performed to observe the effect of dielectric loading of the three volumes on the impedance matching around the lower and upper operating frequencies. Except for VOLUME-1, the impedance matching of the other two blocks deviated, which are shown in Figure 5.12. The dimensions of all the three blocks are shown in Table 5.3.

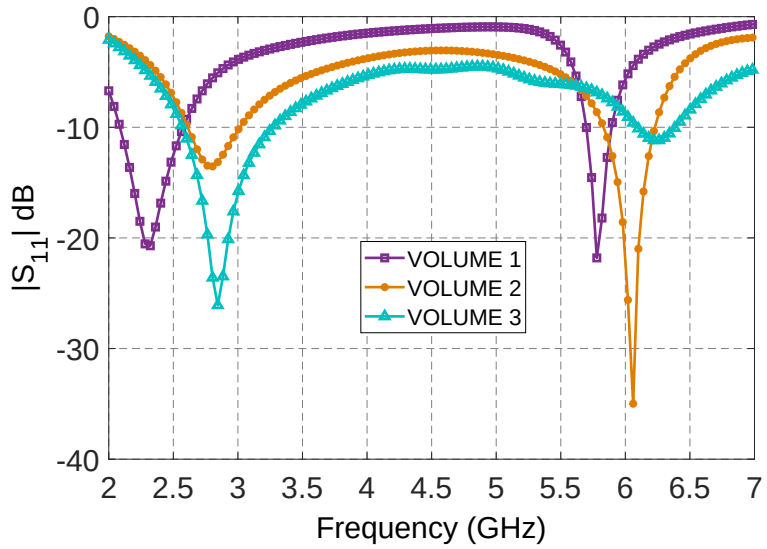

Figure 5.12: $|S_{11}|$ plot for rectangular dielectric volume for changes in dimensions but keeping the volume constant.

5.5.2 Dielectric volume having only one degree of freedom on dimension

Unlike previous geometries, if we assume a dielectric loading from a dielectric block that has only one degree of freedom like in the case of a quarter sphere, we observe poor degree of impedance matching at the operating frequencies. Here, the radius of the dielectric shape, which is the only possible dimension that can be varied, is kept comparable to the height of the metal strip and simulations are performed to observe the effect of loading on the impedance matching as well as resonance around the operating frequencies. A significant deviation on the resonant frequencies as well as impedance matching are observed, for the studies carried out for the cases of different values of dielectric constant and corresponding volumes of this dielectric shape loaded on the monopole. The effect on the impedance matching for two cases, (a) ϵ_r=10.2 for which volume comes out to be around 870 cubic mm and (b) ϵ_r=6.15 for which volume comes out to be 1860 cubic mm are shown in Figure 5.13. It is observed that impedance matching and resonances for the cases of different dielectric volume and ϵ_r for such geometries cannot be adopted using Equation (5.1).

5.5.3 Behaviour of the design when $\epsilon_r < 4$

When the studies are performed to understand the effect of dielectric loading with blocks having $\epsilon_r < 4$, on the impedance matching and resonant frequencies, deviation are observed. The specifications of the dielectric load do not follow the curves of Figure 5.4; however, the trend in which volume

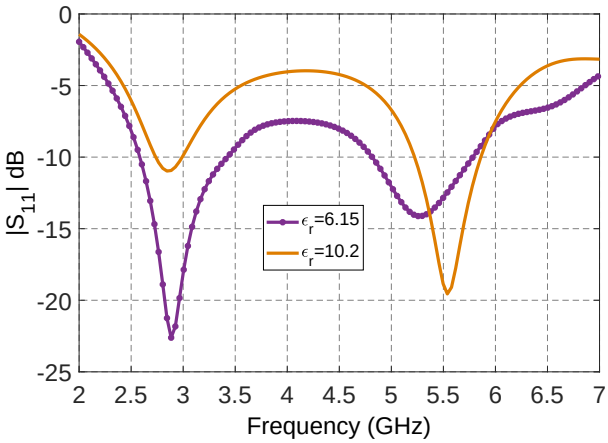

Figure 5.13: $|S_{11}|$ plot for quarter sphere for ϵ_r=6.15 and ϵ_r=10.2.

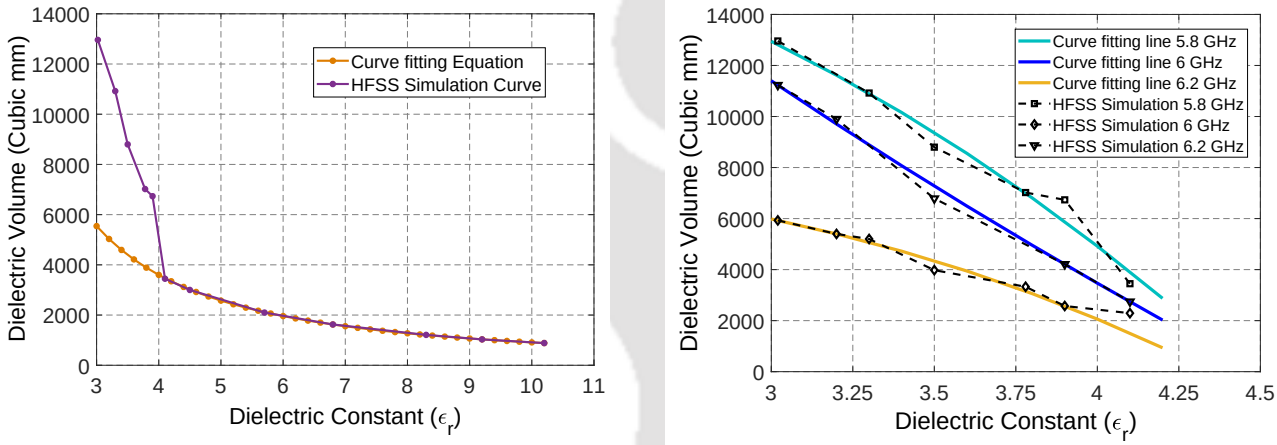

(a) (b)

Figure 5.14: The variation of dielectric volume with ϵ_r for the case of $\epsilon_r < 4$ for (a) upper band around 5.8 GHz and (b) upper band of different operating frequencies

and dielectric constant values are related, takes a different form, which is shown in Figure 5.14(a). The volume of dielectric block corresponding to a value of dielectric constant almost doubled, which demand loading of monopole with bulky dielectric blocks to bring a proper impedance matching and resonance around 5.8 GHz. When simulations are performed for the impedance bandwidths around 6 GHz and 6.2 GHz, parallel curves are obtained with slight variations on their slopes as shown in Figure 5.14(b).

5.6 Practical observations of dielectric loaded dual-band antennas

The dielectric loaded antennas designed to achieve dual-band operation can be used in the operational bandwidths of 2.4-2.5 GHz and 5.75-5.85 GHz, which are suitable for WLAN applications. In the investigation, dielectric loading with various possible geometries have been performed, of which

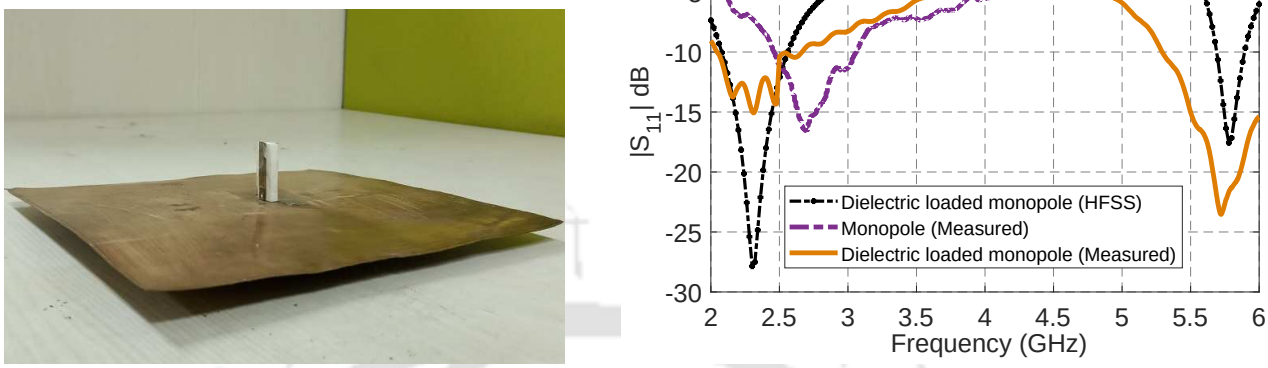

(a) (b)

Figure 5.15: Rectangular dielectric loaded monopole strip antenna: (a) fabricated prototype and (b) $|S_{11}|$ plot.

rectangular, half cylindrical, conical, triangular dielectric shapes are found to be a suitable dielectric load over a metal monopole strip to achieve dual-band antenna operation. We now present the practical behaviour of such a dual-band antenna. Here, we demonstrate the investigation carried on the dielectric loaded dual-band antenna, by choosing the case of a practical rectangular dielectric load. A schematic representation of a dual-band antenna loaded with rectangular dielectric material is shown in Figure 5.2(a). A prototype of one such geometry with rectangular dielectric load over the monopole strip is also fabricated and is shown in Figure 5.15(a). The dielectric load has an $\epsilon_r = 9.2$ and dimensions as 26 mm x 11 mm x 3.6 mm. The dielectric loading effect on the monopole antenna (operated at its resonant frequency near 2.45 GHz) is utilized to bring an operational bandwidth in the range 5.75-5.85 GHz. The return loss for monopole antenna alone, and with dielectric loading are shown in Figure 5.15(b).

The nature of radiation pattern at both the frequency bands are shown in Figure 5.16 and Figure 5.17, at resonant frequencies 2.45 GHz and 5.78 GHz, respectively. The measured as well as simulated plots are presented for comparison. We observe that the simulation and measured radiation plots follow similar pattern. Maximum gain of 4.11 dBi and 6.99 dBi are obtained at 2.45 GHz and 5.78 GHz, respectively through HFSS simulation. The measured gain is obtained 3.95 dB and 5.93 dB at 2.45 GHz and 5.78 GHz, respectively. It is to be noted that, in the 5.75-5.85 GHz band, at $\phi = 0^0$ plane, we observe circular polarization. This is shown in the simulated radiation pattern of Figure 5.17(a). The variation of simulated axial ratio in this plane as shown in Figure 5.18(a) and

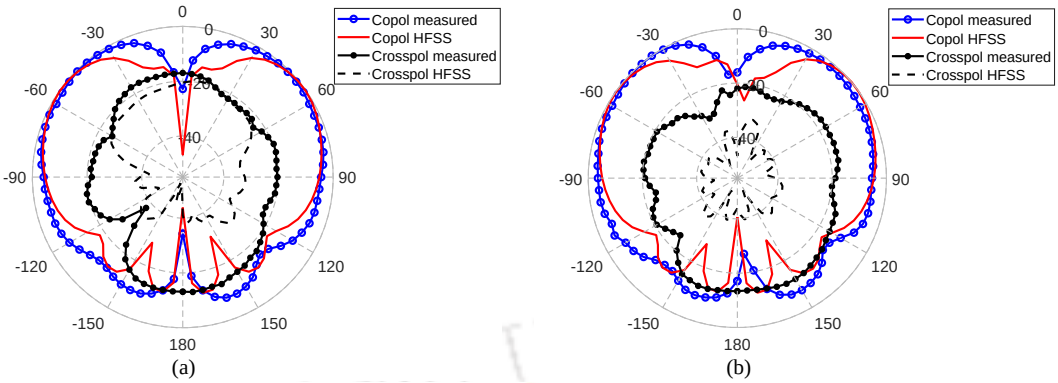

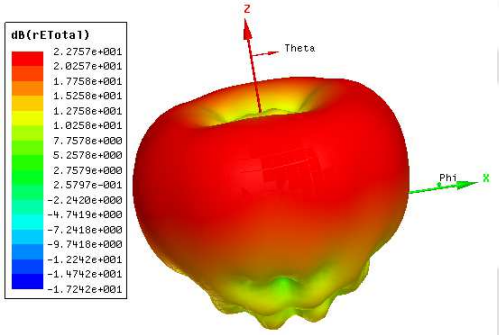

(a)

Figure 5.16: Radiation patterns of the dielectric loaded monopole antenna at 2.45 GHz at (a) $\phi = 0^0$ (E-plane) and (b) $\phi = 90^0$ (E-plane) (c) 3-D pattern.

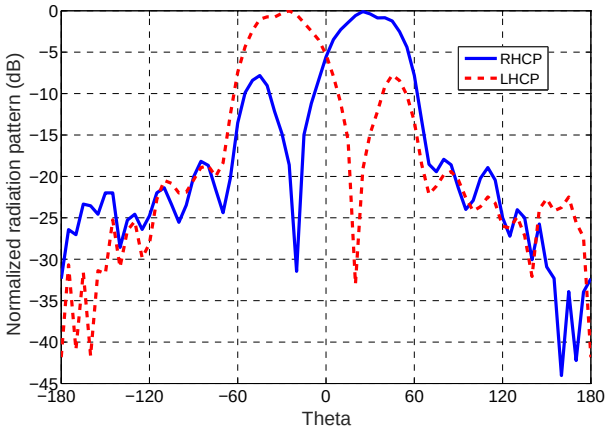

(a)

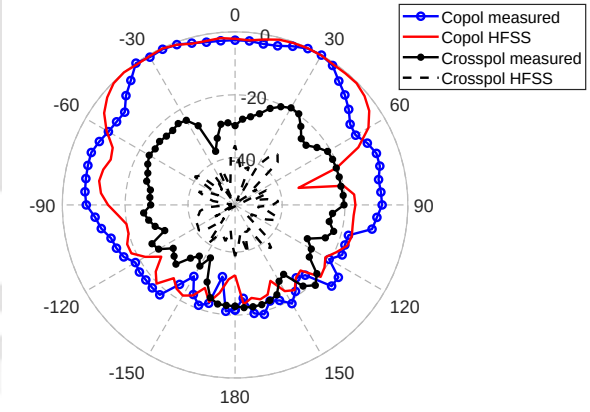

(b)

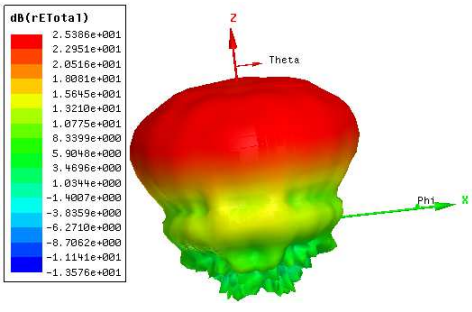

(c)

Figure 5.17: Radiation patterns of the dielectric loaded monopole antenna at 5.78 GHz at (a) $\phi = 0^0$ (E-plane) and (b) $\phi = 90^0$ (E-plane) (c) 3-D pattern.

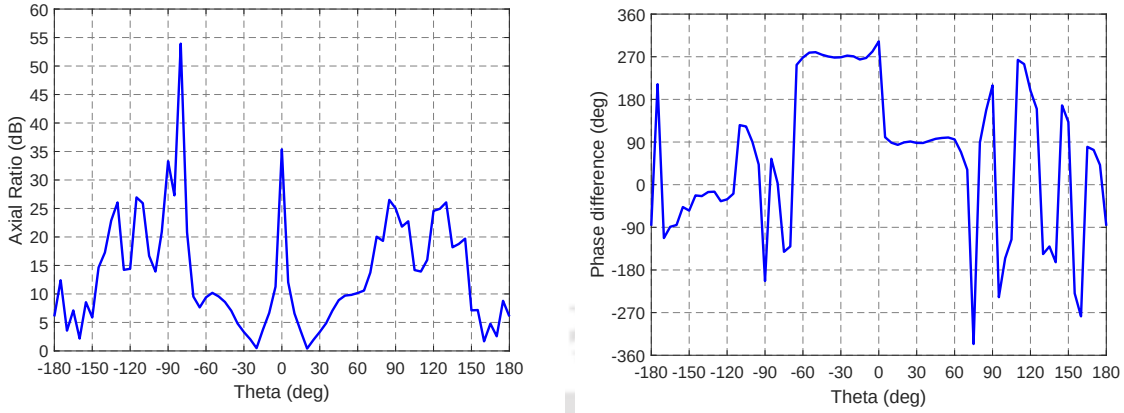

(a) (b)

Figure 5.18: Variation of (a) axial ratio and (b) phase difference at 5.78 GHz for $\phi = 0^0$.

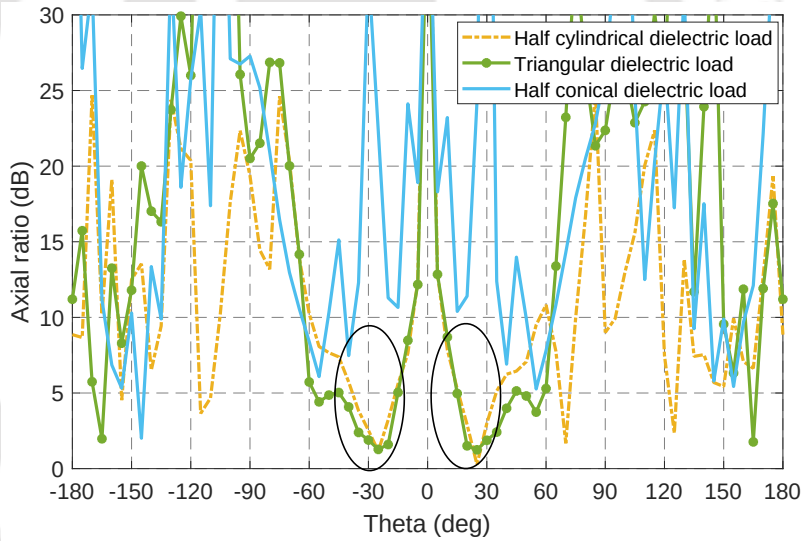

Figure 5.19: Axial ratio variation at $\phi = 0^0$ plane for different dielectric loading at respective resonant frequency in 5.75-5.85 GHz band

the variation of phase difference as shown in Figure 5.18(b) confirms circular polarization. However, with further investigation, we observe that the antenna does not exhibit circular polarization for every shape of dielectric load. Figure 5.19 shows variation of axial ratio at $\phi = 0^0$ for different shape of dielectric loading. We observe an exceptional case with half conical dielectric load for which the antenna does not exhibit circular polarization. However, for half cylindrical and triangular dielectric load, the antenna exhibit circular polarization. Therefore, it is found that the generation of circular polarization is depended on the geometry of the dielectric load. In this investigation, the dielectric loads having basic geometry and, a few of their modified versions have been included. However, as it is noted that circular polarization is generated for only some the geometries of these dielectric loads, it

is expected that, for a few geometries which have not been included in this investigation, the antenna may generate circular polarization. Therefore, a detailed investigation is to be carried out to exactly understand the reason for such behaviour in the 5.75-5.85 GHz band for different dielectric shaped loads. We keep this topic as a future prospect for the research carried out and presented in this thesis.

The objective of the investigation carried out in this chapter is to understand the effect of size, shape, volume and dielectric constant of the dielectric load on the impedance matching around the operating frequency, shifting of operational impedance bandwidth and radiation characteristics of an antenna. We observed that, by suitable choice of the size, shape, volume and the dielectric material of the dielectric load, shifting of the operational impedance bandwidth can be favourably controlled without effecting the impedance matching at the other operating frequency of the antenna. Further we also noted that, such loads can even effect the polarization of the antenna. This investigation carried out on the dielectric loaded monopole antenna to understand various aspects of dielectric loading also demonstrated how such phenomena can be favourably used to design a dual-band antenna. A prototype of the same is fabricated for the case of a rectangular dielectric loaded monopole which can used as a dual-band antenna for WLAN applications.

5.7 Conclusion

In this chapter an investigation on dielectric loaded monopole strip has been presented. Monopole strip designed to resonate at 2.45 GHz is loaded with rectangular dielectric blocks of different volumes to bring a resonance in the band 5.75-5.85 GHz. Appropriate modeling of the design is done and closed form equation is developed through curve fitting. Further studies are carried out with other possible geometries and case studies were done to understand the behaviour of the dielectric loading on the resonant frequency. Applicability of the developed closed form equation is demonstrated and the cases where the deviations are observed are also highlighted. All the studies were carried out using the Ansys HFSS software. A prototype of the monopole antenna loaded with a rectangular dielectric block is also fabricated, and the performance of the same is presented and compared with the simulated data. It is noted that this design has the potential for exhibiting circular polarization in the upper band, for some of the cases of dielectric loading. However, the investigation on this observation is kept as a scope for future research.

6

Summary and Conclusions

Contents

In this thesis, we present the investigation of two geometries of DRA, namely (i) ETDRA and (ii) the Rhombic DRA. We investigated on the Q-factor and impedance bandwidth performance of the dominant $TM_{10\delta}$ mode excited inside an ETDRA. Further, the potential of the ETDRA as a dual-band antenna is also investigated, and two configurations for the same are proposed which can be used for WLAN applications. A basic geometry having a Rhombic cross-section as a DRA, which have not been reported in the literature is also investigated. A Rhombic DRA for wideband application is also proposed by choosing a suitable feeding technique. During various investigations carried out on DRAs, it is observed that, the designs involving multiple DRAs has some effect on the impedance matching due the phenomena of dielectric loading of a DRA at frequencies where they do not excite any radiating mode. On this context, the phenomena of dielectric loading effect as well as some aspects of dielectric loaded antennas are also investigated and presented in this thesis.

In this chapter, the summary of various investigations discussed in this thesis, are presented. Based on these investigations, the scope for future research are also presented. In Section 6.1, the main contributions of this thesis are summarized. Section 6.2 discusses the possible future work for the investigations reported in this thesis. in Section 6.2.

6.1 Summary of the Thesis Contributions

In Chapter 2, we present the nature of Q-factor for various aspect ratios and material dielectric constant values for an ETDRA operated in the dominant $TM_{10\delta}$ mode. A closed form expression for calculating the Q-factor for this excited mode in an ETDRA is developed by applying curve fitting approximation technique over the Q-factor curves. The expression can be used to estimate the Q-factor of the ETDRAs operated in $TM_{10\delta}$ mode for the aspect ratio and dielectric constant values, ranging from $1 \leq a/h \leq 4$ and $9.2 \leq \epsilon_r \leq 15$. Further, an investigation on the impedance bandwidth performance of an ETDRA operated in $TM_{10\delta}$ mode is discussed and an expression for estimating the same for this operating mode is also presented. The proposed technique is expected to be very useful for the antenna engineers for estimating the impedance bandwidth of the practical ETDRA, operated with $TM_{10\delta}$ mode for the aspect ratio and dielectric constant values, ranging from $1.5 \leq a/h \leq 4$ and $9.2 \leq \epsilon_r \leq 15$.

In Chapter 3, an investigation on ETDRA for dual-band application is presented. Through proper understanding of the excited modes, the potential of the ETDRA as a dual-band antenna is inves-

tigated in detail, based on which two configurations of dual-band ETDRA are proposed; namely, Configuration-I and Configuration-II. The configuration-I is a single ETDRA dual-band antenna, which operates in the dominant $TM_{10\delta}$ mode in the lower band and in higher order $TM_{3-3\delta}$ mode for the upper band. The configuration-II presents a dual-band antenna using two ETDRAs having similar radiation characteristics in both the operating bands. The dominant $TM_{10\delta}$ mode is excited in both the DRAs at their respective operating frequency. The two configurations of the dual-band ETDRAs are excited by means of a conventional coaxial feed, which makes them simple and easily realisable dual-band antennas. The proposed configurations of ETDRAs can be used for WLAN applications, in the bands of 2.4-2.5 GHz and 5.75-5.85 GHz. Further, in the context of the proposed dual-band ETDRAs, the importance of dielectric loss tangent value is briefly highlighted and the same is taken into account while evaluating the antenna performance. The chapter also summarizes some of the challenges in the design of practical dual-band and multi-band DRAs.

In Chapter 4, an investigation on a new Rhombic DRA geometry is presented. A few of the possible TE modes that are excited inside this DRA geometry are identified through eigen mode analysis with the aid of CST simulation. Suitable feeding techniques that can be used for exciting these modes are discussed. The identified TE modes were classified into $(TE_n)^y$ and $(TE_n)^x$ modes, and the empirical formulae for calculating the resonant frequencies of these modes are developed through curve-fitting approximation. The nature of radiation characteristics of these modes are also identified, and are presented for a fabricated prototype of this proposed DRA. By suitable choice of the feed, a Rhombic DRA for wideband application is also proposed. A conventional coaxial feed is used to make the antenna configuration, simple and easily realizable. The proposed wideband Rhombic DRA has a percentage impedance bandwidth of 31.64%, which is obtained through measurements. The DRA is also compact at its operating frequency, when compared with other basic DRAs reported in the literature. A preliminary investigation on a special case of the proposed Rhombic DRA geometry in low profile configuration is discussed. The resonant frequency and radiation characteristics of lowest x- and y- polarized TE modes excited in this configuration of the Rhombic DRA are also presented.

In Chapter 5, an investigation on dielectric loaded rectangular monopole strip is presented. The investigation demonstrates the effect of size, shape, volume and dielectric constant of the dielectric load on the impedance matching as well as the radiation performance of a rectangular monopoles strip which is operated at 2.45 GHz. An upper operational bandwidth is achieved by proper choice of the

dielectric load, based on which a dielectric loaded monopole antenna for dual-band operation is proposed. Appropriate modelling of the design is proposed and a closed form equation is presented, which will be useful in the initial design of dielectric loaded monopole antenna for dual-band operation. Applicability of the developed closed form equation is demonstrated and the cases where the deviations are observed are also highlighted. A prototype of the proposed antenna which can be operated in the bands of 2.4-2.5 GHz and 5.75-5.85 GHz, is also fabricated and the practical radiation characteristics at both the operating frequency are discussed. The proposed dielectric loaded monopole can be used as a dual-band antenna, which are suitable for WLAN applications.

6.2 Suggestions for possible Future Work

In this thesis, we presented an investigation on ETDRA and Rhombic DRA. Further, some aspects of dielectric loaded antennas are also presented to understand the effect of dielectric loading on the impedance bandwidth and radiation performance of a monopole antenna. We expect that, these investigations will be very useful in understanding some of the aspects in the realization of a potential Dielectric Resonator and Dielectric Loaded Antennas. We also expect that, some of the objectives which are addressed in this thesis can be extended further in the following directions.

In Chapter 2, we presented the Q-factor curves and impedance bandwidth performance of the dominant $TM_{10\delta}$ mode excited in an ETDRA. The investigation on the same, for higher order radiating modes of an ETDRA can also be carried out and relevant closed form expressions for calculating the Q-factor as well as impedance bandwidth can be developed. This will be very useful in understanding the radiation performance as well as estimating the practical impedance bandwidth achievable with an ETDRA operated in higher order mode.

In Chapter 4, we presented an investigation on Rhombic DRA, which is not reported in the literature, so far. Investigation on some of the excited TE modes, their practical radiation characteristics and the possibility of wide impedance bandwidth using a conventional feeding technique are presented. Further, the potential of this proposed DRA as a circularly polarized antenna as well as an antenna for multi-band and wideband applications by exciting higher order radiating modes can be investigated through proper choice of the feed. Moreover, a special case of this DRA geometry in low profile configuration can also be investigated. A preliminary investigation on this DRA geometry is already presented in this thesis. It is found that, the proposed Rhombic DRA is compact at its operation

frequency, when compared with other DRAs having basic geometry. And therefore, the low profile configuration of the Rhombic DRA can be investigated for its potential, in the designs, where the size of the antenna is very small.

In Chapter 5, we presented a dual-band monopole antenna using the concept of dielectric loading. It is found that, the monopole antenna exhibit circular polarization in the upper operating band when loaded by dielectric blocks of certain geometries. The investigation on the same can be carried out and the radiation performance can be studied to meet the practical antenna applications.

Appendices

A

$TM_{m,n,p}$ mode solutions of Equilateral Triangular Dielectric Resonator Antennas

Contents

A.1 $TM_{m,n,p}$ mode solutions of Triangular shaped DRA

For an ETDRA of side 'a' and height 'h', whose cross-sectional view in the XY-plane is shown in Fig. A.1, the E_z component in case of TM modes ($H_z = 0$) can be expressed as [50, 62];

$$E_z = A_c \left(\frac{\chi^2}{j\omega\varepsilon}\right) T(x,y)P(z) \tag{A.1}$$

where, A_c is a constant. For a magnetic wall boundary condition $T(x,y)$ is expressed using a tri-linear transformation as given in [52] and [54]. If l, m, n are three integers satisfying $l+m+n=0$, then the T-function for transverse magnetic waves is given by;

$$\begin{aligned} T(x,y) = &\cos\left[\left(\frac{2\pi l}{3b}\right)\left(\frac{u}{2}+b\right)\right]\cos\left[\left(\frac{\pi(m-n)(v-w)}{9b}\right)\right] \\ &+\cos\left[\left(\frac{2\pi m}{3b}\right)\left(\frac{u}{2}+b\right)\right]\cos\left[\left(\frac{\pi(n-l)(v-w)}{9b}\right)\right] \\ &+\cos\left[\left(\frac{2\pi n}{3b}\right)\left(\frac{u}{2}+b\right)\right]\cos\left[\left(\frac{\pi(l-m)(v-w)}{9b}\right)\right] \end{aligned} \tag{A.2}$$

Where, b is the distance from one of the sides of an equilateral triangle to its centroid and u, v, w are the coordinates (as shown in Figure A.2) formed by tri-linear transformation given by;

$$u = xcos\alpha + ysin\alpha \tag{A.3}$$

$$v = xcos\beta + ysin\beta \quad ; \quad \beta = \alpha + \frac{2\pi}{3} \tag{A.4}$$

$$w = xcos\gamma + ysin\gamma \quad ; \quad \gamma = \beta + \frac{2\pi}{3} \tag{A.5}$$

Where α, β, γ are the angles made by AO, BO and CO with the X-axis. For α=0; we have u=x and

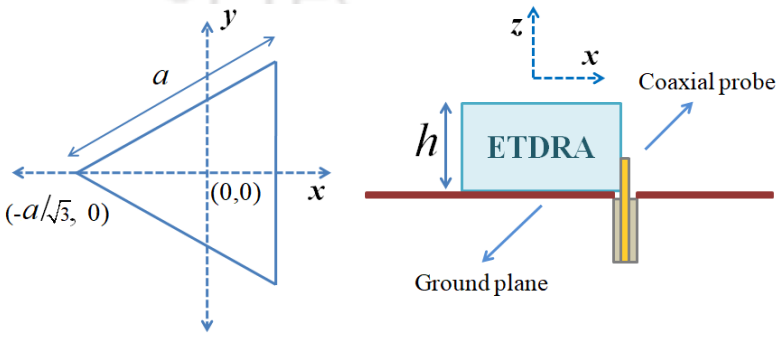

(a) (b)

Figure A.1: Geometry of Equilateral Triangular DRA: (a) 2-D top view and (b) side view.

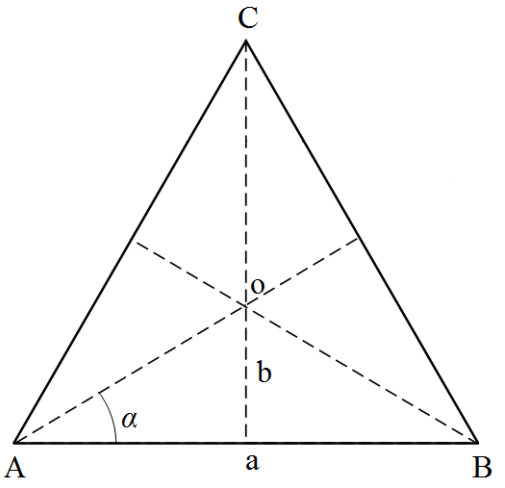

Figure A.2: Cross section of an ETDRA

y=$\frac{v-w}{\sqrt{3}}$. Substituting in (A.2) we get,

$$\begin{aligned} T(x,y) = &\cos\left[\left(\frac{2\pi x}{\sqrt{3A}}+\frac{2\pi}{3}\right)l\right]\cos\left[\left(\frac{2\pi\,(m-n)\,y}{3A}\right)\right] \\ &+\cos\left[\left(\frac{2\pi x}{\sqrt{3A}}+\frac{2\pi}{3}\right)m\right]\cos\left[\left(\frac{2\pi\,(n-l)\,y}{3A}\right)\right] \\ &+\cos\left[\left(\frac{2\pi x}{\sqrt{3A}}+\frac{2\pi}{3}\right)n\right]\cos\left[\left(\frac{2\pi\,(l-m)\,y}{3A}\right)\right] \end{aligned} \tag{A.6}$$

If we assume, $\theta_x = \left(\frac{2\pi x}{\sqrt{3}a}+\frac{2\pi}{3}\right)$ and $\theta_y = \left(\frac{2\pi y}{3a}\right)$, the above equation can be further simplified as;

$$T(x,y)=cos\,(\theta_x l)\,cos\,[\theta_y(m-n)]+cos\,(\theta_x m)\,cos\,[\theta_y(n-l)]+cos\,(\theta_x n)\,cos\,[\theta_y(l-m)] \tag{A.7}$$

The composite wave number χ (along x- and y- direction together) and k_z satisfies the separation equation;

$$\chi^2 + k_z^2 = \varepsilon_r k_0^2 \tag{A.8}$$

where, k_0 is the free space wave number. The composite wave number χ can be expressed as;

$$\chi = \left(\frac{4\pi}{3a}\right)\sqrt{(m^2+mn+n^2)} \tag{A.9}$$

k_z follows the transcendental equation given in [62], which is expressed as;

$$k_z tan\left(k_z h - \frac{\pi}{2}\right) = \varepsilon_r\sqrt{(\varepsilon_r-1)\,k_0^2 - k_z^2} \tag{A.10}$$

where,

$$k_z = \frac{p\pi}{2h}, \qquad p=1,2.. \tag{A.11}$$

$P(z)$ is separately expressed for perfect magnetic conductor (PMC) walls and imperfect magnetic conductor (IPMC) walls as in [62];

$$P(z) = \begin{cases} \sin[(k_z(h-z)], \text{ for PMC} \\ \cos(k_z z), \text{ for IPMC} \end{cases} \tag{A.12}$$

For a practical DRA, we assume imperfect magnetic walls existing around the dielectric surface. The TM field distribution of an ETDRA can be therefore expressed using E_z and the remaining field quantities (E_x, E_y, H_x, H_y) expressed as;

$$E_x = \frac{1}{\chi^2}\frac{\partial^2 E_z}{\partial z \partial x} \tag{A.13}$$

$$E_y = \frac{1}{\chi^2}\frac{\partial^2 E_z}{\partial z \partial y} \tag{A.14}$$

$$H_x = \frac{j\omega\epsilon}{\chi^2}\frac{\partial E_z}{\partial y} \tag{A.15}$$

$$H_y = \frac{-j\omega\epsilon}{\chi^2}\frac{\partial E_z}{\partial x} \tag{A.16}$$

Expanding (A.13), (A.14), (A.15), and (A.16), we obtain;

$$E_x = \left[\frac{A_c(k_z sin(k_z z))}{j\omega\epsilon}\right]\left(\frac{2\pi}{\sqrt{3}a}\right) \times \{lsin(\theta_x l)cos[\theta_y(m-n)] + msin(\theta_x m)cos[\theta_y(n-l)] + nsin(\theta_x n)cos[\theta_y(l-m)]\} \tag{A.17}$$

$$E_y = \left[\frac{A_c(k_z sin(k_z z))}{j\omega\epsilon}\right]\left(\frac{2\pi}{3a}\right) \times \{(m-n)cos(\theta_x l)sin[\theta_y(m-n)] + (n-l)cos(\theta_x m) sin[\theta_y(n-l)] + (l-m)cos(\theta_x n)sin[\theta_y(l-m)]\} \tag{A.18}$$

$$H_x = -A_c(cos(k_z z))\left(\frac{2\pi}{3a}\right) \times \{(m-n)cos(\theta_x l)sin[\theta_y(m-n)] + (n-l)cos(\theta_x m) sin[\theta_y(n-l)] + (l-m)cos(\theta_x n)sin[\theta_y(l-m)]\} \tag{A.19}$$

$$H_y = A_c(cos(k_z z))\left(\frac{2\pi}{\sqrt{3}a}\right) \times \{lsin(\theta_x l)cos[\theta_y(m-n)] + msin(\theta_x m)cos[\theta_y(n-l)] + nsin(\theta_x n)cos[\theta_y(l-m)]\} \tag{A.20}$$

B

Empirical Formula to Calculate Antenna Gain

Contents

B.1 Evaluation of Antenna Gain using Empirical Formula

For any practical antenna an approximate value of gain can be calculated from its radiation pattern. The formula which is widely used can be expressed as;

$$G_0 \backsimeq \frac{30,000}{\phi_{1d}\ \phi_{2d}} \tag{B.1}$$

where,

ϕ_{1d}= Half power beamwidth in one plane (degrees)

ϕ_{2d}= Half power beamwidth in a plane at a right angle to the other (degrees)

Bibliography

[1] S. A. Long, M. McAllister, and Liang Shen, "The resonant cylindrical dielectric cavity antenna," *IEEE Transactions on Antennas and Propagation*, vol. 31, pp. 406–412, May 1983.

[2] R. D. Richtmyer, "Dielectric Resonators," *Journal of Applied Physics*, vol. 10, no. 6, pp. 391–398, 1939.

[3] A. Okaya and L. F. Barash, "The Dielectric Microwave Resonator," *Proceedings of the IRE*, vol. 50, pp. 2081–2092, Oct 1962.

[4] M. W. McAllister, S. A. Long, and G. L. Conway, "Rectangular dielectric resonator antenna," *Electronics Letters*, vol. 19, pp. 218–219, March 1983.

[5] M. W. McAllister and S. A. Long, "Resonant hemispherical dielectric antenna," *Electronics Letters*, vol. 20, pp. 657–659, August 1984.

[6] K. W. Leung, K. M. Luk, K. Y. A. Lai, and D. Lin, "Theory and experiment of a coaxial probe fed hemispherical dielectric resonator antenna," *IEEE Transactions on Antennas and Propagation*, vol. 41, pp. 1390–1398, Oct 1993.

[7] K. W. Leung, K. Y. A. Lai, K. M. Luk, and D. Lin, "Input impedance of aperture coupled hemispherical dielectric resonator antenna," *Electronics Letters*, vol. 29, pp. 1165–1167, June 1993.

[8] K. W. Leung and K. M. Luk, "Radiation characteristics of an aperture-coupled hemispherical dielectric resonator antenna," *Microwave and Optical Technology Letters*, vol. 7, no. 14, pp. 677–679, 1994.

[9] K. W. Leung, K. M. Luk, K. Y. A. Lai, and D. Lin, "On the tm_{101} mode of a hemispherical dielectric resonator antenna," *Microwave and Optical Technology Letters*, vol. 6, no. 11, pp. 626–629, 1993.

[10] R. K. Mongia and P. Bhartia, "Dielectric resonator antennas- a review and general design relations for resonant frequency and bandwidth," *International Journal of Microwave and Millimeter-Wave Computer-Aided Engineering*, vol. 4, no. 3, pp. 230–247.

[11] R. K. Mongia, C. L. Larose, S. R. Mishra, and P. Bhartia, "Accurate measurement of Q-factors of isolated dielectric resonators," *IEEE Transactions on Microwave Theory and Techniques*, vol. 42, pp. 1463–1467, Aug 1994.

[12] R. Kumar Mongia and A. Ittipiboon, "Theoretical and experimental investigations on rectangular dielectric resonator antennas," *IEEE Transactions on Antennas and Propagation*, vol. 45, pp. 1348–1356, Sep. 1997.

[13] A. A. Kishk, B. Ahn, and D. Kajfez, "Broadband stacked dielectric resonator antennas," *Electronics Letters*, vol. 25, pp. 1232–1233, Aug 1989.

[14] R. N. Simons and R. Q. Lee, "Effect of parasitic dielectric resonators on CPW/aperture-coupled dielectric resonator antennas," *IEE Proceedings H - Microwaves, Antennas and Propagation*, vol. 140, pp. 336–338, Oct 1993.

[15] G. P. Junker, A. A. Kishk, A. W. Glisson, and D. Kajifez, "Effect of air gap on cylindrical dielectric resonator antenna operating in TM/sub 01/ mode," *Electronics Letters*, vol. 30, pp. 97–98, Jan 1994.

[16] G. P. Junker, A. A. Kishk, A. W. Glisson, and D. Kajfez, "Effect of fabrication imperfections for ground-plane-backed dielectric-resonator antennas," *IEEE Antennas and Propagation Magazine*, vol. 37, pp. 40–47, Feb 1995.

[17] K. W. Leung, K. M. Luk, K. Y. Chow, and E. K. N. Yung, "Bandwidth enhancement of dielectric resonator antenna by loading a low-profile dielectric disk of very high permittivity," *Electronics Letters*, vol. 33, pp. 725–726, April 1997.

[18] A. Sangiovanni, J. Y. Dauvignac, and C. Pichot, "Embedded dielectric resonator antenna for bandwidth enhancement," *Electronics Letters*, vol. 33, pp. 2090–2091, Dec 1997.

[19] A. A. Kishk, "Tetrahedron and triangular dielectric resonator antenna with wideband performance," in *IEEE Antennas and Propagation Society International Symposium (IEEE Cat. No.02CH37313)*, vol. 4, pp. 462–465 vol.4, June 2002.

[20] K. W. Leung and C. K. Leung, "Wideband dielectric resonator antenna excited by cavity-backed circular aperture with microstrip tuning fork," *Electronics Letters*, vol. 39, pp. 1033–1035, July 2003.

[21] M. A. Sharkawy, A. Z. Elsherbeni, and C. E. Smith, "Stacked elliptical dielectric resonator antennas for wideband applications," in *IEEE Antennas and Propagation Society Symposium, 2004.*, vol. 2, pp. 1371–1374 Vol.2, June 2004.

[22] M. B. Oliver, Y. M. M. Antar, R. K. Mongia, and A. Ittipiboon, "Circularly polarised rectangular dielectric resonator antenna," *Electronics Letters*, vol. 31, pp. 418–419, March 1995.

[23] G. Drossos, Z. Wu, and L. E. Davis, "Circular polarised cylindrical dielectric resonator antenna," *Electronics Letters*, vol. 32, pp. 281–283, Feb 1996.

[24] K. P. Esselle, "Circularly polarised higher-order rectangular dielectric-resonator antenna," *Electronics Letters*, vol. 32, pp. 150–151, Feb 1996.

[25] Chih Yu Huang, Jian Yi Wu, and Kin Lu Wong, "Cross-slot-coupled microstrip antenna and dielectric resonator antenna for circular polarization," *IEEE Transactions on Antennas and Propagation*, vol. 47, pp. 605–609, April 1999.

[26] Chih-Yu Huang and Cheng-Fu Yang, "Cross-aperture coupled circularly polarized dielectric resonator antenna," in *IEEE Antennas and Propagation Society International Symposium. 1999 Digest. Held in conjunction with: USNC/URSI National Radio Science Meeting (Cat. No.99CH37010)*, vol. 1, pp. 34–37 vol.1, July 1999.

[27] M. T. Lee, K. M. Luk, E. K. N. Yung, and K. W. Leung, "Microstrip-line feed circularly polarized cylindrical dielectric resonator antenna," *Microwave and Optical Technology Letters*, vol. 24, no. 3, pp. 206–207, 2000.

[28] Y. Hwang, Y. P. Zhang, K. M. Luk, and E. K. N. Yung, "Gain-enhanced miniaturised rectangular dielectric resonator antenna," *Electronics Letters*, vol. 33, pp. 350–352, Feb 1997.

[29] K. W. Leung, K. M. Chow, and K. M. Luk, "Low-profile high-permittivity dielectric resonator antenna excited by a disk-loaded coaxial aperture," *IEEE Antennas and Wireless Propagation Letters*, vol. 2, pp. 212–214, 2003.

[30] Nasimuddin and K. P. Esselle, "Antennas with dielectric resonators and surface mounted short horns for high gain and large bandwidth," *IET Microwaves, Antennas Propagation*, vol. 1, pp. 723–728, June 2007.

[31] D. M. Pozar, *Microwave Engineering*. John Wiley & Sons Pte. Ltd.

[32] J. Van Bladel, "On the Resonances of a Dielectric Resonator of Very High Permittivity," *IEEE Transactions on Microwave Theory and Techniques*, vol. 23, no. 2, pp. 199–208, 1975.

[33] S. B. Cohn, "Microwave Bandpass Filters Containing High-Q Dielectric Resonators," *IEEE Transactions on Microwave Theory and Techniques*, vol. 16, pp. 218–227, April 1968.

[34] T. Itoh and R. S. Rudokas, "New Method for Computing the Resonant Frequencies of Dielectric Resonators (Short Papers)," *IEEE Transactions on Microwave Theory and Techniques*, vol. 25, pp. 52–54, Jan 1977.

[35] A. Perron, T. A. Denidni, and A. Sebak, "High-Gain Hybrid Dielectric Resonator Antenna for Millimeter-Wave Applications: Design and Implementation," *IEEE Transactions on Antennas and Propagation*, vol. 57, pp. 2882–2892, Oct 2009.

[36] Y. Coulibaly, M. Nedil, A. Hagras, D. Hammou, L. Talbi, and T. A. Denidni, "Comparative study of gain enhancement of a Dielectric Resonator antenna using three superstrates for millimeter-wave applications," in *Proceedings of the 2012 IEEE International Symposium on Antennas and Propagation*, pp. 1–2, July 2012.

[37] M. J. Al-Hasan, T. A. Denidni, and A. R. Sebak, "Millimeter-Wave EBG-Based Aperture-Coupled Dielectric Resonator Antenna," *IEEE Transactions on Antennas and Propagation*, vol. 61, pp. 4354–4357, Aug 2013.

[38] M. Akbari, S. Gupta, M. Farahani, A. R. Sebak, and T. A. Denidni, "Gain Enhancement of Circularly Polarized Dielectric Resonator Antenna Based on FSS Superstrate for MMW Applications," *IEEE Transactions on Antennas and Propagation*, vol. 64, pp. 5542–5546, Dec 2016.

[39] K. M. L. K. W. Leung, *Dielectric Resonator Antennas*. Research Studies Press Limited.

[40] A. Petosa, *Dielectric Resonator Antenna Handbook*. Artech House Publishers.

[41] R. K. Mongia, A. Ittipiboon, P. Bhartia, and M. Cuhaci, "Electric-monopole antenna using a dielectric ring resonator," *Electronics Letters*, vol. 29, pp. 1530–1531, Aug 1993.

[42] M. Verplanken and J. V. Bladel, "The Electric-Dipole Resonances of Ring Resonators of Very High Permittivity (Short Papers)," *IEEE Transactions on Microwave Theory and Techniques*, vol. 24, pp. 108–112, Feb 1976.

[43] M. Verplanken and J. Van Bladel, "The Magnetic-Dipole Resonances of Ring Resonators of Very High Permittivity," *IEEE Transactions on Microwave Theory and Techniques*, vol. 27, pp. 328–333, Apr 1979.

[44] R. De Smedt, "Correction Due to a Finite Permittivity for a Ring Resonator in Free Space," *IEEE Transactions on Microwave Theory and Techniques*, vol. 32, pp. 1288–1293, Oct 1984.

[45] R. K. Mongia, "Small eletric monopole mode dielectric resonator antenna," *Electronics Letters*, vol. 32, pp. 947–949, May 1996.

[46] S. M. Shum and K. M. Luk, "Characteristics of dielectric ring resonator antenna with an air gap," *Electronics Letters*, vol. 30, pp. 277–278, Feb 1994.

[47] M. T. K. Tam and R. D. Murch, "Compact circular sector and annular sector dielectric resonator antennas," *IEEE Transactions on Antennas and Propagation*, vol. 47, pp. 837–842, May 1999.

[48] A. Ittipiboon, A. Petosa, and S. Thirakoune, "Bandwidth enhancement of a monopole using dielectric resonator antenna loading," in *2002 9th International Symposium on Antenna Technology and Applied Electromagnetics*, pp. 1–4, July 2002.

[49] D. Guha, Y. M. M. Antar, A. A. Petosa, and D. Lee, "Improved Design Guidelines for the Ultra Wideband Monopole-Dielectric Resonator Antenna," *IEEE Antennas and Wireless Propagation Letters*, vol. 5, pp. 373–376, 2006.

[50] H. Y. Lo, K. W. Leung, K. M. Luk, and E. K. N. Yung, "Low profile equilateral-triangular dielectric resonator antenna of very high permittivity," *Electronics Letters*, vol. 35, pp. 2164–2166, Dec 1999.

[51] H. Y. Lo and K. W. Leung, "Excitation of low-profile equilateral-triangular dielectric resonator antenna using a conducting conformal strip," *Microwave and Optical Technology Letters*, vol. 29, no. 5, pp. 317–319, 2001.

[52] S. A. Schelkunoff, *Electromagnetics Waves*. D Van Nostrand Company Inc.

[53] Y. Akaiwa, "Operation Modes of a Waveguide Y Circulator (Short Papers)," *IEEE Transactions on Microwave Theory and Techniques*, vol. 22, pp. 954–960, Nov 1974.

[54] J. Helszajn and D. S. James, "Planar Triangular Resonators with Magnetic Walls," *IEEE Transactions on Microwave Theory and Techniques*, vol. 26, pp. 95–100, Feb 1978.

[55] P. L. Overfelt and D. J. White, "TE and TM Modes of Some Triangular Cross-Section Waveguides Using Superposition of Plane Waves (Short Paper)," *IEEE Transactions on Microwave Theory and Techniques*, vol. 34, no. 1, pp. 161–167, 1986.

[56] B. J. Mccartin, "Eigenstructure of the Equilateral Triangle, Part I: The Dirichlet Problem.," *Society for Industrial and Applied Mathematics*, vol. 45, no. 2, pp. 267–287, 2003.

[57] B. J. Mccartin, "Eigenstructure of the equilateral triangle, Part II: The Neumann problem.," *Mathematical Problems in Engineering*, vol. 8, 2002.

[58] A. A. Kishk, "A triangular dielectric resonator antenna excited by a coaxial probe," *Microwave and Optical Technology Letters*, vol. 30, no. 5, pp. 340–341, 2001.

[59] R. Kumari, K. Parmar, and S. K. Behera, "Conformal patch fed stacked triangular dielectric resonator antenna for WLAN applications," in *INTERACT-2010*, pp. 104–107, Dec 2010.

[60] R. Kumari, K. Parmar, and S. K. Behera, "A dual band triangular shaped DRA array for WLAN/WiMAX applications," in *2011 Annual IEEE India Conference*, pp. 1–4, Dec 2011.

[61] S. Maity, "Hybrid triangular dielectric resonator antenna (DRA) for WLAN/ISM application," in *2011 Indian Antenna Week (IAW)*, pp. 1–4, Dec 2011.

[62] S. Maity and B. Gupta, "Theoretical investigations on equilateral triangular dielectric resonator antenna," *IET Microwaves, Antennas Propagation*, vol. 11, no. 2, pp. 184–192, 2017.

[63] A. Sharma, A. Sarkar, A. Biswas, and M. Jaleel Akhtar, "Equilateral triangular dielectric resonator based co-radiator MIMO antennas with dual-polarisation," *IET Microwaves, Antennas Propagation*, vol. 12, no. 14, pp. 2161–2166, 2018.

[64] S. K. K. Dash, T. Khan, and B. K. Kanaujia, "Circularly Polarized Dual Facet Spiral Fed Compact Triangular Dielectric Resonator Antenna for Sensing Applications," *IEEE Sensors Letters*, vol. 2, no. 1, pp. 1–4, 2018.

[65] D. Sur, A. Sharma, R. K. Gangwar, and N. K. Sahu, "A novel wideband Minkowski fractal antenna with assistance of triangular dielectric resonator elements," *International Journal of RF and Microwave Computer-Aided Engineering*, vol. 29, no. 2, p. e21524, 2019.

[66] Z. Song, H. Zheng, M. Wang, Y. Li, T. Song, E. Li, and Y. Li, "Equilateral Triangular Dielectric Resonator and Metal Patch Hybrid Antenna for UWB Application," *IEEE Access*, vol. 7, pp. 119060–119068, 2019.

[67] M. Lopaz, *et al.*, "Analytical expressions of the Q-factor for the complete resonant mode spectrum of the equilateral triangular waveguide cavity," *Electronics Letters*, vol. 55, no. 17, pp. 944–947, 2019.

[68] S. Maity and B. Gupta, "Experimental Investigations on Wideband Triangular Dielectric Resonator Antenna," *IEEE Transactions on Antennas and Propagation*, vol. 64, no. 12, pp. 5483–5486, 2016.

[69] S. Maity and B. Gupta, "Resonant frequency of $30^0-60^0-90^0$ triangular dielectric resonator at fundamental mode," *AEU - International Journal of Electronics and Communications*, vol. 83, pp. 451 – 461, 2018.

[70] S. Maity, M. Gangopadhyaya, and B. Gupta, "$45^0-45^0-90^0$ Triangular dielectric resonator antenna with broadside radiation patterns," *AEU - International Journal of Electronics and Communications*, vol. 94, pp. 51 – 54, 2018.

[71] A. A. Kishk, A. W. Glisson, and Y. Yin, "Conical dielectric resonator antennas excited by a coaxial probe," *Microwave and Optical Technology Letters*, vol. 29, no. 3, pp. 160–161, 2001.

[72] A. A. Kishk, Yan Yin, and A. W. Glisson, "Conical dielectric resonator antennas for wide-band applications," *IEEE Transactions on Antennas and Propagation*, vol. 50, pp. 469–474, April 2002.

[73] R. Chair, A. A. Kishk, K. F. Lee, and C. E. Smith, "Broadband aperture coupled flipped staired pyramid and conical dielectric resonator antennas," in *IEEE Antennas and Propagation Society Symposium, 2004.*, vol. 2, pp. 1375–1378 Vol.2, June 2004.

[74] R. Chair, A. A. Kishk, K. F. Lee, and C. E. Smith, "Wideband flipped staired pyramid dielectric resonator antennas," *Electronics Letters*, vol. 40, pp. 581–582, May 2004.

[75] A. A. Kishk, "An elliptic dielectric resonator antenna designed for circular polarization with single feed," *Microwave and Optical Technology Letters*, vol. 37, no. 6, pp. 454–456, 2003.

[76] Jian-Juang Chen, Yi-Cheng Lin, and Ruey-Beei Wu, "A dual band elliptical dra," in *IEEE Antennas and Propagation Society Symposium, 2004.*, vol. 2, pp. 1355–1358 Vol.2, June 2004.

[77] A. Tadjalli, A. Sebak, and T. Denidni, "Elliptical cylinder dielectric resonator antenna," in *2004 10th International Symposium on Antenna Technology and Applied Electromagnetics and URSI Conference*, pp. 1–3, July 2004.

[78] A. Tadjalli, A. Sebak, and T. Denidni, "Modes of elliptical cylinder dielectric resonator and its resonant frequencies," in *IEEE Antennas and Propagation Society Symposium, 2004.*, vol. 2, pp. 2039–2042 Vol.2, June 2004.

[79] S. L. S. Yang, R. Chair, A. A. Kishk, K. F. Lee, and K. M. Luk, "Single-feed elliptical dielectric resonator antennas for circularly polarized applications," *Microwave and Optical Technology Letters*, vol. 48, no. 11, pp. 2340–2345, 2006.

[80] A. A. Kishk, "Wide-band truncated tetrahedron dielectric resonator antenna excited by a coaxial probe," *IEEE Transactions on Antennas and Propagation*, vol. 51, pp. 2913–2917, Oct 2003.

[81] V. Hamsakutty, A. V. Praveen Kumar, J. Yohannan, and K. T. Mathew, "Hexagonal dielectric resonator antenna for multi-frequency operation," in *2006 IEEE Antennas and Propagation Society International Symposium*, pp. 1329–1332, July 2006.

[82] V. Hamsakutty, A. V. Praveen Kumar, J. Yohannan, G. Bindu, and K. T. Mathew, "Coaxial fed hexagonal dielectric resonator antenna for multifrequency operation," *Microwave and Optical Technology Letters*, vol. 48, no. 5, pp. 878–880, 2006.

[83] V. Hamsakutty, A. V. P. Kumar, J. Yohannan, and K. T. Mathew, "Hexagonal dielectric resonator antenna for 2.4 GHz WLAN applications," *Microwave and Optical Technology Letters*, vol. 49, no. 1, pp. 162–164, 2007.

[84] A. Ittipiboon, A. Petosa, D. Roscoe, and M. Cuhaci, "An investigation of a novel broadband dielectric resonator antenna," in *IEEE Antennas and Propagation Society International Symposium. 1996 Digest*, vol. 3, pp. 2038–2041 vol.3, July 1996.

[85] G. Drossos, Z. Wu, and L. E. Davis, "The air gap effect on a microstrip-coupled cylindrical dielectric resonator antenna," *Microwave and Optical Technology Letters*, vol. 20, no. 1, pp. 36–40.

[86] Sheng-Ming Deng, Ching-Long Tsai, Sheng-Far Chang, and Sheau-Shong Bor, "A CPW-fed suspended, low profile rectangular dielectric resonator antenna for wideband operation," in *2005 IEEE Antennas and Propagation Society International Symposium*, vol. 4B, pp. 242–245 vol. 4B, July 2005.

[87] L. C. Y. Chu, D. Guha, and Y. M. M. Antar, "Conformal Strip-Fed Shaped Cylindrical Dielectric Resonator: Improved Design of a Wideband Wireless Antenna," *IEEE Antennas and Wireless Propagation Letters*, vol. 8, pp. 482–485, 2009.

[88] X. Liang and T. A. Denidni, "Wideband Rectangular Dielectric Resonator Antenna With a Concave Ground Plane," *IEEE Antennas and Wireless Propagation Letters*, vol. 8, pp. 367–370, 2009.

[89] M. Khalily, M. K. A. Rahim, and A. A. Kishk, "Bandwidth Enhancement and Radiation Characteristics Improvement of Rectangular Dielectric Resonator Antenna," *IEEE Antennas and Wireless Propagation Letters*, vol. 10, pp. 393–395, 2011.

[90] Y. Gao, Z. Feng, and L. Zhang, "Compact Asymmetrical T-Shaped Dielectric Resonator Antenna for Broadband Applications," *IEEE Transactions on Antennas and Propagation*, vol. 60, pp. 1611–1615, March 2012.

[91] M. Lapierre, Y. M. M. Antar, A. Ittipiboon, and A. Petosa, "A wideband monopole antenna using dielectric resonator loading," in *IEEE Antennas and Propagation Society International Symposium. Digest. Held in conjunction with: USNC/CNC/URSI North American Radio Sci. Meeting (Cat. No.03CH37450)*, vol. 3, pp. 16–19 vol.3, June 2003.

[92] M. Lapierre, Y. M. M. Antar, A. Ittipiboon, and A. Petosa, "Ultra wideband monopole/dielectric resonator antenna," *IEEE Microwave and Wireless Components Letters*, vol. 15, pp. 7–9, Jan 2005.

[93] K. W. Leung, W. C. Wong, K. M. Luk, and E. K. N. Yung, "Annular slot-coupled dielectric resonator antenna," *Electronics Letters*, vol. 34, pp. 1275–1277, June 1998.

[94] Y. Gao, Chee-Parng Chua, A. P. Popov, and Ban-Leong Ooi, "Integrated wideband rectangular dielectric resonator antenna for WLAN," in *2005 IEEE Antennas and Propagation Society International Symposium*, vol. 2A, pp. 180–183 vol. 2A, July 2005.

[95] Tso-Wei Li and Jwo-Shiun Sun, "A wide U-shape slot fed broadband dielectric resonator antenna," in *11th International Symposium on Antenna Technology and Applied Electromagnetics [ANTEM 2005]*, pp. 1–3, June 2005.

[96] S. K. Menon, B. Lethakumary, P. Mohanan, P. V. Bijumon, and M. T. Sebastian, "Wideband cylindrical dielectric resonator antenna excited using an L-strip feed," *Microwave and Optical Technology Letters*, vol. 42, no. 4, pp. 293–294, 2004.

[97] P. V. Bijumon, S. K. Menon, M. N. Suma, M. T. Sebastian, and P. Mohanan, "Broadband cylindrical dielectric resonator antenna excited by modified microstrip line," *Electronics Letters*, vol. 41, pp. 385–387, March 2005.

[98] T.-H. Huang, H.-J. Chen, T.-M. Chen, L.-S. Chen, C.-C. Liu, C.-I. Hung, Y.-H. Wang, and M.-P. Houng, "A simple design cylindrical dielectric resonator antenna with wide aperture-coupled for broadband applications," *Microwave and Optical Technology Letters*, vol. 49, no. 5, pp. 1064–1067, 2007.

[99] Xiao-ming Wang, Yong-chang Jiao, Zi-bin Weng, and Fu-shun Zhang, "Slot-fed cylindrical dielectric resonator antenna (DRA) for wideband application," in *Proceedings of the 9th International Symposium on Antennas, Propagation and EM Theory*, pp. 263–266, Nov 2010.

[100] X. Liang, T. A. Denidni, and L. Zhang, "Wideband L-Shaped Dielectric Resonator Antenna With a Conformal Inverted-Trapezoidal Patch Feed," *IEEE Transactions on Antennas and Propagation*, vol. 57, pp. 271–274, Jan 2009.

[101] W. Chang and Z. Feng, "Investigation of a Novel Wideband Feeding Technique for Dielectric Ring Resonator Antennas," *IEEE Antennas and Wireless Propagation Letters*, vol. 8, pp. 348–351, 2009.

[102] M. Khalily, M. K. A. Rahim, and A. A. Kishk, "Bandwidth Enhancement and Radiation Characteristics Improvement of Rectangular Dielectric Resonator Antenna," *IEEE Antennas and Wireless Propagation Letters*, vol. 10, pp. 393–395, 2011.

[103] A. Rashidian, L. Shafai, and D. M. Klymyshyn, "Compact Wideband Multimode Dielectric Resonator Antennas Fed With Parallel Standing Strips," *IEEE Transactions on Antennas and Propagation*, vol. 60, pp. 5021–5031, Nov 2012.

[104] A. Rashidian, M. Tayfeh Aligodarz, L. Shafai, and D. M. Klymyshyn, "On the Matching of Microstrip-Fed Dielectric Resonator Antennas," *IEEE Transactions on Antennas and Propagation*, vol. 61, pp. 5291–5296, Oct 2013.

[105] R. K. Chaudhary, R. Kumar, and K. V. Srivastava, "Wideband Ring Dielectric Resonator Antenna With Annular-Shaped Microstrip Feed," *IEEE Antennas and Wireless Propagation Letters*, vol. 12, pp. 595–598, 2013.

[106] C. Prachi, R. K. Chaudhary, and K. V. Srivastava, "Rounded bevel shaped fed cylindrical dielectric resonator antenna for wideband applications," *Microwave and Optical Technology Letters*, vol. 57, no. 10, pp. 2364–2368, 2015.

[107] G. Bit-Babik, C. Di Nallo, and A. Faraone, "Multimode dielectric resonator antenna of very high permittivity," in *IEEE Antennas and Propagation Society Symposium, 2004.*, vol. 2, pp. 1383–1386 Vol.2, June 2004.

[108] T. Chang, Y. Huang, W. Su, and J. Kiang, "Wideband Dielectric Resonator Antenna With a Tunnel," *IEEE Antennas and Wireless Propagation Letters*, vol. 7, pp. 275–278, 2008.

[109] A. S. Al-Zoubi and A. A. Kishk, "Wide band strip-fed rectangular dielectric resonator antenna with improved radiation patterns," in *2009 IEEE Antennas and Propagation Society International Symposium*, pp. 1–4, June 2009.

[110] T. Chang and J. Kiang, "Bandwidth Broadening of Dielectric Resonator Antenna by Merging Adjacent Bands," *IEEE Transactions on Antennas and Propagation*, vol. 57, pp. 3316–3320, Oct 2009.

[111] S. K. Sharma and M. K. Brar, "Aperture-coupled pentagon shape dielectric resonator antennas providing wideband and multiband performance," *Microwave and Optical Technology Letters*, vol. 55, no. 2, pp. 395–400, 2013.

[112] B. Mukherjee, P. Patel, and J. Mukherjee, "A Novel Cup-Shaped Inverted Hemispherical Dielectric Resonator Antenna for Wideband Applications," *IEEE Antennas and Wireless Propagation Letters*, vol. 12, pp. 1240–1243, 2013.

[113] A. Sharma, A. Sarkar, A. Biswas, and M. J. Akhtar, "A-shaped wideband dielectric resonator antenna for wireless communication systems and its MIMO implementation," *International Journal of RF and Microwave Computer-Aided Engineering*, vol. 28, no. 8, p. e21402, 2018.

[114] S. M. Shum and K. M. Luk, "Stacked annular ring dielectric resonator antenna excited by axi-symmetric coaxial probe," *IEEE Transactions on Antennas and Propagation*, vol. 43, pp. 889–892, Aug 1995.

[115] K. M. Luk, K. W. Leung, and K. Y. Chow, "Bandwidth and gain enhancement of a dielectric resonator antenna with the use of a stacking element," *Microwave and Optical Technology Letters*, vol. 14, no. 4, pp. 215–217.

[116] A. A. Kishk, Xiao Zhang, A. W. Glisson, and D. Kajfez, "Numerical analysis of stacked dielectric resonator antennas excited by a coaxial probe for wideband applications," *IEEE Transactions on Antennas and Propagation*, vol. 51, pp. 1996–2006, Aug 2003.

[117] Z. Fan, Y. M. M. Antar, A. Ittipiboon, and A. Petosa, "Parasitic coplanar three-element dielectric resonator antenna subarray," *Electronics Letters*, vol. 32, pp. 789–790, April 1996.

[118] D. Guha and Y. M. M. Antar, "Four-Element Cylindrical Dielectric Resonator Antenna for Wideband Monopole-Like Radiation," *IEEE Transactions on Antennas and Propagation*, vol. 54, pp. 2657–2662, Sep. 2006.

[119] A. A. Kishk, "Experimental study of broadband embedded dielectric resonator antennas excited by a narrow slot," *IEEE Antennas and Wireless Propagation Letters*, vol. 4, pp. 79–81, 2005.

[120] Yong-Xin Guo, Yu-Feng Ruan, and Xiang-Quan Shi, "Wide-band stacked double annular-ring dielectric resonator antenna at the end-fire mode operation," *IEEE Transactions on Antennas and Propagation*, vol. 53, pp. 3394–3397, Oct 2005.

[121] R. K. Chaudhary, H. B. Baskey, K. V. Srivastava, and A. Biswas, "Wideband two-layer rectangular dielectric resonator antenna with $(Zr_{0.8}Sn_{0.2})TiO_4$-epoxy composite system," in *2011 Indian Antenna Week (IAW)*, pp. 1–4, Dec 2011.

[122] R. K. Chaudhary, K. V. Srivastava, and A. Biswas, "Wideband multilayer multi-permittivity half-split cylindrical dielectric resonator antenna," *Microwave and Optical Technology Letters*, vol. 54, no. 11, pp. 2587–2590, 2012.

[123] X. S. Fang and K. W. Leung, "Design of Wideband Omnidirectional Two-Layer Transparent Hemispherical Dielectric Resonator Antenna," *IEEE Transactions on Antennas and Propagation*, vol. 62, pp. 5353–5357, Oct 2014.

[124] Y. M. Pan and S. Y. Zheng, "A Low-Profile Stacked Dielectric Resonator Antenna With High-Gain and Wide Bandwidth," *IEEE Antennas and Wireless Propagation Letters*, vol. 15, pp. 68–71, 2016.

[125] M. R. Hajihashemi and H. Abiri, "Parametric study of novel types of dielectric resonator antennas based on fractal geometry," *International Journal of RF and Microwave Computer-Aided Engineering*, vol. 17, no. 4, pp. 416–424, 2007.

[126] S. Dhar, R. Ghatak, B. Gupta, and D. R. Poddar, "A Wideband Minkowski Fractal Dielectric Resonator Antenna," *IEEE Transactions on Antennas and Propagation*, vol. 61, pp. 2895–2903, June 2013.

[127] B. Mukherjee, P. Patel, and J. Mukherjee, "Hemispherical Dielectric Resonator Antenna Based on Apollonian Gasket of Circles- A Fractal Approach," *IEEE Transactions on Antennas and Propagation*, vol. 62, pp. 40–47, Jan 2014.

[128] S. Dhar, K. Patra, R. Ghatak, B. Gupta, and D. R. Poddar, "A Dielectric Resonator-Loaded Minkowski Fractal-Shaped Slot Loop Heptaband Antenna," *IEEE Transactions on Antennas and Propagation*, vol. 63, pp. 1521–1529, April 2015.

[129] D. V. Kiran, D. Sankaranarayanan, and B. Mukherjee, "Compact Embedded Dual-Element Rectangular Dielectric Resonator Antenna Combining Sierpinski and Minkowski Fractals," *IEEE Transactions on Components, Packaging and Manufacturing Technology*, vol. 7, pp. 786–791, May 2017.

[130] D. Guha, B. Gupta, and Y. M. M. Antar, "New Pawn-Shaped Dielectric Ring Resonator Loaded Hybrid Monopole Antenna for Improved Ultrawide Bandwidth," *IEEE Antennas and Wireless Propagation Letters*, vol. 8, pp. 1178–1181, 2009.

[131] D. Guha, B. Gupta, and Y. M. M. Antar, "Hybrid monopole-DRA: New geometries for improved ultra-wideband operation," in *2010 IEEE Antennas and Propagation Society International Symposium*, pp. 1–4, July 2010.

[132] M. N. Jazi, T. A. Denidni, and A. R. Sebak, "Ultra-wideband dielectric-resonator antenna based on hybrid techniques," in *2010 14th International Symposium on Antenna Technology and Applied Electromagnetics the American Electromagnetics Conference*, pp. 1–4, July 2010.

[133] C. Ozzaim, F. Ustuner, and N. Tarim, "Stacked Conical Ring Dielectric Resonator Antenna Excited by a Monopole for Improved Ultrawide Bandwidth," *IEEE Transactions on Antennas and Propagation*, vol. 61, pp. 1435–1438, March 2013.

[134] K. H. R. Zheng, H. O. Chua, and L. Li, "Analysis and design of UWB monopole-dielectric resonator antenna," in *2010 IEEE International Conference on Ultra-Wideband*, vol. 1, pp. 1–4, Sep. 2010.

[135] L. Huitema, M. Koubeissi, C. Decroze, and T. Monediere, "Ultrawideband Dielectric Resonator Antenna for DVB-H and GSM Applications," *IEEE Antennas and Wireless Propagation Letters*, vol. 8, pp. 1021–1027, 2009.

[136] T. A. Denidni and Z. Weng, "Hybrid ultrawideband dielectric resonator antenna and band-notched designs," *IET Microwaves, Antennas Propagation*, vol. 5, pp. 450–458, March 2011.

[137] M. Niroo-Jazi and T. A. Denidni, "Experimental Investigations of a Novel Ultrawideband Dielectric Resonator Antenna With Rejection Band Using Hybrid Techniques," *IEEE Antennas and Wireless Propagation Letters*, vol. 11, pp. 492–495, 2012.

[138] M. Abedian, S. K. A. Rahim, S. Danesh, M. Khalily, and S. M. Noghabaei, "Ultrawideband Dielectric Resonator Antenna With WLAN Band Rejection at 5.8 GHz," *IEEE Antennas and Wireless Propagation Letters*, vol. 12, pp. 1523–1526, 2013.

[139] M. Abedian, S. K. A. Rahim, S. Danesh, S. Hakimi, L. Y. Cheong, and M. H. Jamaluddin, "Novel Design of Compact UWB Dielectric Resonator Antenna With Dual-Band-Rejection Characteristics for WiMAX/WLAN Bands," *IEEE Antennas and Wireless Propagation Letters*, vol. 14, pp. 245–248, 2015.

[140] Y. Ge, K. P. Esselle, and T. S. Bird, "Compact Dielectric Resonator Antennas With Ultrawide 60% - 110% Bandwidth," *IEEE Transactions on Antennas and Propagation*, vol. 59, pp. 3445–3448, Sep. 2011.

[141] M. Abedian, S. K. A. Rahim, and M. Khalily, "Two-Segments Compact Dielectric Resonator Antenna for UWB Application," *IEEE Antennas and Wireless Propagation Letters*, vol. 11, pp. 1533–1536, 2012.

[142] T. A. Denidni, Z. Weng, and M. Niroo-Jazi, "Z-Shaped Dielectric Resonator Antenna for Ultrawideband Applications," *IEEE Transactions on Antennas and Propagation*, vol. 58, pp. 4059–4062, Dec 2010.

[143] K. S. Ryu and A. A. Kishk, "UWB dielectric resonator antenna mounted on a vertical ground plane edge," in *2009 IEEE Antennas and Propagation Society International Symposium*, pp. 1–4, June 2009.

[144] K. S. Ryu and A. A. Kishk, "Ultrawideband Dielectric Resonator Antenna With Broadside Patterns Mounted on a Vertical Ground Plane Edge," *IEEE Transactions on Antennas and Propagation*, vol. 58, pp. 1047–1053, April 2010.

[145] K. S. Ryu and A. A. Kishk, "UWB dielectric resonator antenna with low cross-polarization," in *2010 IEEE Radio and Wireless Symposium (RWS)*, pp. 551–554, Jan 2010.

[146] K. S. Ryu and A. A. Kishk, "UWB Dielectric Resonator Antenna Having Consistent Omnidirectional Pattern and Low Cross-Polarization Characteristics," *IEEE Transactions on Antennas and Propagation*, vol. 59, pp. 1403–1408, April 2011.

[147] O. M. H. Ahmed, A. R. Sebak, and T. A. Denidni, "Compact UWB printed monopole loaded with dielectric resonator antenna," *Electronics Letters*, vol. 47, pp. 7–8, January 2011.

[148] Y. Sung, C. S. Ahn, and Y.-S. Kim, "Microstripline fed dual-frequency dielectric resonator antenna," *Microwave and Optical Technology Letters*, vol. 42, no. 5, pp. 388–390, 2004.

[149] B. Paul, S. Mridula, P. Mohanan, P. V. Bijumon, and M. T. Sebastian, "A compact very-high-permittivity dielectric-eye resonator antenna for multiband wireless applications," *Microwave and Optical Technology Letters*, vol. 43, no. 2, pp. 118–121, 2004.

[150] A. V. Praveen Kumar, J. Yohannan, C. K. Anandan, and K. T. Mathew, "Microstripline fed cylindrical dielectric resonator antenna for dual-band operation," *Microwave and Optical Technology Letters*, vol. 47, no. 2, pp. 150–153, 2005.

[151] Sheng-Ming Deng, Cho-Kang Hsu, and Ching-Long Tsai, "A slot-coupled rectangular dielectric resonator antenna for dual-band operations," in *2005 IEEE Antennas and Propagation Society International Symposium*, vol. 2A, pp. 188–191 vol. 2A, July 2005.

[152] E. H. Lim and K. W. Leung, "Dual-wideband rectangular dielectric resonator antenna for WLAN communications," *Microwave and Optical Technology Letters*, vol. 48, no. 2, pp. 378–380, 2006.

[153] X. S. Fang and K. W. Leung, "Designs of Single-, Dual-, Wide-Band Rectangular Dielectric Resonator Antennas," *IEEE Transactions on Antennas and Propagation*, vol. 59, pp. 2409–2414, June 2011.

[154] R. Kumari and S. K. Behera, "Miniaturized dual-band dielectric resonator antenna for IEEE 802.16d fixed WiMAX applications," *International Journal of RF and Microwave Computer-Aided Engineering*, vol. 22, no. 6, pp. 682–689, 2012.

[155] E. E. C. Oliveira, A. G. D' Assuncao, J. B. L. Oliveira, A. M. Cabral, P. C. Assis Jr., and M. S. Vieira, "Aperture coupled $BaTiO_3$ based dielectric resonator antenna with dualband," *Microwave and Optical Technology Letters*, vol. 55, no. 11, pp. 2759–2763, 2013.

[156] T. A. Denidni, Q. Rao, and A. R. Sebak, "Two-ring slot-fed dielectric resonator antenna for dual-frequency operation," *Microwave and Optical Technology Letters*, vol. 44, no. 5, pp. 448–451, 2005.

[157] Y. Gao, B.-L. Ooi, and A. P. Popov, "Dual-band hybrid dielectric resonator antenna with CPW-fed slot," *Microwave and Optical Technology Letters*, vol. 48, no. 1, pp. 170–172, 2006.

[158] Z. Wang, S. Kamalraj, C. C. Chiau, X. Chen, B. S. Collins, and S. P. Kingsley, "Dual-band Dielectric Antenna for WLAN Applications," in *2007 International workshop on Antenna Technology: Small and Smart Antennas Metamaterials and Applications*, pp. 151–154, March 2007.

[159] M. Khalily, M. K. A. Rahim, N. A. Murad, N. A. Samsuri, and A. A. Kishk, "Rectangular ring-shaped dielectric resonator antenna for dual and wideband frequency," *Microwave and Optical Technology Letters*, vol. 55, no. 5, pp. 1077–1081, 2013.

[160] Y. Ding, K. W. Leung, and Y. C. Or, "Dualband DRA-slot hybrid slot antenna," in *2007 IEEE Antennas and Propagation Society International Symposium*, pp. 976–979, June 2007.

[161] D. Batra and S. Sharma, "Dual band dielectric resonator antenna for wireless application," *International Journal of Electronics*, vol. 99, no. 9, pp. 1323–1331, 2012.

[162] A. Sharma and R. K. Gangwar, "Compact dual-band ring dielectric resonator antenna with moon-shaped defected ground structure for WiMAX/WLAN applications," *International Journal of RF and Microwave Computer-Aided Engineering*, vol. 26, no. 6, pp. 503–511, 2016.

[163] H. Liu, Y. Liu, M. Wei, and S. Gong, "A novel dual-broadband dielectric resonator antenna based on modified Sierpinski fractal geometry," in *2015 IEEE International Symposium on Antennas and Propagation USNC/URSI National Radio Science Meeting*, pp. 43–44, July 2015.

[164] P. Gupta, D. Guha, and C. Kumar, "Dielectric Resonator Working as Feed as Well as Antenna: New Concept for Dual-Mode Dual-Band Improved Design," *IEEE Transactions on Antennas and Propagation*, vol. 64, pp. 1497–1502, April 2016.

[165] A. Sharma, G. Das, P. Ranjan, N. K. Sahu, and R. K. Gangwar, "Novel Feeding Mechanism to Stimulate Triple Radiating Modes in Cylindrical Dielectric Resonator Antenna," *IEEE Access*, vol. 4, pp. 9987–9992, 2016.

[166] V. Hamsakutty, A. V. Praveen Kumar, G. Bindu, V. Thomas, A. Lonappan, J. Yohannan, and K. T. Mathew, "A multifrequency coaxial-fed metal coated dielectric resonator antenna," *Microwave and Optical Technology Letters*, vol. 47, no. 6, pp. 573–575, 2005.

[167] A. Sangiovanni, J. Y. Dauvignac, and C. Pichot, "Stacked dielectric resonator antenna for multifrequency operation," *Microwave and Optical Technology Letters*, vol. 18, no. 4, pp. 303–306.

[168] R. K. Chaudhary, K. V. Srivastava, and A. Biswas, "A novel triple-band cylindrical dielectric resonator antenna using varying permittivity in ϕ-direction," in *Proceedings of the 2012 IEEE International Symposium on Antennas and Propagation*, pp. 1–2, July 2012.

[169] M. R. Haji-hashemi and M. Moradian, "Dielectric resonator antenna based on fudgeflake geometry," in *2006 IEEE Antennas and Propagation Society International Symposium*, pp. 1325–1328, July 2006.

[170] Y. Coulibaly, H. Boutayeb, T. A. Denidni, and L. Talbi, "Gain enhancement of a dielectric resonator antenna using a cylindrical electromagnetic crystal substrate," in *2007 IEEE Antennas and Propagation Society International Symposium*, pp. 1325–1328, June 2007.

[171] T. A. Denidni, Y. Coulibaly, and H. Boutayeb, "Hybrid Dielectric Resonator Antenna With Circular Mushroom-Like Structure for Gain Improvement," *IEEE Transactions on Antennas and Propagation*, vol. 57, pp. 1043–1049, April 2009.

[172] D. Guha, A. Banerjee, and Y. M. M. Antar, "New radiating mode in a Cylindrical DRA to produce broadside high gain radiation," in *2010 IEEE Antennas and Propagation Society International Symposium*, pp. 1–4, July 2010.

[173] A. Petosa and S. Thirakoune, "Rectangular Dielectric Resonator Antennas With Enhanced Gain," *IEEE Transactions on Antennas and Propagation*, vol. 59, pp. 1385–1389, April 2011.

[174] D. Guha, A. Banerjee, C. Kumar, and Y. M. M. Antar, "Higher Order Mode Excitation for High-Gain Broadside Radiation From Cylindrical Dielectric Resonator Antennas," *IEEE Transactions on Antennas and Propagation*, vol. 60, pp. 71–77, Jan 2012.

[175] S. Fakhte, H. Oraizi, and M. H. Vadjed Samiei, "A High Gain Dielectric Resonator Loaded Patch Antenna," *Progress In Electromagnetics Research C*, vol. 30, pp. 147–158, 2012.

[176] M. Ranjbar Nikkhah, J. Rashed-Mohassel, and A. A. Kishk, "High-Gain Aperture Coupled Rectangular Dielectric Resonator Antenna Array Using Parasitic Elements," *IEEE Transactions on Antennas and Propagation*, vol. 61, pp. 3905–3908, July 2013.

[177] L. Y. Feng and K. W. Leung, "Gain enhancement of omnidirectional dielectric resonator antenna using a higher-order mode," in *2014 IEEE Antennas and Propagation Society International Symposium (APSURSI)*, pp. 1970–1971, July 2014.

[178] A. Rashidian, L. Shafai, and D. M. Klymyshyn, "Tall microstrip transmission lines for dielectric resonator antenna applications," *IET Microwaves, Antennas Propagation*, vol. 8, pp. 112–124, January 2014.

[179] M. Mrnka and Z. Raida, "Enhanced-Gain Dielectric Resonator Antenna Based on the Combination of Higher-Order Modes," *IEEE Antennas and Wireless Propagation Letters*, vol. 15, pp. 710–713, 2016.

[180] K. Dutta, D. Guha, C. Kumar, and Y. M. M. Antar, "New Approach in Designing Resonance Cavity High-Gain Antenna Using Nontransparent Conducting Sheet as the Superstrate," *IEEE Transactions on Antennas and Propagation*, vol. 63, pp. 2807–2813, June 2015.

[181] L. Zhong, J. Hong, and H. Zhou, "A Novel Pattern-Reconfigurable Cylindrical Dielectric Resonator Antenna With Enhanced Gain," *IEEE Antennas and Wireless Propagation Letters*, vol. 15, pp. 1253–1256, Dec 2016.

[182] S. K. K. Dash, T. Khan, B. K. Kanaujia, and Y. M. M. Antar, "Gain improvement of cylindrical dielectric resonator antenna using flat reflector plane: a new approach," *IET Microwaves, Antennas Propagation*, vol. 11, no. 11, pp. 1622–1628, 2017.

[183] S. Fakhte, H. Oraizi, L. Matekovits, and G. Dassano, "Cylindrical Anisotropic Dielectric Resonator Antenna With Improved Gain," *IEEE Transactions on Antennas and Propagation*, vol. 65, pp. 1404–1409, March 2017.

[184] S. Fakhte, H. Oraizi, and L. Matekovits, "Gain Improvement of Rectangular Dielectric Resonator Antenna by Engraving Grooves on Its Side Walls," *IEEE Antennas and Wireless Propagation Letters*, vol. 16, pp. 2167–2170, 2017.

[185] S. Fakhte, H. Oraizi, and L. Matekovits, "High Gain Rectangular Dielectric Resonator Antenna Using Uniaxial Material at Fundamental Mode," *IEEE Transactions on Antennas and Propagation*, vol. 65, pp. 342–347, Jan 2017.

[186] Nasimuddin and K. P. Esselle, "A Low-Profile Compact Microwave Antenna With High Gain and Wide Bandwidth," *IEEE Transactions on Antennas and Propagation*, vol. 55, pp. 1880–1883, June 2007.

[187] Y. . Wang, T. A. Denidni, Q. . Zeng, and G. Wei, "Design of high gain, broadband cylindrical dielectric resonator antenna," *Electronics Letters*, vol. 49, pp. 1506–1507, November 2013.

[188] P. Patel, B. Mukherjee, and J. Mukherjee, "Rectangular Dielectric Resonator Antenna for wideband and high gain applications," in *2014 Asia-Pacific Microwave Conference*, pp. 330–332, Nov 2014.

[189] B. Mukherjee, V. D. Kumar, and M. Gupta, "A novel Hemispherical Dielectric Resonator Antenna on an Electromagnetic Band Gap substrate for broadband and high gain systems," *AEU - International Journal of Electronics and Communications*, vol. 68, no. 12, pp. 1185 – 1190, 2014.

[190] B. Sahu, P. Tripathi, R. Singh, and S. P. Singh, "Dual segment rectangular dielectric resonator antenna with metamaterial for improvement of bandwidth and gain," *International Journal of RF and Microwave Computer-Aided Engineering*, vol. 24, no. 6, pp. 646–655, 2014.

[191] R. M. Hashmi and K. P. Esselle, "A wideband EBG resonator antenna with an extremely small footprint area," *Microwave and Optical Technology Letters*, vol. 57, no. 7, pp. 1531–1535, 2015.

[192] P. F. Hu, Y. M. Pan, X. Y. Zhang, and S. Y. Zheng, "A Compact Filtering Dielectric Resonator Antenna With Wide Bandwidth and High Gain," *IEEE Transactions on Antennas and Propagation*, vol. 64, pp. 3645–3651, Aug 2016.

[193] R. Cicchetti, A. Faraone, E. Miozzi, R. Ravanelli, and O. Testa, "A High-Gain Mushroom-Shaped Dielectric Resonator Antenna for Wideband Wireless Applications," *IEEE Transactions on Antennas and Propagation*, vol. 64, pp. 2848–2861, July 2016.

[194] M. Haneishi and H. Takazawa, "Broadband circularly polarised planar array composed of a pair of dielectric resonator antennas," *Electronics Letters*, vol. 21, pp. 437–438, May 1985.

[195] M. B. Oliver, R. K. Mongia, and Y. M. M. Antar, "A new broadband circularly polarized dielectric resonator antenna," in *IEEE Antennas and Propagation Society International Symposium. 1995 Digest*, vol. 1, pp. 738–741 vol.1, June 1995.

[196] T. Inoue, N. Inagaki, N. Kikuma, and K. Sakakibara, "Design of circularly polarized dielectric resonator antenna using modal polarization current model method," in *IEEE Antennas and Propagation Society International Symposium. Digest. Held in conjunction with: USNC/CNC/URSI North American Radio Sci. Meeting (Cat. No.03CH37450)*, vol. 3, pp. 504–507 vol.3, June 2003.

[197] A. Ittipiboon, D. Roscoe, R. Mongia, and M. Cuhaci, "A circularly polarized dielectric guide antenna with a single slot feed," in *Symposium on Antenna Technology and Applied Electromagnetics [ANTEM 1994]*, pp. 427–430, Aug 1994.

[198] K. W. Leung and S. K. Mok, "Circularly polarised dielectric resonator antenna excited by perturbed annular slot with backing cavity," *Electronics Letters*, vol. 37, pp. 934–936, July 2001.

[199] C.-Y. Huang and J.-S. Kuo, "Frequency-adjustable circularly polarized dielectric resonator antenna," *Microwave and Optical Technology Letters*, vol. 34, no. 3, pp. 211–213, 2002.

[200] Ching-Wei Ling and Chih-Yu Huang, "Dual-band circularly polarized dielectric resonator antenna," in *IEEE Antennas and Propagation Society International Symposium. Digest. Held in conjunction with: USNC/CNC/URSI North American Radio Sci. Meeting (Cat. No.03CH37450)*, vol. 3, pp. 496–499 vol.3, June 2003.

[201] K. K. So, K. W. Leung, and H. K. Ng, "Frequency design of the circularly polarized dielectric resonator antenna," in *IEEE Antennas and Propagation Society Symposium, 2004.*, vol. 1, pp. 1090–1093 Vol.1, June 2004.

[202] B. Li, K. K. So, and K. W. Leung, "A circularly polarized dielectric resonator antenna excited by an asymmetrical U-slot with a backing cavity," *IEEE Antennas and Wireless Propagation Letters*, vol. 2, pp. 133–135, 2003.

[203] K. W. Leung, "Circularly polarized dielectric resonator antenna excited by a shorted annular slot with a backing cavity," *IEEE Transactions on Antennas and Propagation*, vol. 52, pp. 2765–2770, Oct 2004.

[204] D. L. Sounas, N. V. Kantartzis, and T. D. Tsiboukis, "Optimized ADI-FDTD analysis of circularly polarized microstrip and dielectric resonator antennas," *IEEE Microwave and Wireless Components Letters*, vol. 16, pp. 63–65, Feb 2006.

[205] G. Almpanis, C. Fumeaux, and R. Vahldieck, "Offset Cross-Slot-Coupled Dielectric Resonator Antenna for Circular Polarization," *IEEE Microwave and Wireless Components Letters*, vol. 16, pp. 461–463, Aug 2006.

[206] A. Tadjalli, A. Sebak, and T. Denidni, "Design of circularly polarized slot-coupled elliptical dielectric resonator antenna," in *2007 IEEE Antennas and Propagation Society International Symposium*, pp. 4881–4884, June 2007.

[207] B. Li and K. W. Leung, "On the circularly polarized hemi-ellipsoidal dielectric resonator antenna," *Microwave and Optical Technology Letters*, vol. 48, no. 9, pp. 1763–1766, 2006.

[208] Chih-Yu Huang and Ching-Wei Ling, "Frequency-adjustable circularly polarised dielectric resonator antenna with slotted ground plane," *Electronics Letters*, vol. 39, pp. 1030–1031, July 2003.

[209] F.-R. Hsiao, T.-W. Chiou, and K.-L. Wong, "Circularly polarized low-profile square dielectric resonator antenna with a loading patch," *Microwave and Optical Technology Letters*, vol. 31, no. 3, pp. 157–159, 2001.

[210] R. T. Long, R. J. Dorris, S. A. Long, M. A. Khayat, and J. T. Williams, "Use of parasitic strip to produce circular polarisation and increased bandwidth for cylindrical dielectric resonator antenna," *Electronics Letters*, vol. 37, pp. 406–408, March 2001.

[211] H. K. Ng and K. W. Leung, "Excitation of CP aperture-coupled dielectric resonator antenna with a parasitic patch," in *IEEE Antennas and Propagation Society International Symposium. 2001 Digest. Held in conjunction with: USNC/URSI National Radio Science Meeting (Cat. No.01CH37229)*, vol. 4, pp. 202–205 vol.4, July 2001.

[212] K. W. Leung, W. C. Wong, and H. K. Ng, "Circularly polarized slot-coupled dielectric resonator antenna with a parasitic patch," *IEEE Antennas and Wireless Propagation Letters*, vol. 1, pp. 57–59, 2002.

[213] Kwok Wa Leung and Hoi Kuen Ng, "Theory and experiment of circularly polarized dielectric resonator antenna with a parasitic patch," *IEEE Transactions on Antennas and Propagation*, vol. 51, pp. 405–412, March 2003.

[214] S. Dhar, R. Ghatak, B. Gupta, and D. R. Poddar, "Circularly polarized Minkowski fractal dielectric resonator antenna," in *2013 International Symposium on Electromagnetic Theory*, pp. 470–472, May 2013.

[215] A. Altaf, Y. Yang, K. Lee, and K. C. Hwang, "Circularly Polarized Spidron Fractal Dielectric Resonator Antenna," *IEEE Antennas and Wireless Propagation Letters*, vol. 14, pp. 1806–1809, 2015.

[216] M. Haneishi, S. Yoshida, and N. Goto, "A broadband microstrip array composed of single-feed type circularly polarized microstrip antennas," in *1982 Antennas and Propagation Society International Symposium*, vol. 20, pp. 160–163, May 1982.

[217] J. Huang, "A technique for an array to generate circular polarization with linearly polarized elements," *IEEE Transactions on Antennas and Propagation*, vol. 34, pp. 1113–1124, Sep. 1986.

[218] A. Petosa, A. Ittipiboon, and M. Cuhaci, "Array of circular-polarised cross dielectric resonator antennas," *Electronics Letters*, vol. 32, pp. 1742–1743, Sep. 1996.

[219] M. Haneishi and Bing Wu, "Array antenna composed of circularly polarized dielectric resonator antennas," in *IEEE Antennas and Propagation Society International Symposium. 1999 Digest. Held in conjunction with: USNC/URSI National Radio Science Meeting (Cat. No.99CH37010)*, vol. 1, pp. 252–255 vol.1, July 1999.

[220] K. K. Pang, H. Y. Lo, K. W. Leung, K. M. Luk, and E. K. N. Yung, "Circularly polarized dielectric resonator antenna subarrays," *Microwave and Optical Technology Letters*, vol. 27, no. 6, pp. 377–379, 2000.

[221] A. Laisne, R. Gillard, and G. Piton, "Circularly polarised dielectric resonator antenna with metallic strip," *Electronics Letters*, vol. 38, pp. 106–107, Jan 2002.

[222] S. Fakhte, H. Oraizi, and R. Karimian, "A Novel Low-Cost Circularly Polarized Rotated Stacked Dielectric Resonator Antenna," *IEEE Antennas and Wireless Propagation Letters*, vol. 13, pp. 722–725, 2014.

[223] K. X. Wang and H. Wong, "A Circularly Polarized Antenna by Using Rotated-Stair Dielectric Resonator," *IEEE Antennas and Wireless Propagation Letters*, vol. 14, pp. 787–790, 2015.

[224] K. Khoo, Y. Guo, and L. C. Ong, "Wideband Circularly Polarized Dielectric Resonator Antenna," *IEEE Transactions on Antennas and Propagation*, vol. 55, pp. 1929–1932, July 2007.

[225] E. H. Lim and K. W. Leung, "Compact wideband circularly polarized dielectric resonator antenna with an underlaid hybrid coupler," in *2008 IEEE Antennas and Propagation Society International Symposium*, pp. 1–4, July 2008.

[226] Y. Pan and K. W. Leung, "Wideband Circularly Polarized Trapezoidal Dielectric Resonator Antenna," *IEEE Antennas and Wireless Propagation Letters*, vol. 9, pp. 588–591, 2010.

[227] Y. M. Pan and K. W. Leung, "Wideband Omnidirectional Circularly Polarized Dielectric Resonator Antenna With Parasitic Strips," *IEEE Transactions on Antennas and Propagation*, vol. 60, pp. 2992–2997, June 2012.

[228] R. Han, S. Zhong, and J. Liu, "Broadband circularly polarised dielectric resonator antenna fed by wideband switched line coupler," *Electronics Letters*, vol. 50, pp. 725–726, May 2014.

[229] M. Zou and J. Pan, "Wideband hybrid circularly polarised rectangular dielectric resonator antenna excited by modified cross-slot," *Electronics Letters*, vol. 50, pp. 1123–1125, July 2014.

[230] J. Patin and S. K. Sharma, "Dual band single feed dielectric resonator antenna with linear and circular polariziations for Ku-band," in *2011 IEEE International Symposium on Antennas and Propagation (APSURSI)*, pp. 1678–1681, July 2011.

[231] Hon San Ngan, X. S. Fang, and K. W. Leung, "Design of dual-band circularly polarized dielectric resonator antenna using a higher-order mode," in *2012 IEEE-APS Topical Conference on Antennas and Propagation in Wireless Communications (APWC)*, pp. 424–427, Sep. 2012.

[232] X. Fang, K. W. Leung, and E. H. Lim, "Singly-Fed Dual-Band Circularly Polarized Dielectric Resonator Antenna," *IEEE Antennas and Wireless Propagation Letters*, vol. 13, pp. 995–998, 2014.

[233] S. Dhar, R. Ghatak, B. Gupta, and D. R. Poddar, "Wideband rhombic dielectric resonator antenna with CPW slot excitation for IEEE 802.11a/HiperLAN application," *International Journal of Electronics*, vol. 100, no. 9, pp. 1270–1282, 2013.

[234] W. Huang, A. W. Glisson, and A. A. Kishk, "Electromagnetic characteristics of a thick monopole antenna with dielectric loading," in *Proceedings IEEE Southeastcon '92*, pp. 314–317 vol.1, April 1992.

[235] I. Ida, J. Sato, H. Yoshimura, and K. Ito, "Improvement in efficiency-bandwidth product in small dielectric loaded antennas," *Electronics Letters*, vol. 36, pp. 861–862, May 2000.

[236] H. F. Pues and A. R. Van de Capelle, "An impedance-matching technique for increasing the bandwidth of microstrip antennas," *IEEE Transactions on Antennas and Propagation*, vol. 37, pp. 1345–1354, Nov 1989.

[237] Ansys, "High Frequency Structure Simulator (HFSS) v 15.0."

[238] R. Vila, M. González, J. Mollá, and A. Ibarra, "Dielectric spectroscopy of alumina ceramics over a wide frequency range," *Journal of Nuclear Materials*, vol. 253, no. 1, pp. 141 – 148, 1998.

[239] H. Chen, Y. Wang, Y. Lin, S. Lin, and S. Pan, "A Compact Dual-Band Dielectric Resonator Antenna Using a Parasitic Slot," *IEEE Antennas and Wireless Propagation Letters*, vol. 8, pp. 173–176, 2009.

[240] X. S. Fang and K. W. Leung, "Linear-/Circular-Polarization Designs of Dual-/Wide-Band Cylindrical Dielectric Resonator Antennas," *IEEE Transactions on Antennas and Propagation*, vol. 60, pp. 2662–2671, June 2012.

[241] Y. M. Pan, S. Y. Zheng, and B. J. Hu, "Design of Dual-Band Omnidirectional Cylindrical Dielectric Resonator Antenna," *IEEE Antennas and Wireless Propagation Letters*, vol. 13, pp. 710–713, 2014.

[242] C. A. Balanis, *Antenna Theory Analysis and Design*. Wiley India (P.) Ltd.

[243] D. Guha, B. Gupta, C. Kumar, and Y. M. M. Antar, "Segmented Hemispherical DRA: New Geometry Characterized and Investigated in Multi-Element Composite Forms for Wideband Antenna Applications," *IEEE Transactions on Antennas and Propagation*, vol. 60, pp. 1605–1610, March 2012.

[244] M. Zou and J. Pan, "Investigation of Resonant Modes in Wideband Hybrid Omnidirectional Rectangular Dielectric Resonator Antenna," *IEEE Transactions on Antennas and Propagation*, vol. 63, pp. 3272–3275, July 2015.

[245] I. Ida, J. Sato, T. Sekizawa, H. Yoshimura, and K. Ito, "Dependence of the efficiency-bandwidth product on electrical volume of small dielectric loaded antennas," *IEEE Transactions on Antennas and Propagation*, vol. 50, pp. 821–826, June 2002.

[246] H. Lebbar, M. Himdi, and J. P. Daniel, "Transmission line analysis of printed monopole," *Electronics Letters*, vol. 28, pp. 1326–1327, July 1992.

[247] H. Lebbar, M. Himdi, and J. P. Daniel, "Analysis and optimization of reduced size printed monopole," in *Proceedings of IEEE Antennas and Propagation Society International Symposium*, pp. 1858–1861 vol.3, June 1993.

[248] H. Lebbar, M. Himdi, and J. P. Daniel, "Analysis and size reduction of various printed monopoles with different shapes," *Electronics Letters*, vol. 30, pp. 1725–1726, Oct 1994.

[249] N. P. Agrawall, G. Kumar, and K. P. Ray, "Wide-band planar monopole antennas," *IEEE Transactions on Antennas and Propagation*, vol. 46, pp. 294–295, Feb 1998.

[250] K. Girish Kumar, *Broadband Microstrip Antennas*. Artech House Publishers.

[251] Y. . Lin, C. . Lin, H. . Chen, and P. S. Hall, "A Miniature Dielectric Loaded Monopole Antenna for 2.4/5 GHz WLAN Applications," *IEEE Microwave and Wireless Components Letters*, vol. 16, pp. 591–593, Nov 2006.

List of Publications

Journal Publications

1. P. Anoop and R. Bhattacharjee, "Investigation on a new compact wideband rhombic dielectric resonator antenna", in *Int J RF Microw Comput Aided Eng*, vol.29, no.9, e21864, September 2019. https://doi.org/10.1002/mmce.21864.

2. Anoop P, Bhattacharjee R, "Investigation on Dual-band Equilateral Triangular shaped Dielectric Resonator Antennas for WLAN Applications", in *Int J RF Microw Comput Aided Eng*, vol.31, no.7, e22672, July 2021. https://doi.org/10.1002/mmce.22672.

Conference Publications

1. P. Anoop and R. Bhattacharjee, " Impedance bandwidth performance of $TM_{10\delta}$ mode in Equilateral Triangular DRA", *2020 14th European Conference on Antennas and Propagation (EuCAP)*, Copenhagen, Denmark, 2020, pp. 1-5, doi: 10.23919/EuCAP48036.2020.9135190.

2. P. Anoop and R. Bhattacharjee, "Expression for Quality factor of $TM_{10\delta}$ mode in Equilateral Triangular DRA", in *Proceedings of IEEE-INAE Workshop on Electromagnetics (IIWE 2018)*; Dec.2018, Trivandrum, India. (Best Student Paper Award)

3. P. Anoop and R. Bhattacharjee, "Investigation on Dielectric Loaded Monopole Antennas for Dual Band Application", *2016 Twenty Second National Conference on Communication (NCC)*, Guwahati, 2016, pp. 1-6, doi: 10.1109/NCC.2016.7561178.

4. P. Anoop and R. Bhattacharjee, "Design of Dual Band Triangular DRA for WLAN Application", *2015 IEEE Applied Electromagnetics Conference (AEMC)*, Guwahati, 2015, pp. 1-2, doi: 10.1109/AEMC.2015.7509114.

Bio-Data

1	Name:	P. Anoop
2	Date of Birth:	13-August-1986
3	Educational Qualification:	December-2007, B.Tech. in Electronics Engineering (62.58 %), Government College of Engineering, Kannur, Kerala, India July-2013, M.Tech. in Communication Engineering (6.87/10 CGPA), Indian Institute of Technology Guwahati, Guwahati, Assam, India
4	Permanent Address:	S/O M. Balachandran Sayoojyam, Parakkadavu Post: Anchampeedika District: Kannur Kerala, India Pincode-670331
5	Contact Address:	Communication Lab II, Department of Electronics & Electrical Engineering, Indian Institute of Technology Guwahati, Guwahati, Assam, India Pincode-781039
6	Contact Number:	(+91)-8011919339